UiT
THE ARCTIC UNIVERSITY OF NORWAY

Faculty of Science and Technology

Department of Geosciences

Reconstructing the Paleoproterozoic sulfur cycle

Insights from the multiple sulfur isotope record of the Zaonega Formation, Karelia, Russia

—

Kärt Paiste

A dissertation for the degree of Philosophiae Doctor – September 2018

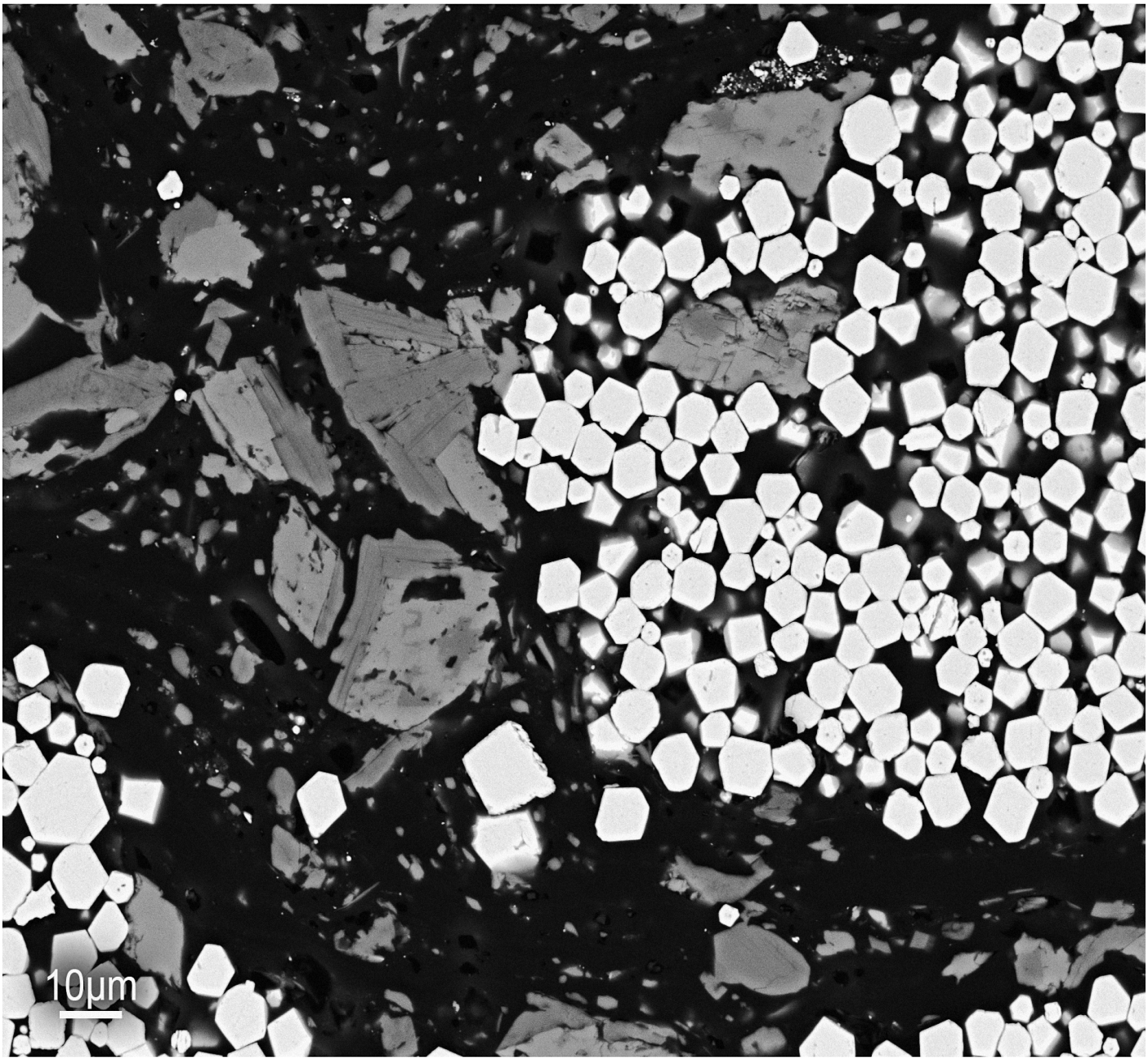

UNIVERSITY OF TROMSØ

Dissertation for the degree of Philosophiae Doctor

Reconstructing the Paleoproterozoic sulfur cycle

Insights from the multiple sulfur isotope record of the Zaonega Formation, Karelia, Russia

Kärt Paiste

UiT - The Arctic University of Norway

Faculty of Sciences and Technology

Department of Geosciences

September 2018

Supervisors:

Dr. Aivo Lepland
Geological Survey of Norway (NGU)
Trondheim, Norway
CAGE—Centre for Arctic Gas Hydrate,
Environment and Climate
UiT The Arctic University of Norway,
Tromsø, Norway
University of Tartu, Tartu, Estonia
Tallinn University of Technology, Tallinn, Estonia

Dr. Aubrey L. Zerkle
School of Earth and Environmental Sciences
and Centre for Exoplanet Science
University of St Andrews, St Andrews, Scotland

Dr. Boswell A. Wing
Department of Geological Sciences
University of Colorado Boulder, Boulder, USA

Dr. Giuliana Panieri
CAGE—Centre for Arctic Gas Hydrate,
Environment and Climate
Department of Geosciences
UiT The Arctic University of Norway
Tromsø, Norway

Preface

This doctoral thesis was conducted over the course of four years (September 2014–2018) as part of the Centre for Arctic Gas Hydrate, Environment and Climate (CAGE) at UiT - The Arctic University of Norway. Research presented in this thesis was supervised by A. Lepland, A. L. Zerkle, B. A. Wing, G. Panieri and during the initial stages of the project by H. Oduro. Writing of the thesis was completed at the Geological Survey of Norway (NGU), while laboratory work and data acquisition were carried out at the University of St Andrews, University of Tartu and McGill University. Funding was provided from the Centre for Arctic Gas Hydrate, Environment and Climate which is supported by the Research Council of Norway through its Centres of Excellence funding scheme grant No. 223259.

Research results of this thesis have been presented at several international conferences, including Goldschmidt (2015, 2016, 2017) and the Gordon Research Conference on geomicrobiology (2018). I have also attended international courses such as Carbonate Sediments as Archives of Earth Evolution (Estonia, 2018), BUBBLES 2017 (Tromsø, 2017) and the Astrobiology Summer School on Volcanism, Plate Tectonics, Hydrothermal Vents and Life (Azores, 2016). Throughout the course of my studies I have gained geological fieldwork experience from Paleoproterozoic terranes in Karelia and the Kola peninsula in Russia and joined a scientific cruise (HH2015) to the west coast of Svalbard. I have participated in field trips in northern Italy, Sicily, Scotland and Japan and been involved in several drill core inspection and sampling parties at NGU.

Assigned duty work has been part of the doctoral program at UiT and included various tasks in organisation of seminars, meetings and administration of the AMGG official web page. Additionally, as a doctoral candidate at CAGE I have been a member of the AMGG – Arctic Marine Geology and Geophysics research school, which involved participation at various activities and seminars.

Acknowledgements

Collaboration is the backbone of science, thus, I have had the amazing opportunity to meet and work with a wealth of young researchers and top scientists at different facilities, who have all contributed to the development of the scientific rationale of this thesis. I'm very grateful to the people I have met at at various conferences, CAGE, NGU, the University of St Andrews, McGill University and the University of Colorado Boulder, were everyone has been very welcoming.

I'm also grateful to my supervisors Aivo, Aubrey, Giuliana and Boswell who have been fantastic to work with and guided and supported me throughout the last four years. Especially I want to thank Aivo and Aubrey as you have always encouraged me to pursue my own ideas and goals.

A very special gratitude goes out to Kalle and Tony, with whom I have enjoyed numerous interesting discussions about geology which have significantly influenced my development throughout completing this thesis. It is beyond words how much I appreciate your insights and contribution into this research. Also, for your precious advice to arm myself with plenty of toilet paper as a precautionary measure for a scientific career that may involve episodes of mud throwing.

Most of all, I have loved the numerous meetings, field trips and excursions with my fellow peers at different institutions but mostly at Tromsø, St Andrews, Tartu and Trondheim. It has been always a fun combination of gaining new knowledge and having a great time!

With a special mention to Aave as you have been the voice of reason reminding me that there is also another life outside research and of course Melanie for the smooth and joyful sampling parties.

I would like to thank all my friends in Estonia and worldwide for finding the time for my sporadic visits and the adventures we have shared.

And finally, I would not have made it this far without the encouragement and moral support of Tõnn and the countless hours of intermittent skype connectivity!

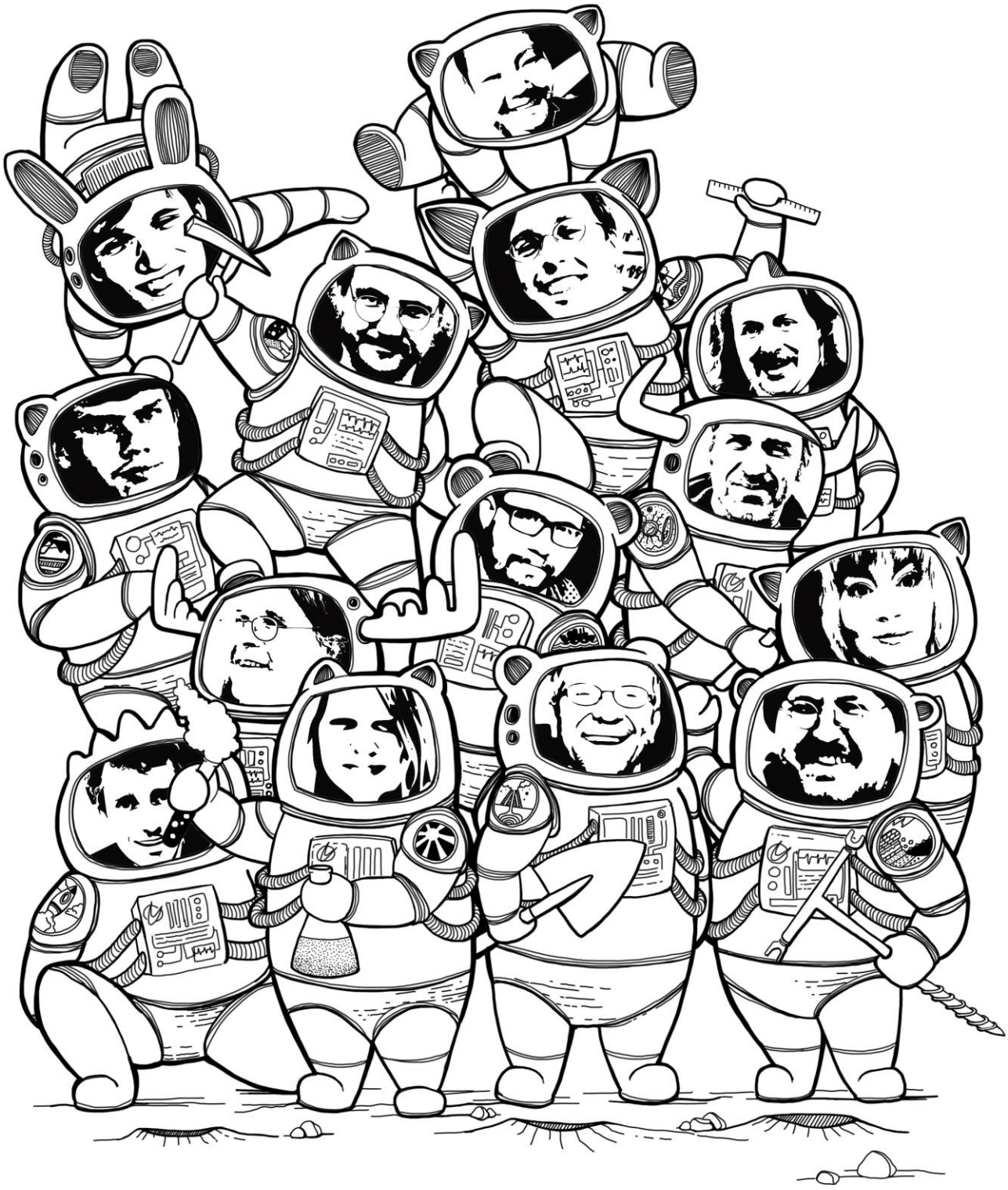

Contents

List of papers

Paper 1

Paiste K., Lepland A., Zerkle A.L., Kirsimäe K., Izon G., Patel N.K., McLean F., Kreitsmann T., Mänd K., Bui T.H., Romashkin A.E., Rychanchik D.V., Prave A.R., 2018. Multiple sulphur isotope records tracking basinal and global processes in the 1.98 Ga Zaonega Formation, NW Russia: *Chemical Geology*. https://doi.org/10.1016/j.chemgeo.2018.09.025

Paper 2

Paiste K., Wing B. A., Zerkle A. L., Kirsimäe K., Pellerin A., Bui T. H., Prave A. R., Romashkin A. E., Lepland A. Biogeochemical sulphur cycling in a semirestricted basin – modelling the pyrite multiple sulphur isotope record of the 1.98 Ga Zaonega Formation, *to be submitted to Earth and Planetary Science Letters*.

Paper 3

Paiste K., Lepland A., Zerkle A. L., Wing B. A., Kirsimäe K., Kreitsmann T., Mänd K., Romashkin A. E., Rychanchik D. V., Prave A. R. Global vs. basinal controls on Paleoproterozoic sulfur isotope records: new insights from the Zaonega Formation, NW Russia, *to be submitted to Earth-Science Reviews*.

Co-author papers and papers in preparation for submission

Mänd K., Robbins L. J., Thoby M., Paiste K., Kreitsmann T., Lalonde S. V., Kirsimäe K., Lepland A., Konhauser K. O. Extreme trace metal enrichments in the Zaonega Formation indicate a post-Lomagundi O_2 overshoot, *to be submitted*.

Kreitsmann T., Külaviir M., Kirsimäe K., Lepland A., Paiste K., Paiste P., Prave A. R., Sepp H., Romashkin A. E., Rychanchik D. V. Insights into the Paleoproterozoic C cycle: dedolomitization and hydrothermal alteration of carbonate rocks of the Zaonega Formation, NW Russia, *to be submitted*.

Blättler C.L., Claire M.W., Prave A.R., Kirsimäe K., Higgins J.A., Medvedev P.V., Romashkin A.E., Rychanchik D.V., Zerkle A.L., Paiste K., Kreitsmann T., Millar I.L., Hayles J.A., Bao H., 2018. Two-billion-year-old evaporites capture Earth's great oxidation: *Science*, p. eaar2687. https://doi.org/10.1126/science.aar2687

Joosu L., Lepland A., Kreitsmann T., Üpraus* K., Roberts N.M.W., Paiste P., Martin A.P., Kirsimäe K., 2016. Petrography and the REE-composition of apatite in the Paleoproterozoic Pilgujärvi Sedimentary Formation, Pechenga Greenstone Belt, Russia: *Geochimica et Cosmochimica Acta*, v. 186, p. 135–153. https://doi.org/10.1016/j.gca.2016.04.043

Lepland A., Joosu L., Kirsimae K., Prave A.R., Romashkin A.E., Crne A.E., Martin A.P., Fallick A.E., Somelar P., Üpraus* K., Mand K., Roberts N.M.W., van Zuilen M.A., Wirth R., 2014. Potential influence of sulphur bacteria on Palaeoproterozoic phosphogenesis: *Nature Geoscience*, v. 7, p. 20–24. https://doi.org/10.1038/NGEO2005

* Surname changed from Üpraus to Paiste.

1. Introduction

The chemical composition of Earth's atmosphere and oceans is governed by biogeochemical cycling of material between deep-Earth and surface reservoirs (Canfield, 1998; Farquhar et al., 2014; Holland, 1984). Both biotic and abiotic pathways are involved in the transfer of material between different sinks and sources and intrinsically link the evolution of Earth's environment and life. In the Phanerozoic, several well documented global climatic fluctuations varying from warm greenhouse periods to ice ages, have been associated with changes in tectonic activity, volcanism, silicate weathering rates and carbon burial fluxes. Changes in continental emergence and elemental cycles ultimately impact global surface temperatures, nutrient availability and, hence, can influence the nature and distribution of habitats. Therefore, large-scale perturbations in Earth's environmental conditions can modify significantly ecosystems and their complex interactions and, if severe enough, lead to global destabilisation of ecological networks and biotic interactions and even major mass-extinction events. However, one's loss is another one's gain as life adjusts to the changing world. Organisms unable to adapt are quickly replaced by others who take advantage of the newly available niches. Although the direct fossil record is sparse for Deep Time, the first mass-extinction or significant rearrangement of ecosystems in Earth's history possibly occurred during the Great Oxidation Event (GOE) at ~2.3-2.4 Ga. During this hallmark event, biogenic oxygen production by photosynthetic cyanobacteria surpassed the consumption of oxygen by chemical reactions allowing it to accumulate in the atmosphere. Consequently, the GOE signifies a transition from a reducing to oxidizing world as atmospheric oxygen levels rose to above 0.001% of present levels (Bekker et al., 2004; Gumsley et al., 2017; Guo et al., 2009; Luo et al., 2016).

Multiple lines of evidence, including changes in accumulation of iron formations (Bekker et al., 2014; Konhauser et al., 2017; Planavsky et al., 2010), retention of iron in paleosols (Rye and Holland, 1998), the first economic-grade manganese deposits (Bekker et al., 2003; Roy, 2006), the disappearance of detrital pyrite and uraninite grains (Holland, 2006) and perhaps, most significantly, the loss of mass-independent sulfur isotope fractionations (Farquhar et al., 2011, 2001; Guo et al., 2009; Johnston, 2011; Luo et al., 2016), indicate that pO_2 increased at ~ 2.4–2.3 Ga with possible earlier 'whiffs' of oxygenation at 2.5 Ga (Anbar et al., 2007; Reinhard et al., 2009) or even at 2.9 Ga (Kato et al., 2002; Planavsky et al., 2010). Nevertheless, diversification and speciation of complex multicellular life forms lagged behind the initial expansion of oxygenated environments. Most ecosystems were

dominated by microbes until the radiation of the Ediacaran fauna at ~575 Ma (Shen et al., 2008) and Cambrian explosion at ~541 Ma (Maloof et al., 2010). It is not clear, what caused this long-lasting period of mid-Proterozoic evolutionary stagnation but it may relate to oxygen concentrations in the environment. Microbes are capable of utilising electron acceptors such as manganese oxides, ferrous iron, nitrate or sulfate to harvest energy. However, the free energy gained by anaerobic respiration is not sufficient to sustain complex multicellular organisms. Oxygen is the most effective oxidizing agent and considered essential to meet the high energetic needs of large animals. Therefore, the lack of multicellular organisms has been proposed to reflect oxygen deficiency in Proterozoic environments. This has caused significant debate considering the extent and duration of the GOE with interpretations ranging from a monotonous increase (Ohmoto et al., 2014) to a two-step oxygenation (Canfield et al., 2013; Kump, 2011; Ossa Ossa et al., 2018) or a transitional Earth system state characterized by oscillating atmosphere-ocean redox conditions lasting until the late Neoproterozoic (Planavsky et al., 2018; Sheen et al., 2018).

The numerous opinions on the nature of the GOE's is not surprising considering the patchy preservation of the Archean and Proterozoic rock record. Moreover, sedimentary basins from this time period that have escaped recycling by plate tectonics have experienced at least some degree of metamorphism. Therefore, the causative relationships and exact mechanisms responsible for this irreversible shift in surface redox conditions are difficult to investigate and interpret. In addition, abiotic and biotic cycles operate on different time scales. Microbes are efficient in concentrating reactants and forming low-temperature mineral deposits between days to thousands or millions of years, whereas the influence exerted by geological processes on the cycling of bioessential elements often requires tens to hundreds of millions of years. This interrelation between geological and biological cycling of material highlights the different and distinct response times to global change that would be influenced by a particular setting in a sedimentary basin and the openness of its depositional systems. Therefore, it is necessary to evaluate the dynamic relationships between local and global processes in each individual paleobasin to be able to comprehensively develop and test a model of the ancient Earth System functioning.

The focus of this thesis is the ~2.0 Ga Zaonega Formation in the Paleoproterozoic Onega Basin in Russian Karelia. This formation is considered to be one of the finest archives from which to characterise and assess the physical and chemical conditions, as well as the role of local- vs. global-scale processes, under which biogeochemical sulfur and carbon cycling occurred in the aftermath

of the GOE. This study applies multiple sulfur and organic carbon isotope, bulk-rock chemical and mineralogical analyses combined with petrographical and lithological observations on new and published drill core records on this Formation from across the Onega Basin. The obtained results are integrated with existing data from the Zaonega Formation and placed into a global context by comparing the Onega Basin with other Paleoproterozoic basins elsewhere, such as the Francevillian and Animikie basins and the Pechenga Greenstone belt.

My findings show that the pyrite sulfur isotope record of the Zaonega Formation reflects changes in organic carbon fluxes and depositional conditions that indicate restructuring of the local microbial community at different stages of basin evolution. Moreover, modelling results and comparisons with other basins infer that the underlying mechanisms (e.g. changes in sedimentation and microbial processes) responsible for generating broadly similar sulfur isotope records were operating in different basins at discrete times. Therefore, following the establishment of a substantial seawater sulfate reservoir after the GOE, its size and isotope composition may have remained stable at least during accumulation of the Zaonega Formation and possibly throughout most of the Paleoproterozoic. In summary, this thesis highlights the importance of evaluating spatial and temporal geochemical variability in the context of individual basinal history before reaching global-scale conclusions.

2. The Archean-Paleoproterozoic transition: a synthesis

Turbulent reorganization of the Solar System at ~4 Ga triggered intense cometary-asteroidal bombardment, the so-called Late Heavy Bombardment (LHB). As a result of that as well as plate tectonics, no crustal rocks have been preserved from the earliest history of Earth immediately after its formation at ~4.5 Ga (Fig. 1). Nonetheless, ~4.4 Ga detrital zircons from Jack Hills, Western Australia, suggest that continental crust and oceans capable of harbouring life existed by that time (Wilde et al., 2001). Although the origin of life is unknown, it has been speculated that if life arose early (before 4 Ga) it was constrained to deep-marine hydrothermal systems where primitive organisms could have survived the LHB (Maher and Stevenson, 1988).

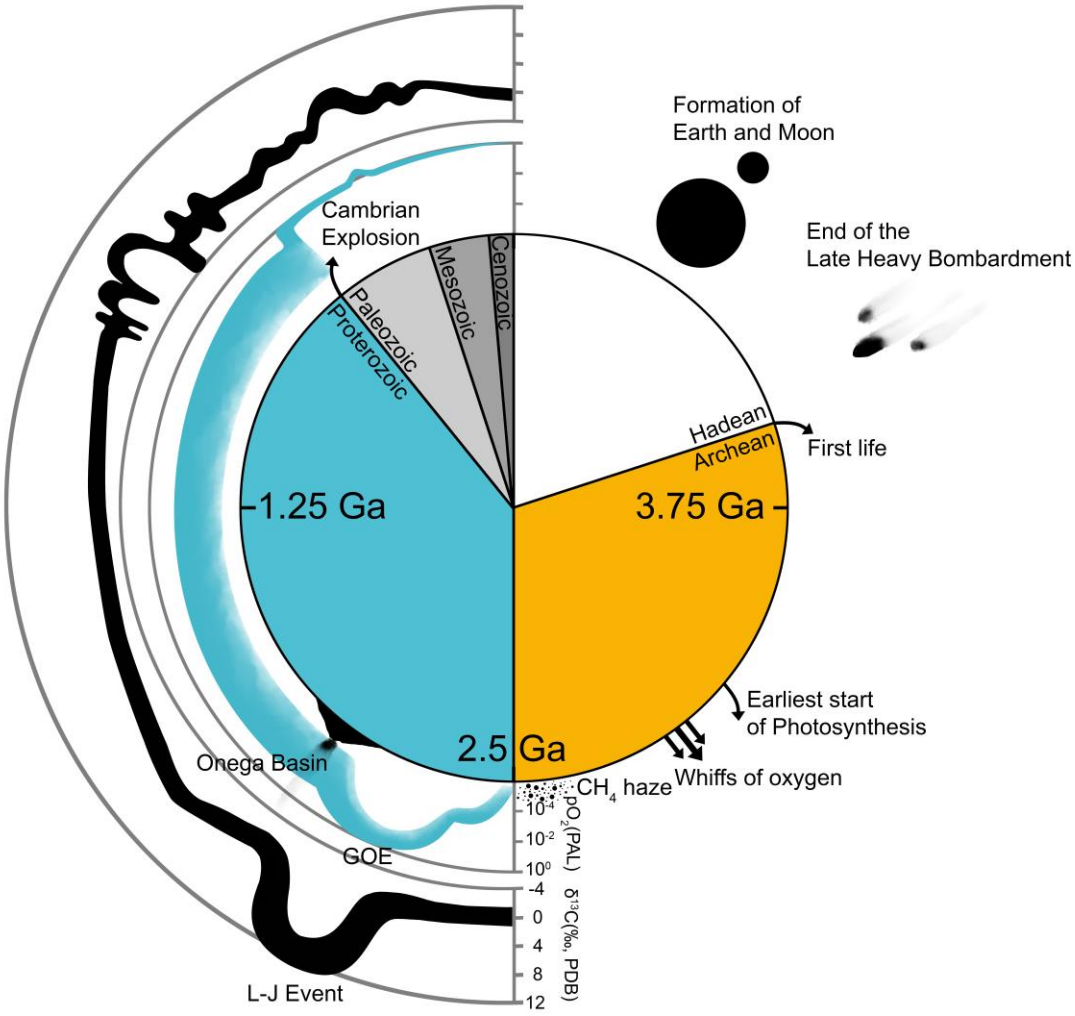

Figure 1. Key geobiological events through Earth's history and along with post-Archean trends of $\delta^{13}C_{carb}$ (from Farquhar et al. 2014) and evolution of atmospheric oxygen (modified from Kump et al. 2007).

In deep-sea hydrothermal systems, high geothermal gradients induce fluid circulation and fluid-rock interactions in the subseafloor leaching reduced compounds (e.g. ferrous iron, hydrogen sulfide, molecular hydrogen or ammonia) from the host rocks. As the ascending hot fluids mix with seawater, oversaturation with respect to different mineral phases is reached promoting mineral precipitation and formation of chimney structures. Such chimneys act as conduits for fluid flow where steep heat and redox gradients could have provided the necessary conditions to overcome energetic barriers to trigger the first metabolic reactions to sustain life (Baross and Hoffman, 1985; Russell and Hall, 1997). A close look at prokaryotic genomes has revealed a set of genes that could be traced back to the Last Universal Common Ancestor (LUCA) and are characteristic for thermophilic organisms inhabiting anoxic environments with abundant H_2, CO_2 and iron such as hydrothermal vent sites (Weiss et al., 2016).

In concert with abiogenesis in submarine-hydrothermal environments, recent discoveries from the Nuvvuagittuq belt in Quebec, Canada have been used to argue for putative microfossils dating possibly as far back as ~4.3 Ga (Dodd et al., 2017). This study is controversial and the inferred age contrasts with the previous estimate of ~3.8 Ga for the Nuvvuagittuq belt (Cates and Mojzsis, 2007; Dauphas et al., 2007). Other evidence for microbial life comes from the carbon isotope signatures of graphite in the ~3.7 Ga Isua Supracrustal Belt, Greenland (Rosing, 1999) and more recently from putative microbial structures there (Nutman et al., 2016) and younger Archean successions (e.g. ~3.5 Ga Dresser Formation in the Pilbara Craton Western Australia; (Djokic et al., 2017). Whether the first organisms inhabited Earth's environments before or shortly after the LHB remains a matter of debate, however, life originated and evolved in conditions that differ significantly from the modern.

2.1 The early Earth and its atmosphere

Residual heat from planetary accretion and grater abundance of radioactive elements were responsible for higher heat production on early Earth (Kasting, 1993; Reddy and Evans, 2009). As a consequence, the mantle was significantly hotter than at present and it is generally agreed that the core was entirely liquid (Davies et al., 2015; Jacobs, 1953; Reddy and Evans, 2009). Precise timing of the inner core's nucleation is a matter of debate with estimates ranging from a relatively late < 1 Ga (Davies et al., 2015; Gubbins et al., 2008) to an early crystallisation at ~3.8 Ga (Hildebrand et al., 2018; Kleine et al., 2002). This has important implications for the redox state of the atmosphere,

since loss of iron to the core early in Earth's history would have impacted the oxidation state of volcanic gasses favouring a weakly reducing or neutral atmosphere (Farquhar et al., 2014; Holland, 1962; Kasting, 1993). Magmatic rocks in Archean and early Proterozoic successions are characterized by komatiites, which form from Fe- and Mg-rich magmas that have a melting point of >1600 °C, much hotter than 1100–1250°C of basaltic magmas (Nisbet et al., 1993). Therefore, a hotter and more reduced mantle relative to the present could have induced high inputs of ferrous iron into the oceans via hydrothermal systems and "weakly reduced" volcanic gases such as CO_2, N_2, CO, H_2, reduced sulfur compounds and possibly CH_4 (Kasting, 1993). Proof for a reduced atmosphere-ocean system is found in Superior-type iron formations that accumulated in various marine settings during the Archean and Paleoproterozoic, disappeared in the Mesoproterozoic but reappeared at the end of the Neoproterozoic (Bekker et al., 2014, 2010; Konhauser et al., 2017; Planavsky et al., 2010). The accumulation of such large-scale iron-rich deposits requires a ferruginous ocean, implying that the flux of ferrous iron overwhelmed oxygen and sulfate inputs to marine environments. This would be unlikely under an oxygenated atmosphere since iron rapidly reacts with oxygen and sulfide (produced by microbial sulfate reduction) forming insoluble minerals (ferric oxides/oxyhydroxides and Fe-sulfides) (Holland, 1973).

Warm climate resulting from an atmosphere rich in greenhouse gases is further implied by the scarcity of glacial deposits in the Archean. The oldest putative glacial diamictites formed at ~2.9 Ga in the Witwatersrand Supergroup of South Africa (Young et al., 1998) and were followed by a long-lasting ice-free period until the three episodes of Huronian glaciation in the earliest Paleoproterozoic at 2.4-2.2 Ga (Bekker et al., 2005; Young et al., 1998). A warm greenhouse climate is supported by $\delta^{18}O$ investigations of chert deposits that have been used to argue for surface temperatures as highs as 70 $\pm$ 15°C (Knauth and Epstein, 1976; Robert and Chaussidon, 2006). However, more recent evaluations of seawater $\delta^{18}O$ evolution suggest more moderate 25–40°C temperatures (Blake et al., 2010; Hren et al., 2009; Marin et al., 2010). Even though glacial deposits are scare in the Archean, their presence favours a temperate global climate not significantly warmer than ~20°C (Kasting, 1993). Regardless whether the planet was hot or temperate, higher contributions of greenhouse gases into the atmosphere were necessary in order to maintain largely ice-free climatic conditions and compensate for lower solar luminosity on early Earth (Farquhar et al., 2014; Kasting, 1993).

Under low atmospheric oxygen levels, increased pCO_2 would lower pH in rain water and consequently soil water leading to aggressive weathering regimes and intense leaching of iron from the initial Fe-rich substrate (ultramafic and mafic lavas and plutons). Mature paleosols in Archean successions (e.g. ~3.2 Ga Moodies Group in South Africa and ~2.75 Ga Mt Roe in Western Australia) attest to such conditions and display weathering profiles with pronounced iron depletions (Farquhar et al., 2014; Hessler and Lowe, 2006; Kump et al., 2013; Murakami et al., 2011; Rye and Holland, 1998). Additional evidence for low pO_2 is provided by detrital grains of redox sensitive minerals such as pyrite, uraninite and siderite that are common constituents in Archean and early Proterozoic sedimentary rocks (Farquhar et al., 2014; Holland, 2006). These minerals are unstable under oxic conditions and quickly weather when transported into sedimentary basins, unless extremely high erosion, transport and sedimentation rates prevent exposure and oxidation of such minerals (Maynard et al., 1991). Consequently, in modern conditions detrital pyrite and uraninite minerals are rare, contrary to rock successions predating ~2.3 Ga where such well-rounded grains are often observed in various fluvial and marine-lacustrine settings (Berkner and Marshall, 1965; Cloud, 1968; Farquhar et al., 2014; Roscoe and Minter, 1993).

Geochemical proxies such as rare earth element (REE) patterns also indicate oxygen-poor terrestrial and marine environments during this time. Archean and early Paleoproterozoic phosphate minerals in paleosols (Murakami et al., 2001) and iron formations (Bau et al., 1997; Bau and Dulski, 1996; Bau and Möller, 1993; Planavsky et al., 2010) lack characteristic negative Ce anomalies in their REE profiles, which are typically attributed to Ce fractionation under oxic conditions. Similarly, abundances of redox sensitive metals such as Mo, Re, V and U in sedimentary rocks have been used to constrain inputs of these elements via oxidative weathering relative to their removal via reductive oceanic sinks (Anbar et al., 2007; Partin et al., 2013; Scott et al., 2008; Sheen et al., 2018; Shields-Zhou and Och, 2011). The magnitude of trace metal enrichments in sedimentary successions is typically related to their concentrations in seawater, thus their low abundances in Archean shales have been interpreted to reflect limited oxidative weathering of continental crust (Partin et al., 2013; Scott et al., 2008; Sheen et al., 2018). Perhaps, transient atmospheric oxygenation, so-called whiffs of oxygen, at that time are indicated by episodic Mo and Re enrichments in 2.65–2.5 Ga sedimentary rocks (Anbar et al., 2007).

Utilization of trace metal abundances is most straight-forward when they are quantitatively removed from the water column under euxinic conditions. Interpretation of water column redox

status has taken advantage of iron speciation techniques that enable identifying ferruginous, euxinic and oxic depositional conditions by assessing the relative distribution of iron among different mineral phases (Clarkson et al., 2014; Poulton and Canfield, 2011, 2005; Poulton and Raiswell, 2002; Raiswell et al., 1994; Raiswell and Canfield, 2012). Applying this method on ancient rocks has revealed that Archean oceans were largely ferruginous and deep waters remained predominantly anoxic until the Neoproterozoic-Cambrian transition (Planavsky et al., 2011; Poulton and Canfield, 2011). However, euxinic water column conditions have been described on continental margins already at ~2.66 Ga (Scott et al., 2011). The development of euxinia requires reduction of sulfate suggesting that the relative input of sulfate from continental weathering overturned the flux of iron, which might signify rising atmospheric oxygen levels at that time (Scott et al., 2011). Alternatively, decreasing supply of iron from hydrothermal sources into early Earth's oceans could also promote euxinia without necessitating changes in pO_2 (Farquhar et al., 2011; Scott et al., 2011). Further, in modern environments, water column euxinia forms in a variety of settings depending on basin circulation, configuration, specific depositional conditions, nutrient fluxes, distribution of microbial communities, bioproductivity and microbial sulfate reduction (MSR) rates (Brüchert, 2004; Dale et al., 2009; Gomes and Hurtgen, 2013; Gomes and Johnston, 2017; Meyer and Kump, 2008). All these factors reflect local rather than global conditions. The use of iron proxies in ancient paleoredox studies must also take into consideration iron mobility and reactivity during diagenesis and metamorphism, which can be difficult to untangle from primary signatures (Slotznick et al., 2018).

Even though all of the above noted metal redox proxies comply with reducing Archean environments, the strongest evidence for low atmospheric oxygen is provided by the preservation of mass-independently fractionated sulfur isotope (S-MIF) signatures in rock successions older than ~2.3 Ga (Farquhar et al., 2007, 2000; Johnston, 2011; Luo et al., 2016). Sulfur has four stable isotopes (^{32}S, ^{33}S, ^{34}S and ^{36}S) that, according to normal equilibrium and kinetic mass laws, are fractionated by biogeochemical processes in a predictable manner such that, depending on their relative mass differences, the generated isotope effects converge on a linear fractionation trend (Farquhar et al., 2003; Johnston, 2011; Seal, 2006; Thode et al., 1991). Small deviations from the mass-dependent relationship can be produced by microbial processes, which are expressed as a few tenths of a per mil fractionations in the minor sulfur isotope ratios ($\Delta^{33}S$ and $\Delta^{36}S$) (Canfield et al., 2010; Johnston et al., 2005; Ono et al., 2006; Seal, 2006; Zerkle et al., 2016, 2010). However, rock successions predating ~2.3 Ga exhibit anomalously large $\Delta^{33}S$ (larger than ±0.3‰) and $\Delta^{36}S$ values and a

$\Delta^{36}S/\Delta^{33}S$ relationship (~1) that diverges from thermodynamical predictions for mass-dependent processes ($\Delta^{36}S/\Delta^{33}S$ of ~7) (Farquhar et al., 2014; Ono et al., 2006; Zerkle et al., 2016, 2010). These non-equilibrium signatures in pre-2.3 Ga rocks have been attributed to (i) dissociation of volcanically released SO_2 by atmospheric photochemical reactions involving UV radiation (Danielache et al., 2008; Farquhar et al., 2001; Masterson et al., 2011; Ueno et al., 2009; Zerkle et al., 2012), (ii) transfer of sulfur species carrying a S-MIF signature from atmosphere to marine environments and (iii) their preservation in sedimentary successions (Farquhar et al., 2014; Pavlov and Kasting, 2002). These conditions are met in the absence of an ozone layer that shields against UV radiation and when contributions of atmospherically sourced sulfur species are high relative to weathering inputs into sedimentary basins. Further, the S-MIF record provides quantitative constraints on atmospheric oxygen concentrations of ~1 ppm, since above this threshold the S-MIF would be homogenized by oxidation reactions of sulfur aerosols (Farquhar et al., 2007, 2000; Pavlov and Kasting, 2002). This does not exclude the production of S-MIF in a modern-type atmosphere as recently reported (Guo et al., 2009; Romero, 2003) and stratospheric volcanic eruptions (Baroni et al., 2007; Savarino et al., 2003) but merely denotes its limited role in modern-type sulfur cycling. At present such sulfur species are effectively diluted in the ocean environment and not transferred widely into sediments. Thus, it is generally accepted that the S-MIF record signifies the dominance of anoxic surface environments until 2.3 Ga (Farquhar et al., 2014; Guo et al., 2009; Luo et al., 2016).

Experimental studies have been used to argue that thermochemical sulfate reduction (TSR) could provide an alternative mechanism for explaining the anomalous minor sulfur isotope fractionations (Lasaga et al., 2008; Watanabe et al., 2009). These studies showed that a combination of abundant labile organic matter, sulfate-rich seawater and extensive submarine hydrothermal activity could induce TSR and facilitate anomalous fractionations in $\Delta^{33}S$ and $\Delta^{36}S$. Follow up work by Oduro et al. (2011) further demonstrated that these isotope effects could be attributed to magnetic isotope effects that fractionate $\Delta^{33}S$ without significantly affecting $\Delta^{36}S$. Thus, although TSR could be an important mechanism in natural systems where heat induced reactions between organic and sulfur compounds occur, it has been considered unlikely to explain the S-MIF in both $\Delta^{33}S$ and $\Delta^{36}S$ in Archean successions (Farquhar et al., 2014; Oduro et al., 2011).

In summary, the formation and preservation of the Archean S-MIF record combined with insights from several paleoredox proxies and geological observations is most parsimoniously explained by a

greenhouse atmosphere, dominated by CO_2 gas and the prevalence of reducing surface environments in the Archean and early Paleoproterozoic.

2.2 Neoarchean and early Paleoproterozoic environmental changes

The tipping point towards a permanently oxygenated atmosphere was reached at the Neoarchean and Paleoproterozoic transition. Regardless of an early or late start of modern-type plate tectonics, there is considerable evidence for extensive juvenile crust formation and stabilisation of continental cratons at the Neoarchean-Paleoproterozoic transition (Kump and Barley, 2007; Reddy and Evans, 2009; Taylor et al., 1981). The scarcity of komatiites in post-Archean rock successions (Grove and Parman, 2004) and the increased contribution of subaerial relative to submarine large igneous provinces (LIP's) at ~2.7–2.5 Ga (Kump and Barley, 2007) infer a shift in tectonic evolution accompanied by changes in mantle composition and temperature. Widespread continental emergence enhanced silicate weathering and drawdown of atmospheric greenhouse gases (Bekker et al., 2005; Eriksson et al., 2005), whereas decreased submarine volcanism reduced the overall sink for oxygen (Kump and Barley, 2007). This helped to establish the prerequisites that allowed for the first-time biogenic oxygen production to surpass its consumption by chemical reactions and its accumulation in the atmosphere and overturning of the greenhouse effect.

The contingent nature of continental emergence and weathering affected the global climate by reducing the overall greenhouse effect, which initiated the low-latitudinal ice sheets and triggered the Huronian glaciations between ~2.45–2.22 Ga (Bekker, 2011; Evans et al., 1997; Kirschvink et al., 2000; Kopp et al., 2005). Glacial diamictites from this time interval have been identified in South Africa, eastern and northern Canada, United States, Russia, Finland, and Western Australia (Bekker, 2011; Bekker et al., 2006). These glacial deposits also associate with the first appearance of hematite coated detrital sediments known as red beds (Fig. 2a) (Bekker et al., 2004; Eriksson and Cheney, 1992; Melezhik et al., 2005; Ojakangas et al., 2001; Twist and Cheney, 1986). The formation of red beds denotes a shift in iron redox from ferrous to ferric iron and the relatively higher oxidizing capacity of early Paleoproterozoic terrestrial settings. This observation is reinforced by the immobilisation of iron in paleosols (Rye and Holland, 1998) and the presence of highly oxidized ~2.3–2.06 Ga volcanic rocks in Fennoscandia (Fig. 2b) (Rybacki et al., 2013). The latter advocate for increased oxidation of the upper mantle and/or deep oxidative weathering of these lavas.

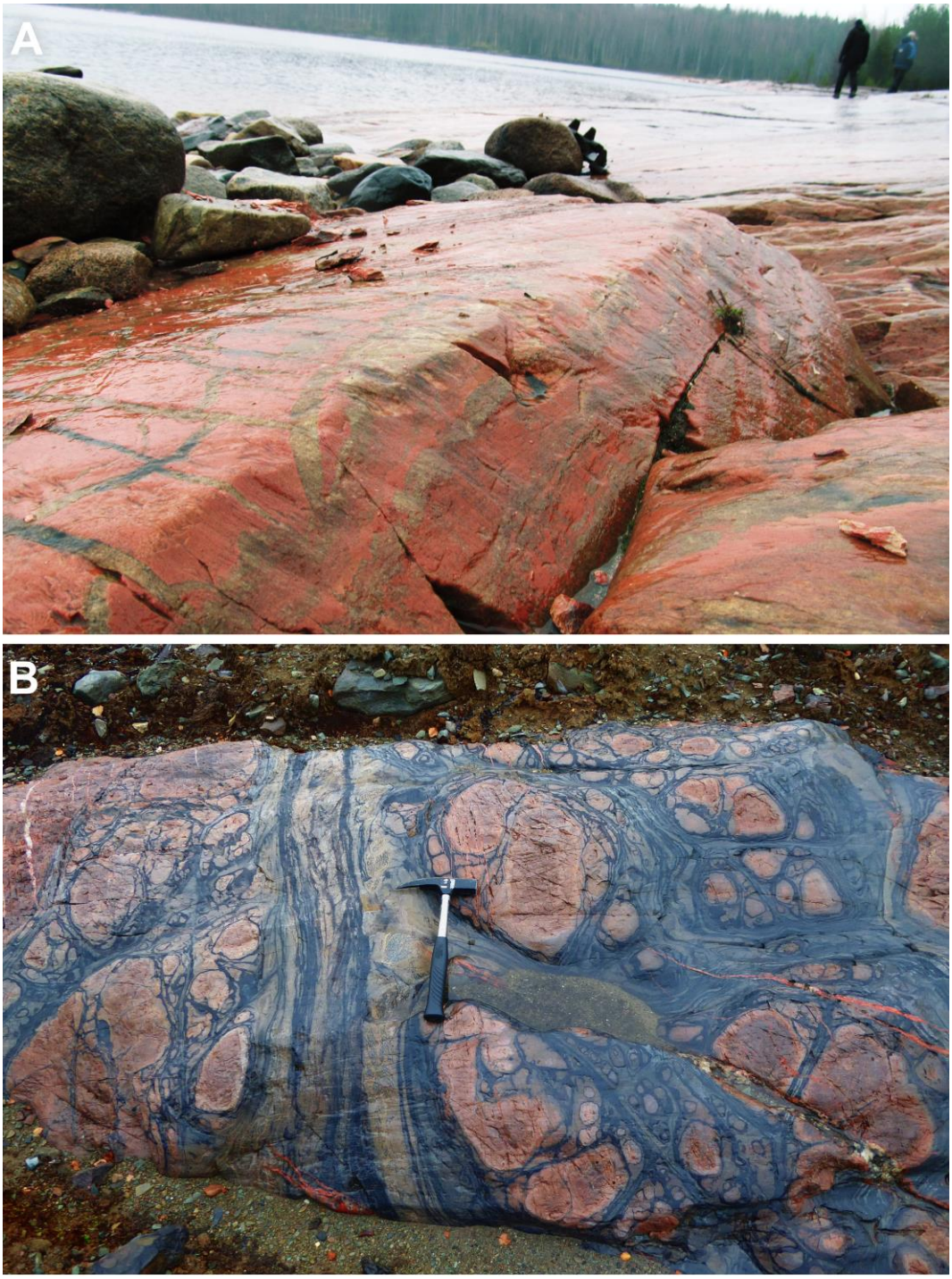

Figure 2. A. Red beds in the lower part of the Tulomozero Formation at Lake Segozero in Karelia, Russia. The alternating red mudstone and beige sandstone beds indicate shallow water sedimentation and exhibit sand filled desiccation cracks within mudstone, formed during exposure to an oxic atmosphere. B. Oxidized lava flow from the 2.06 Ga Kuetsjärvi Volcanic Formation in the Pechenga Greenstone Belt.

This shift in surface redox is thought to signify the irreversible accumulation of atmospheric oxygen at the Neoarchean-Proterozoic transition (Holland, 2006). The expansion of Earth's surface oxidant reservoirs is further indicated by the declining preservation of detrital pyrite, siderite and uraninite grains in post-Archean successions (Holland, 2006), augmented mineral evolution (Hazen et al.,

2008) and enhanced riverine inputs of sulfate, phosphate and metals into the global ocean. It is interesting to note that the biogeochemical processes occurring at the Neoarchean-Paleoproterozoic transition may have affected the variety and relative abundances of near-surface mineral phases and contributed to the largest expansion of mineral diversity in Earth's history. The number of different mineral species at least doubled between ~2.5–1.9 Ga and rose to over 4000 (4300 are currently known) with the advent of new oxide/hydroxide minerals (Hazen et al., 2008).

Evaporites are considered as direct precipitates from seawater, thus the lack of sulfate minerals in Archean successions (Eriksson et al., 2005) and their appearance at ~2.2–2.0 Ga manifests a transformation in the major ion composition of the oceans. The discovery of a thick ~2.0 Ga modern-type marine evaporite sequence containing abundant Ca-sulfate minerals in Karelia and the presence of Ca-sulfate pseudomorphs identified in other 2.2–2.1 Ga sedimentary rocks in Australia, Canada, South Africa and USA provide unequivocal evidence for an expanding seawater sulfate (SWS) reservoir (Blättler et al., 2018; Melezhik et al., 2005; Morozov et al., 2010; Reuschel et al., 2012b; Schröder et al., 2008). Further, these evaporite-carbonate successions preserve stromatolitic structures and their carbonate carbon isotope composition exhibits a pronounced ^{13}C-enrichment. This positive $\delta^{13}C_{carb}$, excursion termed the Lomagundi-Jatuli Event (LJE), has been interpreted to reflect an imbalance between oxidized and reduced carbon reservoirs (Bekker et al., 2001; Karhu and Holland, 1996; Melezhik et al., 2005). It has been proposed that during the LJE pO_2 rose to near modern levels enhancing oxidative weathering and the delivery of electron acceptors and macro/micro nutrients (e.g. SO_4^{2-}, PO_4^{3-}, NO_3^-, Fe, Cu, Ni, Zn, Mn) into marine settings. This seems to be supported by the first appearance of economic grade sediment-hosted manganese deposits in western Africa and India that imply redox-controlled Mn cycling at the interface of oxic surface and anoxic deep waters (Bekker et al., 2003; Planavsky et al., 2010; Roy, 2006). Increased availability of nutrients stimulated primary productivity leading to the accumulation of Paleoproterozoic organic-rich shales (Kump, 2011; Melezhik et al., 1999; Strauss et al., 2013) and the first appearance of phosphorous-rich sedimentary deposits (Lepland et al., 2013; Papineau, 2010). Enrichments in Mo, Re and other trace metals in these organic-rich rocks point to the expansion of their respective reservoirs as a consequence of enhanced oxidative weathering (Partin et al., 2013; Scott et al., 2008; Sheen et al., 2018).

Combined, these transitional changes in Earth's surface environment, along with the permanent disappearance of S-MIF at ~2.3–2.4 Ga recorded in the Huronian Supergroup in North America

(Papineau et al., 2007) and Transvaal Supergroup in southern Africa (Guo et al., 2009; Luo et al., 2016), provide abundant evidence for global oxygenation in the time interval between 2.5–2.0 Ga (but see Ohmoto et al., 2014). It has been argued that the GOE involved several rises and falls in pO_2 based on transient fluctuations in S-MIF in the Rooihoogte and overlying Duitschland Formations of the Transvaal Supergroup (Guo et al., 2009). A more recent re-evaluation of the depositional model and investigation of the sediment facies in the Transvaal Supergroup, however, demonstrated that the Rooihoogte and overlying Duitschland Formations may be correlative; if so, then these represent a singular event (Warke and Schröder, 2018) and the loss of S-MIF could be utilized in chemostratigraphical correlations (Warke and Schröder, 2018). Further, recent modelling of Ca isotope fractionation in 2.0 Ga LJE evaporites constrain SWS concentration at 10 mM. Such a large SWS reservoir just after the GOE, would correspond to oxidant capacity equivalent to 23% of modern atmosphere and ocean combined or to an atmospheric O_2 inventory equivalent to 62% of present atmospheric level (Blättler et al., 2018). However, recent paleoenvironmental reconstructions utilising different geochemical tools, including stable sulfur and carbon isotopes, have suggested that the oxygenation of Earth's atmosphere was dynamic and marked by spatiotemporal heterogeneities (Luo et al., 2016; Ossa Ossa et al., 2018; Planavsky et al., 2018, 2012; Scott et al., 2014; Sheen et al., 2018).

2.3 Deciphering Paleoproterozoic ocean redox conditions

The coupled sulfur and carbon cycles regulate atmospheric oxygen levels through their long-term burial fluxes of oxidized versus reduced forms (Canfield, 1991; Fike et al., 2015; Fry et al., 1988; Habicht et al., 2002). Thus, the sulfur and carbon isotope have been extensively utilized to decipher Paleoproterozoic environmental changes. Most notable are the anomalously positive $\delta^{13}C_{carb}$ values of the LJE that characterise shallow-water carbonate rocks; these have been related to the GOE by enhanced burial of ^{13}C-depleted organic matter (Karhu and Holland, 1996) or, alternatively, by carbonate precipitation in the methanogenic zone where dissolved inorganic carbon (DIC) is enriched in ^{13}C due to microbial methane cycling (Hayes and Waldbauer, 2006). The former inference would require permanent sequestration of large amount of organic matter in rock formations, which is not supported by geological evidence and, instead and paradoxically, organic-rich sediments typically postdate the LJE (Farquhar et al., 2014). The second explanation for positive $\delta^{13}C_{carb}$ is inconsistent with precipitation in environments with intense methanogenesis (Planavsky et al., 2012). Additionally, based on new radiometric ages that expand the canonical LJE time

window, it has been questioned if the LJE was a singular or diachronous event (Gumsley et al., 2017; Adam P. Martin et al., 2013; A.P. Martin et al., 2013). Thus, the timing (~2.2–2 Ga) along with the exact underlying mechanisms behind the LJE isotope excursion remain to be determined. Despite such uncertainties, the LJE shallow-water stromatolitic carbonates and Ca-sulfate evaporites provide clear evidence for an expanding SWS reservoir at the height of the GOE (Blättler et al., 2018; Canfield et al., 2013; Melezhik et al., 2005; Planavsky et al., 2012; Reuschel et al., 2012b).

The occurrence of broadly similar chemostratigraphic trends with negative $\delta^{13}C_{org}$ and positive $\delta^{34}S$ shifts that postdate the LJE in the Paleoproterozoic Onega Basin (Kump, 2011; Scott et al., 2014) and the Francevillian Group (Canfield et al., 2013; Kump, 2011) have been proposed to reflect a return to more reducing atmosphere-ocean redox conditions (Canfield et al., 2013; Havig et al., 2017; Ossa Ossa et al., 2018; Planavsky et al., 2012; Scott et al., 2014). The distinct negative trend in $\delta^{13}C_{org}$ values in the upper part of the sedimentary successions in the Francevillian (i.e. FC and FD Formations) and Onega basins (i.e. Zaonega Formation) were used to argue for massive oxidation of organic matter deposited during the LJE (Kump, 2011). Exhumation of large amounts of organic matter was hypothesised to cause a global and synchronous shift towards ^{12}C-enriched atmospheric and oceanic carbon reservoirs triggering formation of strongly ^{13}C-depleted biomass. It was further demonstrated that the upper part of the Francevillian succession that encompasses the most ^{13}C-depleted biomass ($\delta^{13}C_{org}$ values between -40‰ and -50‰) has preserved ^{34}S-enriched pyrites (Canfield et al., 2013). These pyrites were interpreted as precipitates from a low-sulfate euxinic water column. Thus, this coupling between the $\delta^{13}C_{org}$ and pyrite $\delta^{34}S$ record was thought to be a corollary of the massive remineralisation of organic carbon. This would have provided a sink for O_2 allowing the expansion of euxinic seas and drawdown of SWS levels by MSR (Canfield et al., 2013). Subsequently, the notion of a global decrease in SWS concentrations was reinforced by the close association of negative $\delta^{13}C_{org}$ (~-45‰), increasingly positive $\delta^{34}S$ values (up to 21‰), an opposing $\Delta^{33}S$-$\delta^{34}S$ relationship and Fe speciation results indicating euxinic conditions in the Zaonega Formation in the Onega Basin (Scott et al., 2014). The negative $\delta^{13}C_{org}$ shift was interpreted as a biogeochemical response to very low SWS concentrations that would have allowed enhanced methanogenesis and causing methanotrophy in the water-column (Scott et al., 2014). A similar conclusion was reached by Ossa-Ossa et al. (2018) for the coupled negative $\delta^{13}C_{org}$ and positive pyrite $\delta^{34}S$ records of the Francevillian succession. Thus, it was reasoned that the occurrence of

broadly similar $\delta^{13}C_{org}$ and $\delta^{34}S$ profiles in two separate localities in Russia and Gabon reflected a global ocean-atmosphere deoxygenation (Ossa Ossa et al., 2018).

The global implication of these results rests mainly on correlation of Paleoproterozoic strata that are assumed to be of similar age but preserved within different basins. However, several authors have questioned the correlation between the Francevillian FC (or FD) and the Zaonega Formations as available ages suggest that the latter may be as much as ~100 Ma younger than the former (Martin et al., 2015). Moreover, by combining new and published radiometric ages Martin et al. (2015) concluded that the organic-rich rocks in Russia, Gabon and Australia accumulated at discrete times between the 2.1–1.85 Ga interval. In addition, thorough investigation of the organic-rich rocks of the Zaonega Formation revealed significant differences with the Francevillian $\delta^{13}C_{carb}$ and $\delta^{13}C_{org}$ profiles, as well as evidence for local hydrocarbon migration and spillage (Črne et al., 2014; Qu et al., 2018, 2012; Weber and Gauthier-Lafaye, 2013). This led to the hypothesis that the organic-rich sediments encompassing the ^{13}C-depleted biomass in the Onega Basin may partly be explained by a local bloom in methanotrophic organisms (Qu et al., 2018, 2012). As a consequence, increased methane flux and high organic carbon loading could have favoured AOM and high MSR rates in the shallow sediments (Lepland et al., 2014; Qu et al., 2012) leading to closed-system MSR and precipitation of ^{34}S-enriched pyrites. If true, this would imply high, not low, SWS levels worldwide given that maintaining high MSR over several hundred metres of strata would require a substantial SWS reservoir. Thus, these results highlight the plausible role of local factors in governing the sulfur and carbon cycles rather than necessitating a return to low atmospheric oxygen concentrations.

Documentation of sulfur isotope records from younger Paleoproterozoic sedimentary successions have also produced results that are ambiguous and open to differing interpretations. Until recently the organic-rich sediments of the Pilgujärvi Sedimentary Formation in the Pechenga Greenstone Belt were considered time contemporaneous with the Zaonega Formation. As the former also contains pyrites with positive $\delta^{34}S$ values (up to 18.7‰) the combined Zaonega and Pilgujärvi results were apparently strengthening the notion of global fluctuations in seawater sulfate levels (Havig et al., 2017; Planavsky et al., 2012). However, new age constraints suggest that the Pilgujärvi Sedimentary and Zaonega Formations are not correlative, with the former being significantly younger (1.92 Ga instead of 1.98 Ga; (Martin et al., 2015). Moreover, Reuschel et al. (2012a) demonstrated that a combination of fast sedimentation rates, rapid MSR due to increased organic

carbon loading and effective pyrite sequestration were more likely the causes for the ^{34}S-enriched pyrites.

Similarly, the initial sulfur isotope and Fe speciation results for the ~1.84 Ga Rove Formations of the Animikie Basin were used to infer a SWS $\delta^{34}S_{SO4}$ composition of ~17‰ and the expansion of euxinic seas (Poulton et al., 2004). This interpretation was subsequently questioned by (Pufahl et al., 2010) who argued for increasing restriction and freshening effects in the Animikie Basin. The latter interpretation has been debated (Fralick et al., 2011) and further work in the Animikie Basin has provided important insights about spatial and temporal variability of geochemical proxies across the area (Fralick et al., 2017; Planavsky et al., 2018; Poulton and Canfield, 2011). For example, analyses of trace metal abundances in meteoric calcite cements in the Gunflint Formation were interpreted to reflect an imbalance between oxygenated terrestrial and reduced ocean environments (Fralick et al., 2017). A multi-proxy investigation of the Stambaugh Formation, a deep-water facies in the Animikie Basin, obtained evidence for bottom-water oxygenation at ~1.85 Ga (Planavsky et al., 2018). It was further suggested that the Animikie Basin had a limited connection to the global ocean, resembling the Baltic Sea, where local anoxia can develop due to fluctuations in basin connectivity (Planavsky et al., 2018). This interpretation has important implications for the sulfur isotope record of the 1.84 Ga Rove and 1.85 Ga Stambaugh Formations which are considered in part time-equivalent (Planavsky et al., 2018). The deep-water Stambaugh Formation contains pyrites with $\delta^{34}S$ values ranging from −21.6 to +2.2‰ (average −6.3 ± 6.5‰), whereas in the shallower Rove Formation pyrites have dominantly positive $\delta^{34}S$ values of around 17‰. This discrepancy in $\delta^{34}S$ implies that facies differences and different sulfur cycling (MSR) rates are governing the observed sulfur isotope variations within the Animikie Basin. Moreover, if pyrites recording 17‰ $\delta^{34}S$ from the Rove Formation represent a SWS signature as previously proposed (Poulton et al., 2004), then a large fractionation between sulfate and sulfide in the range of ~38‰ could be estimated. This supports the conclusion of Poulton et al. (2004) that sulfate concentrations within the Animikie Basin exceeded 0.2 mM. This threshold was thought to represent a lower limit required to induce large fractionations by MSR but more recent work has shown this to be equivocal (Crowe et al., 2014; Wing and Halevy, 2014). Therefore, although firm constraints on SWS concentrations are yet to be determined, the presence of such large fractionations speak for a sizeable SWS reservoir at ~1.85 Ga contradicting models that infer low-sulfate oceans for this time. Additional work is clearly

needed before resolving which of the two contrasting models is more correct, which highlights the importance of thorough evaluation of facies and local factors before making large-scale conclusions.

To sum up, there is little doubt that a reduced Archean atmosphere transformed to a more oxidizing atmosphere-ocean system at the Neoarchean-Paleoproterozoic transition. However, there is significant debate regarding the duration, magnitude and extent of this transformation. Current interpretations range from ocean deoxygenation at the end of the LJE (Luo et al., 2016; Ossa Ossa et al., 2018; Planavsky et al., 2012; Scott et al., 2014) to episodic deep-water oxygenation and spatiotemporal ocean redox variability that persisted until the late Neoproterozoic (Diamond et al., 2018; Planavsky et al., 2018; Sheen et al., 2018; Sperling et al., 2015, 2014). Given the complexity in deconvolving local from global processes in reconstructions of Paleoproterozoic ocean chemistry (Aller et al., 2010; Diamond et al., 2018; Fike et al., 2015; Gomes and Johnston, 2017; Jones and Fike, 2013; Pasquier et al., 2017; Slotznick et al., 2018), this discrepancy in opinions is not surprising. The ambiguous reconstructions of ocean paleoredox in different Paleoproterozoic basins (including the Francevillian, Animikie and Onega basins) remain to be solved and reflect the need for better constraints of local depositional conditions and robust age constraints (Črne et al., 2014; Fralick et al., 2017; Kump, 2011; Martin et al., 2015; Melezhik et al., 2015; Ossa Ossa et al., 2018; Poulton et al., 2004; Pufahl et al., 2010; Qu et al., 2018, 2012; Sheen et al., 2018; Warke and Schröder, 2018; Weber and Gauthier-Lafaye, 2013).

3. Organic carbon and pyrite sulfur isotope records

Organic carbon and sulfur isotope proxies have been extensively used as indirect paleoenvironmental proxies for microbial processes and biogeochemical cycling during periods of significant change in Earth's surface. Biological processes preferentially utilise ^{12}C and ^{32}S isotopes over ^{13}C and ^{34}S, respectively, producing isotope effects that leave the reductant pool enriched and the products depleted in the heavier isotopes. Differences in isotopic abundances are reported by using standard delta notations, where

$\delta^{13}C_{org} = 1000 \cdot (^{13}R_{organic\text{-}C}/^{13}R_{V\text{-}PDB} - 1)$, $^{13}R = {}^{13}C/{}^{12}C$ and $^{13}R_{V\text{-}PDB}$ refers to the Vienna PeeDee Belemnite standard, whereas

$\delta^{3x}S = 1000 \cdot (^{3x}R_{sample}/^{3x}R_{V\text{-}CDT} - 1)$, $^{3x}R = {}^{3x}S/{}^{32}S$, x= 33, 34 or 36 and $^{34}R_{V\text{-}CDT}$ represents the international standard Vienna Canyon Diablo Troilite. The minor isotope values are expressed by using the capital delta notation,

$\Delta^{3x}S = \delta^{3x}S - 1000 \cdot [(1 + \delta^{34}S/1000)^{3x\lambda} - 1]$, where 3x is 33 or 36 and $\lambda = 0.515$ or 1.90 for ^{33}S and ^{36}S respectively.

The microbial isotope effects are fully expressed only under favourable conditions and can vary depending on the depositional conditions and environmental factors such as temperature, pH, salinity, the availability and type of electron donors and acceptors (Canfield, 2001; Fike et al., 2015; Seal, 2006). Furthermore, post-depositional alteration can overprint primary isotope signatures leading to $\delta^{13}C_{org}$ and $\delta^{34}S$ values that cannot be attributed to a specific process. In order to resolve some of these issues, recent studies have focused on investigations of minor sulfur isotope ratios ($\Delta^{33}S$ and $\Delta^{36}S$). Small mass-dependent fractionations in $\Delta^{33}S$ and $\Delta^{36}S$ can provide additional information about redistribution of sulfur isotopes by biogeochemical cycling in marine settings (Canfield et al., 2010; Johnston, 2011; Johnston et al., 2005; Seal, 2006; Zerkle et al., 2016, 2010). Therefore, coupled organic carbon ($\delta^{13}C_{org}$) and multiple sulfur isotope data ($\delta^{34}S$, $\Delta^{33}S$, $\Delta^{36}S$) can provide insights to a multitude of processes. However, distinguishing between primary and secondary isotope signatures requires thorough understanding of the mechanisms that can affect isotope fractionations and the specific geological context.

3.1 The role of local carbon fixation pathways in the $\delta^{13}C_{org}$ record

Sedimentary organic matter represents a mixture of biological materials. Regardless of compositional variation, its isotope signature is mostly governed by CO_2-fixing autotrophic organisms (Eigenbrode and Freeman, 2006; Freeman, 2001). These organisms typically produce organic matter with $\delta^{13}C_{org}$ values between -10‰ to -30‰ depending on their carbon fixation pathway (Fig. 3) (Preuß et al., 1989; Zerkle et al., 2005). On average the primary producers discriminate against ^{13}C by ~-20‰, thus in terrestrial environments where the main carbon source is atmospheric CO_2 (~-7‰ $\delta^{13}C$) the produced biomass carries a $\delta^{13}C_{org}$ signature of ~-27%. In aqueous settings carbon is sourced from DIC (0‰ $\delta^{13}C$) leading to sedimentary organic matter with ~-20% $\delta^{13}C_{org}$ (Meyers, 2014). Additionally to autotrophs, heterotrophs represent a significant fraction of sedimentary biomass but generate only small (up to ~2‰) isotope effects and are virtually indistinguishable from their carbon source (Freeman, 2001; Hayes, 1993; Hayes et al., 1999). Therefore, the relatively consistent $\delta^{13}C_{org}$ (-25 to -35‰) record throughout Earth's history is thought to reflect the antiquity of autotrophic carbon fixation metabolisms and fairly uniform biomass burial through geologic time (Hayes, 1983; Hayes and Waldbauer, 2006; Marais, 2001; Schidlowski, 2001; Zerkle et al., 2005).

Despite that, exceptions can occur in mixed substrate environments (e.g. cold seeps) where available carbon sources (e.g. CH_4 and other organic substrates) carry isotope signatures that are already fractionated. Maturation and oil-to-gas cracking of buried organic matter releases ^{13}C-depleted hydrocarbons that can migrate through fracture zones and seep on the seafloor providing a suite of substrates to the local environment (Clayton, 1991; Hayes, 1983; Lewan, 1983). In such settings complex microbial communities that are able to use and even switch between carbon sources can become established (Joye et al., 2004). For example, consumption of CH_4 that can have a $\delta^{13}C_{CH4}$ signature ranging from -20‰ to -50‰ from thermogenic or ~-50‰ to -90‰ from biogenic sources produces biomass significantly more depleted in ^{13}C (Fig. 3) (Sackett, 1978; Schoell, 1983; Whiticar, 1999). However, in seep environments the relative fluxes of methane and other organic substrates are highly variable. Fluctuations in substrate availability and type can induce competition for electron acceptors between metabolic pathways and ultimately impact the structure of the microbial community (Joye et al., 2004). Therefore, the preserved $\delta^{13}C_{org}$ values in ancient sediments are closely linked to the available carbon sources and the prevailing metabolisms operating in the local environment.

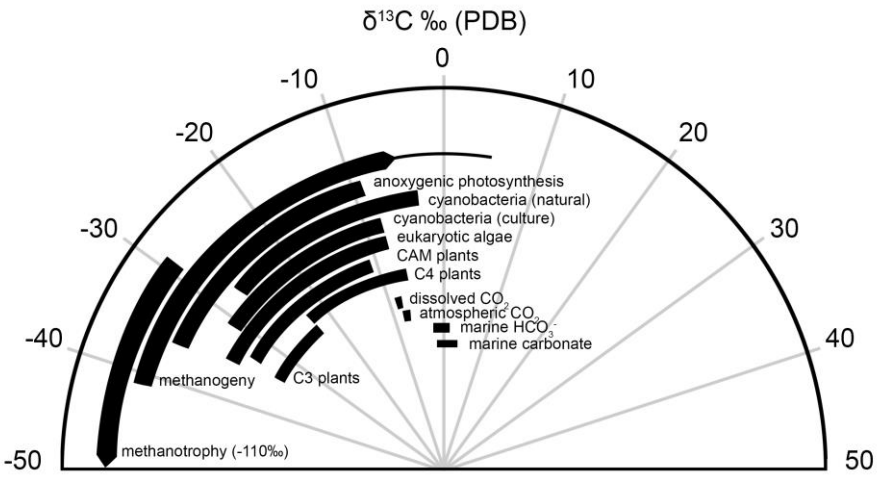

Figure 3. Range of $\delta^{13}C$ values of various organisms and inorganic carbon species in the environment (modified after Schidlowski, 2001).

Later in the burial history of sedimentary rocks the isotope composition of primary organic matter can be altered by metamorphic processes. In basins with high geothermal gradients ^{13}C-depleted hydrocarbons can be devolatilised leaving the residual organic matter enriched in ^{13}C. These isotope effects are generally small (< 3‰) and will exclusively shift the preserved $\delta^{13}C_{org}$ to more positive values (Clayton, 1991; Lewan, 1983). In general, however, low grade (greenschist) metamorphic alteration is unlikely to obscure signatures of biological processes recorded in the $\delta^{13}C$ values of ancient organic matter. Given that, localised oil and gas seepage can provide additional substrates to local environments, the presence of unusually ^{13}C-depleted biomass in the rock record does not necessarily reflect global changes in carbon cycling. Similarly, recycling of ^{13}C-depleted organic carbon can impact DIC in restricted and/or stratified environments and produce exceptionally depleted biomass without the need of methane. For example, organic matter with values as low as -45‰ $\delta^{13}C_{org}$ have been reported in a modern mountain lake and -34‰ $\delta^{13}C_{org}$ in a Norwegian fjord (Rau, 1978; van Breugel et al., 2005). Therefore, the principal way to discriminate between local and global mechanisms is to place the $\delta^{13}C_{org}$ isotope record into its depositional context.

3.2 Mechanisms governing the sulfur isotope system

Sulfur is intensely cycled through various but intrinsically linked biological and geological reservoirs that generate distinct isotope effects as sulfur mass is redistributed along different pathways. Over geological time SWS concentrations and isotope composition is governed by the balance between the relative fluxes of sulfur into and out of the ocean. Sulfur is mainly delivered into the global ocean via riverine runoff and volcanic outgassing and removed by burial of oxidized (e.g. gypsum,

anhydrite, barite or carbonate/phosphate associated sulfate) and reduced (e.g. pyrite, pyrrhotite, sphalerite, chalcopyrite, etc.) sulfur-bearing minerals or organic sulfur (Raven et al., 2018, 2016; Werne et al., 2004). Different formation pathways of these minerals, either biological (e.g. microbial reduction/oxidation/disproportionation) or abiogenic (e.g. evaporation, thermogenic sulfate reduction, photolysis) are manifested in their sulfur isotope composition (Fig. 4.) (Berner, 1964; Berner and Raiswell, 1983; Canfield, 2001; Johnston et al., 2007, 2005; Seal, 2006; Sim et al., 2011). Ultimately, if the oxidized and reduced sulfur species are transferred to the rock record, the difference between their isotopic composition can be used to trace variations in the redox structure of past oceans (Canfield, 2001; Canfield and Raiswell, 1999; Habicht et al., 2002; Halevy et al., 2012; Havig et al., 2017; Kah et al., 2004; Lowenstein et al., 2003; Luo et al., 2016; Planavsky et al., 2012; Wortmann and Paytan, 2012). As an example the scarcity of Ca-sulfate deposits prior to the GOE is considered as evidence for anoxic sulfate-limited environments. On the other hand, the appearance of sulfate pseudomorphs in Paleoproterozoic successions and the occurrence of thick ~2.0 Ga evaporite beds with abundant Ca-sulfates in Karelia, NW Russia, signifies a transitional change towards oxygenated surface conditions and build-up of the SWS reservoir (Blättler et al., 2018; Melezhik et al., 2005; Morozov et al., 2010). Such bedded evaporites provide the most direct information on SWS concentration and isotopic composition, but their preservation in the Deep Time geological record is scarce since evaporite minerals are easily dissolved. Consequently, most reconstructions of past ocean sulfate concentrations and isotope composition are based on pyrite records.

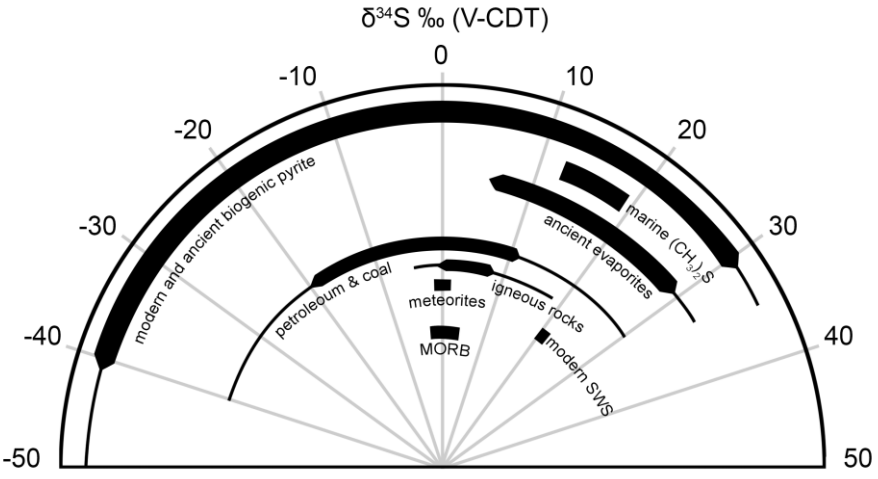

Figure 4. Range of $\delta^{34}S$ values for sulfides from various deposits and environments compared to modern seawater sulfate (SWS) and sulfate in ancient evaporites (modified after Seal, 2006).

Although, pyrites are relatively stable under post-depositional conditions, alteration under diagenetic or hydrothermal conditions and regional metamorphism can promote degradation, secondary mineralisation or overgrowth of earlier pyrite generations and contribute to sulfur isotope variations in pyrite records (Craig, 1993; Gregory et al., 2017; Meyer et al., 2017; Picard et al., 2018; Wagner and Boyce, 2006). Despite that, isotope effects (equilibrium and/or magnetic isotope effects) that associate with post-depositional processes can be identified and assessed by proper screening (petrographical analyses, Secondary Ion Mass Spectrometry (SIMS), REE patterns) of samples (Cui et al., 2018; Fischer et al., 2014; Gregory et al., 2017; Large et al., 2014; Meyer et al., 2017; Picard et al., 2018; Xiao et al., 2010).

Even before burial deep enough for late-stage processes to take effect, several factors can impact the sulfur isotope composition of sedimentary pyrites. This is most evident in Phanerozoic sulfate-rich marine environments where strictly anaerobic MSR operates within the shallow sediments and can produce even under steady-state conditions sulfides with $\delta^{34}S$ and $\Delta^{33}S$ signatures predicted for closed-system sulfur cycling (Aller et al., 2010, 2008; Berner, 1964; Bradley et al., 2016; Fike et al., 2015; Jørgensen et al., 2004; Rees et al., 1978; Ries et al., 2009; Sim et al., 2011; Zaback et al., 1993). Based on experimental studies the maximum fractionation imparted by MSR between sulfate and sulfide is 70‰ (Bradley et al., 2016; Canfield et al., 2010; Canfield and Teske, 1996; Sim et al., 2011). However, in sedimentary environments the full magnitude of microbial fractionations is seldom expressed. Intermediate fractionations between 0‰–70‰ result from variations in the type of organisms and their metabolic rates that mainly depend on temperature, available substrates, sulfate concentrations and ultimately sedimentary processes (e.g. sedimentation rates, porosity, permeability, reworking of sediments). Therefore, limited exchange between pore space and seawater can develop for a variety of reasons, e.g. situations in which sulfate consumption exceeds its replenishment due to rapid MSR or settings with fast sedimentation rates that disconnect pore space from the water column. Subsequently, closed-system and Rayleigh distillation effects attenuate biological fractionations and the produced sulfide $\delta^{34}S$ composition will approximate or even exceed that of SWS (Aller et al., 2010; Berner, 1964; Fike et al., 2015; Goldhaber and Kaplan, 1975; Johnston et al., 2007; Pasquier et al., 2017; Ries et al., 2009; Zaback et al., 1993). The final isotopic composition of pyrite will also depend on iron availability. If reactive iron is limiting only the first formed ^{34}S-depleted sulfide is scavenged and secreted. Such pyrite would preserve $\delta^{34}S$ values which could be misinterpreted as signs for open-system sulfur cycling (Zaback et al., 1993).

Further, if pore water sulfide is not re-oxidized or precipitated as Fe-sulfide minerals, sulfidic conditions can develop within the early-diagenetic environment or even in the water column (Brüchert, 2004; Dale et al., 2009; Meyer and Kump, 2008).

It has been proposed that the link between pyrite isotope composition and SWS concentrations is most straightforward when pyrites precipitate directly from an euxinic water column (Canfield et al., 2010; Lyons, 1997; Scott et al., 2014). In this case MSR is assumed to operate in the water column where rate limitation by sulfate transport is less likely to affect biological isotope fractionations. Thus, in sulfate replete conditions the produced sulfide is expected to reflect stratigraphically consistent ^{34}S-depletions (Bradley et al., 2016; Habicht et al., 2002; Werne et al., 2003). If, though, sulfate becomes limiting then sulfide is expected to display progressive ^{34}S-enricments. It has further been proposed that under very low sulfate concentrations sulfate reducers stop discriminating against ^{34}S and the isotopic composition of produced sulfide approaches that of the original sulfate (Habicht et al., 2002). This relationship between SWS concentrations and the magnitude of biological fractionations could be utilized in paleoenvironmental reconstructions; however, there are several caveats. Firstly, sulfate reducers have been observed to produce large isotope effects at extremely low sulfate concentrations (<0.01 mM) (Crowe et al., 2014). Secondly, this requires that euxinia formed in an openly connected basin that captures global fluctuations in SWS levels. Modern sulfidic-waters typically develop in confined settings with restricted circulation (e.g. fjords, the Black Sea, the Baltic Basin) where eustatic fluctuations and/or seasonal stratification can induce localised Rayleigh distillation effects and pyrites with ^{34}S-enriced signatures (Gomes and Hurtgen, 2013; Gomes and Johnston, 2017; Jørgensen, 1979; Jørgensen et al., 2004; Meyer and Kump, 2008). Sulfidic bottom waters have also been observed in upwelling zones on the coast of Namibia (Brüchert, 2004; Dale et al., 2009). Regardless of an open shelf setting in Namibia, the distribution and development of sulfidic waters is laterally and temporally variable (Brüchert, 2004; Dale et al., 2009). Thus, even in basins that are openly connected to the ocean, the pyrite isotope composition could be strongly influenced by spatial-temporal differences in sedimentation, geochemical gradients, microbial communities and seasonal variability and may or may not reflect fluctuations in ocean chemistry.

To summarise, sedimentary pyrites can form via various and complex pathways and information about past sulfur cycling and ocean redox needs to be extracted by careful evaluation of the sulfur isotope record in the context of basinal history, depositional framework and microbial processes.

4. The Paleoproterozoic Onega Basin

Understanding a basin's evolution is of key importance as it governs nutrient fluxes and biogeochemical element cycling within the local environment, which in turn determine the geochemical signatures preserved in the rock record. The Paleoproterozoic Onega Basin, located on the eastern flank of the Fennoscandian shield (NW Russia), provides an opportunity to investigate the interplay of regional processes against the backdrop of global forcing's throughout its depositional history (Fig. 5). The Onega Basin rock succession (Fig. 6) encompasses both the end of the LJE and the succeeding "Shunga Event" (Kump, 2011; Melezhik et al., 2015, 1999; Strauss et al., 2013). The LJE is recorded in the carbonate rocks of the Tulomozero Formation and the "Shunga Event" is represented by the organic-rich rocks of the Zaonega Formation (Melezhik and Hanski, 2013). The Onega Basin succession has been mildly deformed into a series of open folds cut by high-angle faults as it underwent greenschist facies metamorphism during the 1.89–1.79 Ga Svecofennian orogeny (Ojakangas et al., 2001; Stepanova et al., 2014). Thus, the distribution of recently recovered cores across the Onega Basin provides the means to extract information about spatial and temporal changes throughout its evolution.

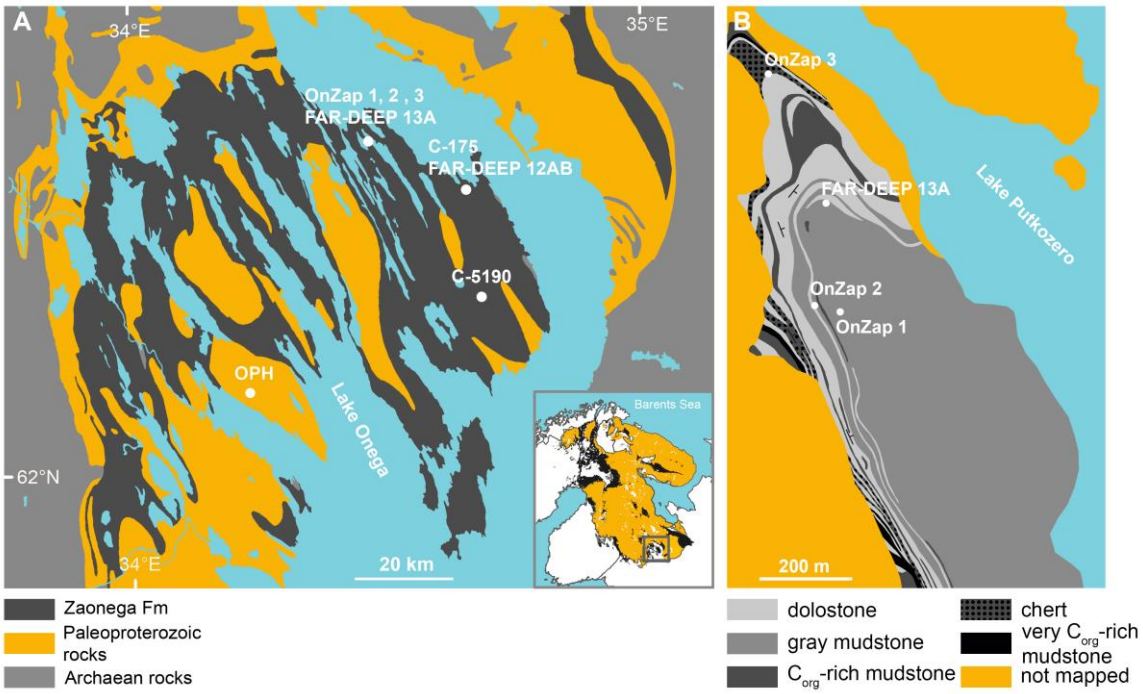

Figure 5. A. Generalised geological map of the Onega Basin, NW Russia, and drill core locations (white circles). Inset map shows location of the Onega Basin and Paleoproterozoic rocks (black) across the eastern Fennoscandian Shield. B. Simplified geological map of the upper Zaonega Formation near the village of Shunga where cores OnZap 1-3 and FARDEEP 13A were drilled (after Melezhik et al., 2013a).

4.1 General geological evolution of the basin

It has been proposed that the Onega Basin accumulated in an intraplate rift or active continental margin depositional setting (Črne et al., 2014; Melezhik et al., 2015) that was established after the opening of the Paleoproterozoic Kola Ocean and Svecofennian Sea (Lahtinen et al., 2008; Melezhik et al., 1999). Initial stages of rifting in Fennoscandia and the earliest deposition in the Onega Basin began prior to 2.5 Ga and was followed by the emplacement of voluminous continental flood basalts at ~2.5–2.4 Ga. The subsequent period between the onset of the Huronian glaciations at ~2.4 Ga and advanced rifting at ~2.2 Ga is characterised by uplift and deep weathering of the flood basalts and minimal igneous activity (Marmo and Ojakangas, 1984; Melezhik et al., 2015; Melezhik and Hanski, 2013). By ~2.2–2.0 Ga, deposition began in a restricted marine embayment characterised by sabkha-coastal plain and shallow marine stromatolite reef environments of the Tulomozero Formation (Blättler et al., 2018; Melezhik and Hanski, 2013; Morozov et al., 2010). As accumulation continued the basin gradually deepened and the initial phase of evaporite precipitation was replaced by shallow marine stromatolitic carbonates in the upper part of the Formation (Fig. 6).

Contrastingly to the overlying successions, the lack of igneous bodies (except one sill) in the Tulomozero Formation implies deposition at a period of relative magmatic quiescence. Continued subsidence generated the accommodation space for deposition of the deeper-water organic-rich siliciclastic and carbonate rocks of the Zaonega Formation. At that time a more stable connection with the global ocean and a deep-water shelf-slope-basin setting was established (Črne et al., 2014; Melezhik et al., 2015). Numerous thick packages of mafic lava flows and co-magmatic intrusions (some of which show peperite contacts) alternating with the sedimentary units indicate that sedimentation was accompanied by extensive syn-depositional magmatism, volcanism and tectonic activity (Črne et al., 2013a, 2013b; Melezhik et al., 1999; Strauss et al., 2013). The Suisari Formation, which overlies the Zaonega Formation, is mainly composed of sub-aqueously extruded basalts and volcaniclastic rocks. These are interpreted as one of the oldest continental flood basalt provinces (Melezhik et al., 2013b; Puchtel et al., 1999). Above these, the rhythmically-bedded siliciclastic rocks of the Kondopoga Formation constitute the youngest part of the Paleoproterozoic succession (Galdobina, 1987; Melezhik et al., 2013b).

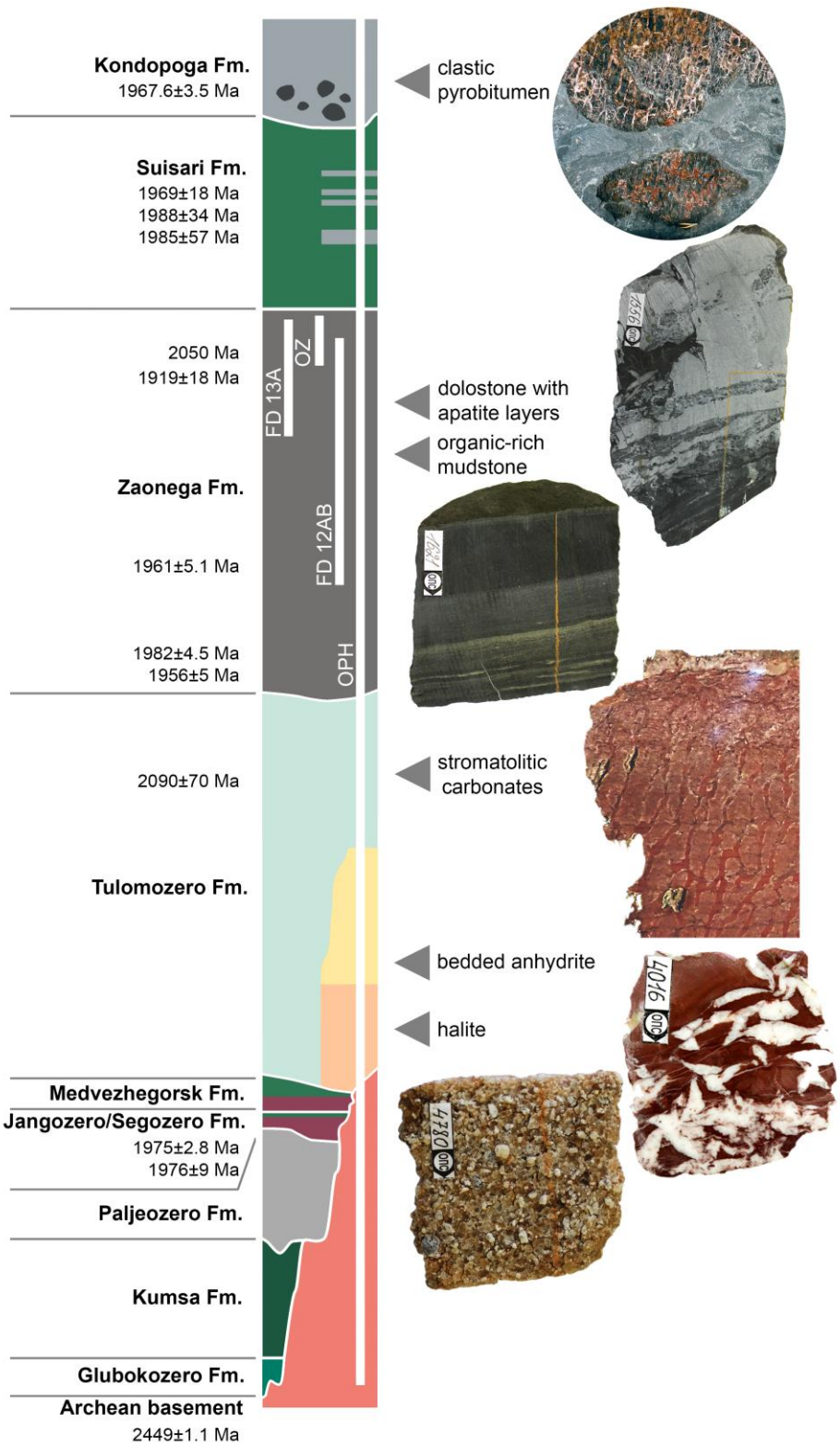

Figure 6. Generalised lithostratigraphic column of the Onega Basin with positions of the FAR-DEEP (FD), OnZap (OZ) and Onega Parametric Hole (OPH) cores. Different colours keyed to lithology: pink – granite, green – mafic magmatic rocks, grey – mudstones, purple – quartzite, orange – halite, yellow – bedded anhydrite and light blue – carbonate rocks (modified after (Melezhik et al., 2015). Radiometric ages are discussed in text. Images on the right show characteristic rock types.

4.2 The Zaonega Formation

The Zaonega Formation has been the focus of much study due to its role in recording environmental change during the aftermath of the LJE. It forms a ~1.5 km thick volcano-sedimentary succession that mainly consists of alternating organic-rich siliciclastic and carbonate rocks interlayered with abundant mafic intrusions and lava flows. Finely laminated mudstones dominate in the lower part of the formation whereas the upper part is characterised by alteration of mudstones and massive to faintly laminated carbonate rocks (Črne et al., 2014, 2013a, 2013b; Galdobina, 1987; Melezhik et al., 2015). Deposition in the otherwise low-energy environments was occasionally disrupted by the emplacement of coarser-grained sediment-gravity flow and turbidity-current deposits, which are common in the lower part of the succession (Črne et al., 2014, 2013a, 2013b; Melezhik et al., 2015). Thus, deep-water facies sediments that accumulated below storm-wave base (>100–200 m) typify most of the Zaonega Formation, whereas marly carbonates displaying faint lamination and cross bedding with mud drapes imply shallowing in the uppermost part of the Formation (Paiste et al., paper 1).

The middle part of the Zaonega Formation has been associated with the formation of the world's oldest petrified oilfield (Melezhik et al., 2013a, 1999). It is characterised by high organic carbon content (up to 40% in mudstones and 90% in pyrobitumen-filled veins) and the occurrence of thick intervals of massive, organic-rich rocks (popularly termed "shungites"). Peperitic contacts of mafic sills are evidence for syn-depositional magmatism and the close association of pyrobitumen-rich intervals with magmatic bodies indicate that locally generated high heat gradients were responsible for inducing hydrocarbon generation and oil migration. This resulted in the impregnation of the sedimentary rocks by pyrobitumen contemporaneously or shortly after deposition (Črne et al., 2013a, 2013b; Qu et al., 2012). The occurrence of such organic-rich rocks in the upper part of the Zaonega Formation is well documented in several outcrops and drill cores across the Onega Basin (Filippov and Yesipko, 2016; Galdobina, 1987; Melezhik et al., 2013a). Moreover, the organic matter within this interval is typified by $\delta^{13}C_{org}$ values <-30‰ (Kump, 2011; Lepland et al., 2014; Qu et al., 2012). This distinct isotope trend of the organic matter ($\delta^{13}C_{org}$ <-30‰) occurs in several sections across the basin and serves as a chemostratigraphical marker horizon for intra-basin correlations (Filippov and Yesipko, 2016; Melezhik et al., 2013a).

4.2.1 Age of the Zaonega Formation

The long-held view and postulated age models for the Onega Basin, including inter-craton correlations with the ~2.1 Ga Francevillian Group and the postulated synchronicity of the Shunga-Francevillian Event (Canfield et al., 2013; Kump, 2011; Ossa Ossa et al., 2018) have been challenged lately. Prior to the most recent age determinations, the maximum age of the Zaonega Formation was constrained by the inferred termination of the LJE at ~2.06 Ga in Fennoscandia (Karhu, 1993; Karhu and Holland, 1996). Initially, this constraint was based on correlations to other LJE-bearing rocks (Karhu, 1993; Karhu and Holland, 1996) and such a correlation is supported by radiometric age determinations on post-LJE bearing rocks in the eastern Fennoscandian Shield: 2058 ± 2 Ma (Melezhik et al., 2007) and 2056.6 ± 0.8 Ma (A.P. Martin et al., 2013) for the Kolosjoki Sedimentary Formation in the Pechenga Greenstone Belt, 2055.5 ± 2.3 Ma for the Il'mozero Sedimentary Formation in the Imandra-Varzuga Greenstone Belt (Martin et al., 2015), and a 2050 ± 8 Ma age on felsic volcanic rocks in the Peräphoja Belt, Finland (Perttunen and Vaasjoki, 2001). Further, the Tulomozero Formation has a carbonate whole rock Pb-Pb age of 2090 ± 70 Ma (Ovchinnikova et al., 2007) and a ~2050 Ma Re-Os age on organic-rich siltstone from the Zaonega Formation has been reported in a conference abstract by Hannah et al. (2008). Given the convergence of these ages, the notion of a synchronous termination of the LJE in Fennoscandia at around 2.06 Ga has been widely used to constrain the maximum age of the Zaonega Formation.

More recent geochronology from NW Russia, however, has revealed radiometric ages that dispute previous correlations and the inference that the termination of the LJE was a globally synchrounous event (e.g. Martin et al., 2013a, 2013b, 2015). For example, zircon U-Pb ages of 1922.8 ±1.6 and 1919.2 ±1.3 Ma from the Pilgujärvi Sedimentary Formation render the previous correlations with the Zaonega Formation equivocal. Additionally, dykes cross-cutting the Zaonega Formation have yielded ages of 1919 ± 18 Ma (Priyatkina et al., 2014), 1956 ± 5 Ma (Stepanova et al., 2014) and 1961.6 ± 5.1 Ma (Martin et al., 2015). Ages between 1969 ± 18 Ma (Puchtel et al., 1998) and 1988 ± 34 Ma (Puchtel et al., 1999) have been obtained from several gabbro sills in the overlying Suisari Formation. Further, the most recent high-precision U-Pb zircon ages indicate deposition of the Zaonega Formation between 1975.3 ± 2.8 and 1967.6 ± 3.5 Ma (Martin et al., 2015). The former age is for a putative lava flow of the Jangozero Formation below the base of the LJE-bearing Tulomozero Formation (which overlaps within error of a previously reported U-Pb age on the same unit of 1976 ±9 Ma; Puchtel et al., 1998) and the latter is detrital zircon age of 1967.6 ± 3.5 Ma from the

Kondopoga Formation. Lastly, zircon derived from a felsic tuff in the lower Zaonega Formation has yielded an age of 1982.0 ±4.5 Ma (Martin et al., 2015). Combined these ages advocate for earlier deposition of the Zaonega Formation, between ~1985 and 1965 Ma, but do require additional scrutiny and confirmation. Until then, in the context of this thesis ~1.98 Ga will be used as the timing of accumulation of the Zaonega Formation.

5. Materials

Within the last decade several drilling projects targeted the Zaonega Formation with the specific focus on organic- and phosphorous-rich intervals; these include the International Continental Drilling Program's Fennoscandia Arctic Russia-Deep Early Earth Project (FAR-DEEP) in 2007, the Onega Parametric Hole (OPH) drilled between 2007–2009 and the OnZap drilling that took place in 2012. As a result, an outstanding set of drill cores intersecting the entire volcano-sedimentary succession of the Onega Basin has been recovered and made available for scientific investigations. This research is based on geochemical and lithological studies of five drill cores that recovered the Zaonega Formation strata: OnZap1 and OnZap3, OPH, FAR-DEEP 12AB and 13A. Additional sedimentological and petrographical information was derived from the OnZap2 core drilled ~70 m from the site of OnZap1. The two 60 m long OnZap1 (62.5870 N, 34.9310 E) and OnZap3 (62.5920 N, 34.9280 E) cores were drilled ~500 m apart near the village of Shunga in the north-western part of the Onega Basin. These two cores intersect ~102 m of stratigraphy from the upper part of the Zaonega Formation. The middle and upper part of the Zaonega Formation is represented by the ~240 m long FAR-DEEP 13A core (62.5891 N, 34.9273 E) located between the OnZap1 and 3 sites, and the ~504 m long FAR-DEEP 12AB core (62.4947 N, 35.2887 E) located near Tolvuja ~25 km south-east from the village of Shunga (Črne et al., 2013a, 2013b). The OPH core was drilled in the southeastern part of the Onega Basin and intersects ~3000 m of Paleoproterozoic rocks and 600 m of the Archean basement (Krupenik et al., 2011; Morozov et al., 2010).

Lithological descriptions of the OPH and FAR-DEEP cores are available in Krupenik et al. (2011) and Črne et al. (2013a, b), whereas lithological logging of the OnZap cores was performed as part of this PhD project and reported in Paiste et al. (paper 1). From the latter, a total of 127 samples was obtained at roughly 1 metre intervals spanning the lengths of the OnZap cores. Less dense sampling was performed on the FAR-DEEP 12AB (29 samples) and FAR-DEEP 13A (18 samples) cores and the OPH (120 samples) core. Sampling of the OPH core focused on the 2115–525 m depth interval that comprises the Zaonega Formation and most of the overlying Suisari Formation. In this study I have also taken advantage of a previously published geochemical data set from the C-175 core (220 m long) and C-5190 core (842 m long; Melezhik et al., 2013b; Scott et al., 2014). These two cores were drilled 500 m to the northwest and ~15 km south of the FAR-DEEP 12AB location, respectively.

5.1 Correlation of studied sections

In order to integrate the different data sets a firm stratigraphic framework has to be established. Lateral facies differences and varied igneous bodies within the lower part of the Zaonega Formation complicate making correlations within the basin. In contrast, cores from the upper part of the Zaonega Formation in all studied locations display broadly similar lithologies (Fig. 7), including a prominent dolomite unit that can be identified readily as a basin-wide lithostratigraphic marker (Črne et al., 2014, 2013a, 2013b; Melezhik et al., 2015; Qu et al., 2012). This unit consists of massive, nearly pure, dolomite beds intersected by black chert veins that are commonly bed-parallel following thin mudstone interlayers within dolostone. The chert veins can be several meters thick and their frequency varies among the cores but they have a distinctive massive structure and contain relicts of the altered dolostone. The base of the dolomite unit is always defined by massive grey dolomite containing infrequent intervals of black up to 1 cm thick, discontinuous apatite layers (Fig. 7) (Joosu et al., 2015; Lepland et al., 2014). It's base sits sharply on underlying very organic-, P- and trace metal-rich mudstone which can be identified at 53 m depth in the OnZap1 and at 10.8 m depth in OnZap3 core. This has been the basis for correlation of the two OnZap cores, that combined provide a 102 m thick composite record, henceforth referred to as the OnZap succession. The OnZap succession has been further subdivided into three Units A, B and C, which are discussed in more detail in Paiste et al. (paper 1). The base of the dolomite unit is also recognised at 9.25 m depth in the FAR-DEEP 12AB, at 43.1 m depth in the FAR-DEEP 13A and 1112 m depth in the OPH core. Additionally, the rocks in the upper Zaonega Formation are marked by ^{13}C-depleted biomass ($\delta^{13}C_{org}$ <-30‰), a pattern that has been recognised by numerous workers across the Onega Basin (Filippov and Yesipko, 2016; Kump, 2011; Lepland et al., 2014; Melezhik and Hanski, 2013; Qu et al., 2012). These combined characteristics are used to subdivide the Zaonega Formation into three Members A, B and C (Paiste et al., paper 2, 3). Using the OPH core as a reference section: Member A is at 2115–1330 m depth in the OPH core and 504–234 m in FAR-DEEP 12AB core; Member B occurs at 1330–1080 m depth in the OPH core and 234–1.6 m, 240–14 m and 102–21 m depths in FAR-DEEP 12AB, FAR-DEEP 13A and the OnZap succession, respectively; Member C defines the 1080–528 m depth interval in the OPH core (the upper part of the Zaonega Formation and the lower part of the overlaying Suisari Formation), 14–1.6 m in FAR-DEEP 13A and 21–1.7 m in the OnZap succession (Figs. 7, 8).

Two other cores have figured prominently in study of the Zaonega Formation, cores C-5190 and C-175. Although no lithological descriptions were provided, Scott et al. (2014) nevertheless assumed that these cores were stacked one on the other i.e. defining a successive stratigraphy. Further, available data show that the C-5190 core evidently corresponds to a stratigraphic interval that is below the dolomite unit. However, C-175 exhibits ^{13}C-depleted biomass throughout its entirety and in C-5190 such biomass occurs in the 184-16 m depth interval. Moreover, these $\delta^{13}C_{org}$ values match well those in the upper part of FAR-DEEP 12AB, with both sets of cores exhibiting an up-section $\delta^{13}C_{org}$ shift from -25‰ to values between -30‰ and -40‰. Given such compatibilities and similarities, correlation of cores C-5190 and C-175 with the upper Zaonega Formation strata is the most objective conclusion to make. This indicates that the former two cores partly overlap and, based on the $\delta^{13}C_{org}$ profiles, the depth interval between 296–184 m in C-5190 core can be assigned to Member A and those in 184–16 m in C-5190 and 219–17 m in C-175 core to Member B (Fig. 8). This is in good agreement with previous correlations of the C-5190 and FAR-DEEP 12AB cores by Melezhik et al. (2013b). Thus, until the establishment of firmer stratigraphic controls of the C-175 and C-5190 cores, these correlations based on $\delta^{13}C_{org}$ values can be considered reasonable and testable.

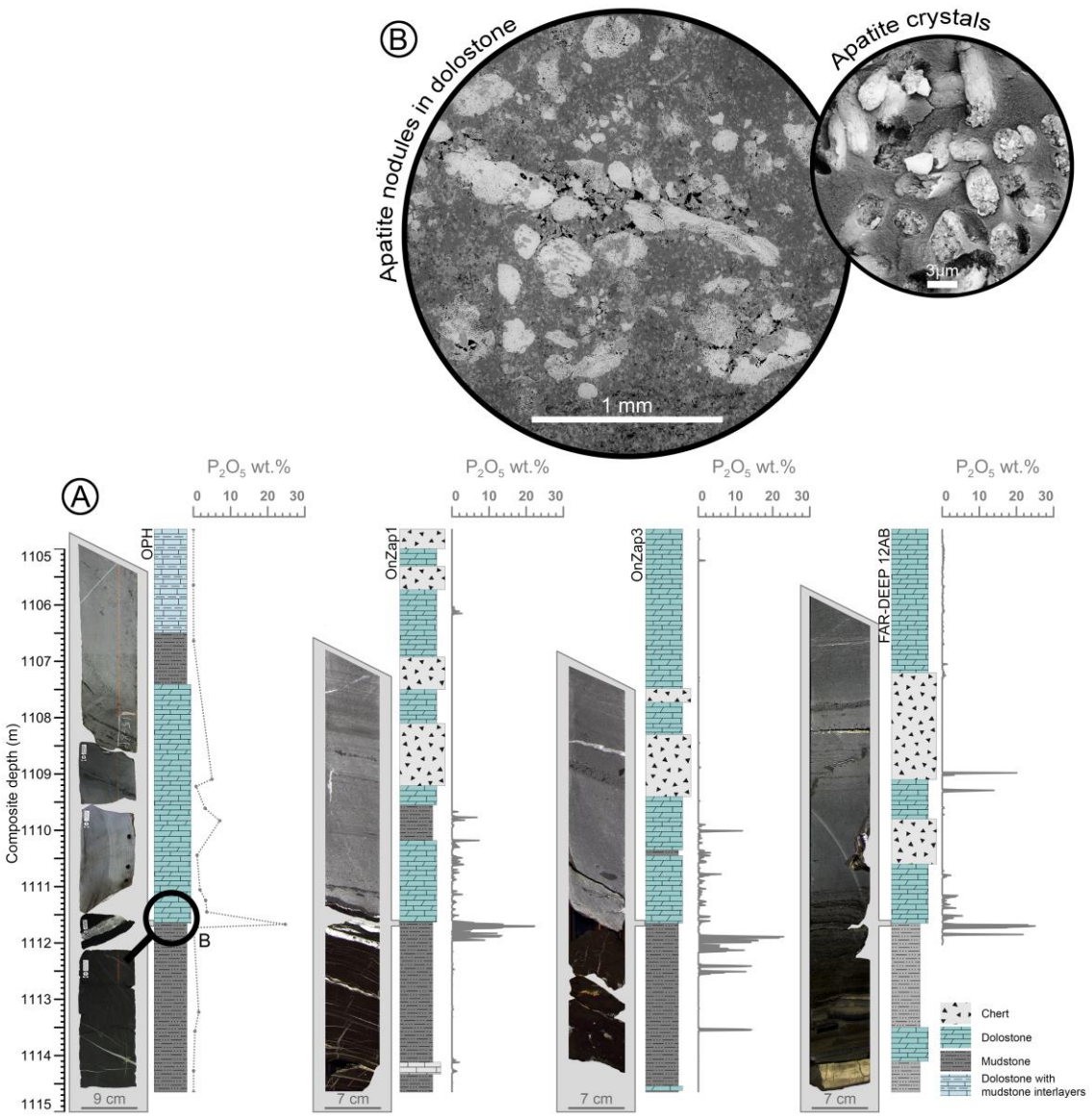

Figure 7. A. Lithological profiles of the of the prominent dolostone unit used for correlating the OPH, OnZap 1 and 3, and FAR-DEEP 12AB cores (each 10 m thick). Core photos from the contact with underlying organic-rich mudstone, show the occurrence of mm- to cm-thick discontinuous black apatite layers in the lower part of the massive dolostone unit. Phosphate (expressed as P_2O_5) concentration logs displayed to the right of the profiles represent semi-quantitative determinations undertaken by XRF logging directly on OnZap 1 and 3 and FAR-DEEP 12AB cores; data for the OPH core are from bulk XRF quantitative determinations on extracted subsamples. Note the high P_2O_5 concentration immediately below the dolostone unit. B. SEM-BSE image of apatite nodules in dolostone (left image) and close-up of cylindrical apatite crystals in apatite nodules within mudstone (right image).

6. Methods

6.1 Petrographical, mineralogical and major element analyses

The petrographic characterisation of thin sections was performed by means of scanning electron microscope (SEM) analysis using a ZEISS EVO MA15 SEM at the University of Tartu. The SEM images were captured in backscattered electron (BSE) mode. To complement the SEM imaging, chemical characterisation by point analyses and elemental mapping of the samples was performed using an Oxford AZTEC-MAX energy-dispersive spectroscopy (EDS).

Major element composition was determined by Bureau Veritas Minerals, Vancouver, Canada by inductively coupled plasma optical emission spectroscopy (ICP-OES). Powdered samples were fused at 950 °C with lithium metaborate flux and the fusion beads were digested with a combination of hydrofluoric and perchloric acids prior to analysis. Loss on ignition data were obtained from heating samples in a furnace at 950 °C for 1 h. Average percent relative standard deviation (average RSD%) was less than 5% for all elements. The mineralogical composition of whole rock samples was determined on unoriented powdered samples using a Bruker D8 Advance X-ray diffractometer using Cu *Kα* radiation and LynxEye positive sensitive detector in 2–70° 2-Theta range at the University of Tartu. The obtained diffractograms were interpreted and modelled with the Rietveld algorithm-based program Topaz and/or Siroquant. The content of crystalline phases determined by XRD analysis were normalised to account for X-ray amorphous organic carbon using the TOC abundance data determined from the same samples.

6.2 Sulfur and carbon content

The concentration of total carbon (TC), total organic carbon (TOC) and total sulfur (TS) were quantified by using 100 mg of powdered samples with the Leco SC-444 analyser at the Geological Survey of Norway. The TOC content was determined on acid-treated (10% HCl) material. Detection limits for TS, TC and TOC were 0.02 wt.%, 0.06 wt.% and 0.1 wt.%, respectively, and the precision was <2.5% for TC, and <10% for TS and TOC.

6.3 Sulfur isotope analyses

Powdered samples were subjected to a two-step sulfur extraction procedure (Canfield et al., 1986). In this sequential extraction method sulfur is liberated as H_2S first from acid volatile sulfur (AVS; monosulfides such as pyrrhotite, sphalerite, mackinawite or greigite) via a 6 M HCl distillation, and

pyrite is released via hot chromium(II) chloride distillation (CRS). The resulting H_2S was converted into Ag_2S upon addition of 0.1 M $AgNO_3$.The precipitate was then cleaned using 1M $NH_4(OH)$ and rinsed to neutrality using MilliQ water (Oduro et al., 2013).

The sulfur isotope analyses were conducted at McGill University under supervision of Dr. T. H. Bui. The Ag_2S samples were reacted overnight with excess fluorine gas in Ni bombs at 250 °C to produce SF_6. The SF_6 was first purified cryogenically and then via gas chromatography. The sulfur isotope composition of purified SF_6 was measured by dual-inlet gas-source mass spectrometry monitoring ion beams at m/e of 127, 128, 129, and 131 using a Thermo Finnigan MAT 253 gas source mass spectrometer. Sample reproducibility, as determined by replicate analyses of the in-house standard MSS-1, was generally better than 0.1‰ for $\delta^{34}S$ values, 0.015‰ for $\Delta^{33}S$ and 0.2‰ for $\Delta^{36}S$.

6.4 Organic carbon isotope analyses

Between 0.2 to 2 g of sample powders were reacted with 10% hydrochloric acid at room temperature in centrifuge tubes for 24 h. The decarbonation step was then repeated until no further reaction was observed and the remaining residues were rinsed to neutrality using deionised water and dried at 45 °C. Aliquots of dry decarbonated residue (0.2 mg) were then weighed into tin capsules and the organic carbon isotopes ($\delta^{13}C_{org}$) were determined by flash combustion using an Elemental Analyser Continuous Flow Isotope Ratio Mass Spectrometer (EA-CF-IRMS: ThermoScientific Delta V Plus with Costech EA) at the NERC Life Sciences Mass Spectrometry Facility at the Scottish Universities Environmental Research Centre. Accuracy and precision were monitored via replicate analyses of the international standard USGS40 L-glutamic acid ($\delta^{13}C$= –26.39 ± 0.04‰ V-PDB) which yielded the $\delta^{13}C$ value of –26.19 ± 0.04‰. Decarbonation and preparation of OnZap 1 core samples was part of F. McLean's Bachelors Thesis (McLean, 2015).

6.5 Iron partitioning in mineral phases

6.5.1 Sequential extraction of iron

To complement the sulfur isotope analyses the sequential iron extraction technique, commonly referred to as "Fe speciation", was performed according to (Poulton and Canfield, 2005). In short, at the first extraction step carbonate-associated iron was liberated by reacting 100 mg of homogenised sample powder with 10 mL of sodium acetate solution for 48 h at 50 °C. The resulting supernatant was separated from the solid residue, whereas the latter was treated with 10 mL sodium dithionite solution for 2 h at room temperature for ferric oxide extraction. Again, the

supernatant was separated and the remaining sample was treated with 10 mL ammonium oxalate solution for 10 h at room temperature to mobilise magnetite iron. Iron contents of the sequential extracts were determined using a Thermo Scientific iCAP 6300 inductively coupled plasma optical emission (ICP-OES) spectrometer at the University of St Andrews via external calibration. Synthetic, matrix matched 1 ppm Fe standards (n > 5 in each run) reproduced better than 2% (1σ relative standard deviation; RSD) and replicate extractions of PACS-2 (n= 5) reproduced better than 5% (1σ RSD) for all Fe pools. The Fe speciation method was only applied on samples from the OnZap succession. Extractions of OnZap1 core samples and analyses were performed by N. Patel as part of his Bachelors Thesis (Patel, 2015).

6.5.2 X-ray diffraction based iron distribution

In order to test the utility of the conventional Fe speciation method on the OnZap succession, I used a combination of XRD and SEM-EDS analyses to estimate Fe partitioning in the main Fe-bearing minerals split into carbonates (Fe_{Carb} = iron-rich dolomite to ankerite solid-solution phase and siderite), sulfides (Fe_{PY} = pyrite + pyrrhotite) and silicates (Fe_{SIL}). The main advantage of XRD analyses is that quantifications are not influenced by incomplete dissolution, however, the final results depend on the analysers experience and knowledge of the specific samples. Thus, petrographic investigations are necessary to avoid misinterpretations. Overall, the XRD and wet-chemical extraction approaches on iron distribution should display good agreement as the mineral phases from which iron concentrations are determined are the same. Iron-oxides and iron-oxyhydroxides were below the XRD quantification limit (< 0.3 wt.%) in all examined samples. The silicate iron (Fe_{SIL}) pool is defined as the sum of Fe in phyllosilicates (K-mica, Fe/Mg-mica and chlorite), the only Fe-carrying silicate phases identified in samples.

Owing to the variable Fe contents of the micas and carbonates, multiple measurements by SEM-EDS were made from several representative crystals throughout the OnZap succession to calculate an average iron content of the individual phases. The average iron content of muscovite-type K-mica was found to be 3.2 wt.% Fe and chlorite was found to be 1.6 wt.% Fe. Multiple analyses demonstrated that these values were constant throughout all examined samples. The iron content of Fe/Mg-mica phases was found to be variable throughout the succession, with low iron contents (1.4 wt.%) typifying the lower part and high iron (20.8 wt.%) mica dominating in the upper part. Iron-rich carbonate phases in the dolomite to ankerite solid-solution series contained up to 10 wt.% iron and were confined to the upper part of the OnZap succession. Siderite, with a stoichiometric

Fe abundance, is present in few samples near the top of the section. Total XRD-derived iron ($Fe_{T\text{-}XRD}$) abundances were calculated as the sum of Fe_{Carb}, Fe_{PY} and Fe_{SIL}. Generally, the calculated $Fe_{T\text{-}XRD}$ and total Fe ($Fe_{T\text{-}OES}$) determined by ICP-OES after fusion and dissolution displayed a good fit ($R^2 = 0.92$). There are a few samples, typically the ones that are very low in iron, where $Fe_{T\text{-}XRD}$ diverged more than 20% from the $Fe_{T\text{-}OES}$. This divergence is likely due to the higher quantification limit (~0.3–0.5 wt.%) of XRD compared to ICP-OES. These samples were excluded from iron distribution assessments as recommended by previous studies (Clarkson et al., 2014).

7. Results

The bulk geochemical and petrographic analyses were used to better characterise the physical and chemical conditions under which biogeochemical sulfur and organic carbon cycling occurred during accumulation of the Zaonega Formation. In this thesis I only report results obtained from sulfur and organic carbon isotope analyses combined with TS and TOC concentrations (Fig. 8) and distribution of iron in mineral phases (Fig. 9). More detailed lithological descriptions, petrographical observations, major element and mineral distribution patterns are presented in the papers accompanying this thesis (Paiste et al., papers 1, 2, 3).

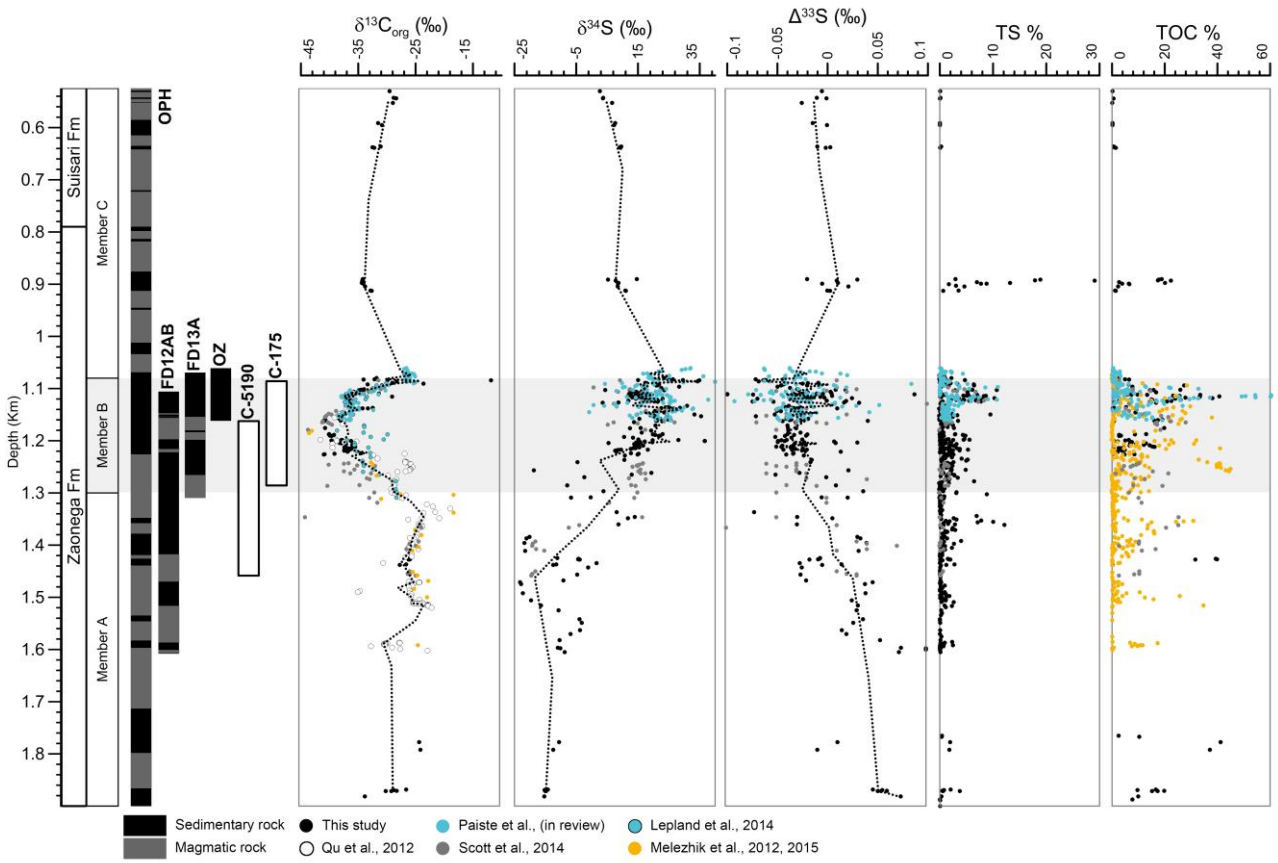

Figure 8. Compilation of $\delta^{13}C_{org}$, $\delta^{34}S$, $\Delta^{33}S$, TS and TOC profiles for the studied cores from the Zaonega Formation (includes data from this study; Lepland et al., 2014; Melezhik et al., 2013b, 2015; Qu et al., 2012; Scott et al., 2014). Using the OPH core as a reference, the Zaonega Formation and the lower part of the Suisari Formation have been subdivided into Members A, B and C. Black and grey bars on the core profiles show sedimentary and igneous intervals, respectively. C-5190 and C-175 cores have no bars since the lithological character of these cores has not been provided in the literature.

7.1 Organic carbon and sulfur isotope profiles

Member B of the Zaonega Formation houses a pronounced negative $\delta^{13}C_{org}$ excursion, with values as low as -42‰ (Fig. 8), whereas Members A and C are characterised by relatively invariant $\delta^{13}C_{org}$ of -26 ± 3‰ and -29 ± 4‰, respectively. Sulfur isotopes in Member A feature negative $\delta^{34}S$ and positive $\Delta^{33}S$, ~-11.3 ± 10.5‰ and ~0.03 ± 0.04‰, respectively, and shift to positive $\delta^{34}S$ and negative $\Delta^{33}S$, 18.3 ± 7.8‰ and -0.03‰ ± 0.03, respectively, in Member B. There are several pronounced positive spikes in $\delta^{34}S$, up to 44‰, and parallel negative spikes in $\Delta^{33}S$, down to -0.12‰. Contrastingly, upwards through Member C, $\delta^{34}S$ exhibits a declining trend to ~+3‰ and a positive trend to ~0‰ in $\Delta^{33}S$. Members A and C have relatively low TOC and TS abundances (mostly between 3–13 wt.% and 1–3 wt.%, respectively) and Member B has the highest enrichments (up to 65 wt.% TOC and 11 wt.% TS).

7.2 Iron speciation results

The iron speciation results for the OnZap succession are illustrated in Figure 9. Fe_{HR} is the biogeochemically highly reactive iron pool comprising a sum of Fe_{Carb}, Fe_{Ox}, Fe_{Mag}, Fe_{PY}. Fe_{Carb} represents iron in carbonate, Fe_{Ox} is the iron in oxide, Fe_{Mag} is the iron in magnetite, Fe_{PY} shows iron in pyrite, and Fe_T is the total iron. Most Fe_{HR}/Fe_T values in the lower part of the OnZap succession (OnZap Unit A and B) plot above 0.38, whereas the upper part (OnZap Unit C) is dominated by Fe_{HR}/Fe_T values below 0.22. The Fe_{PY}/Fe_{HR} values from the OnZap succession are mainly below 0.7, with only a few samples that exceed 0.8. The silicified interval from ~53 to 43 m depth in the OnZap succession exhibits highly variable Fe_{HR}/Fe_T and Fe_{PY}/Fe_{HR} values and very low Fe_T.

The phase distribution of iron calculated from XRD data is also illustrated in Figure 9. Herein, the biogeochemically reactive iron pool (Clarkson et al., 2014; Poulton and Canfield, 2011; Poulton and Raiswell, 2002; Raiswell et al., 1994), is defined as $(Fe_{PY}+Fe_{Carb})/Fe_{T\text{-}XRD}$. The proportion of pyrite in the reactive iron pool is defined as $Fe_{PY}/(Fe_{PY}+Fe_{Carb})$. The majority of $(Fe_{PY}+Fe_{Carb})/Fe_{T\text{-}XRD}$ ratios in OnZap Units A and B are above 0.5 due to abundant pyrite. This is in good agreement with the Fe_{HR}/Fe_T estimates from the conventional Fe speciation method. Contrastingly to Fe_{PY}/Fe_{HR} ratios of <0.7, the XRD derived $Fe_{PY}/(Fe_{PY}+Fe_{Carb})$ in OnZap Units A and B approximate unity. Given the strong linear correlation between TS and $Fe_{T\text{-}OES}$ this indicates that pyrite is the main iron-bearing phase in these intervals. In OnZap Unit C, however, sulfur and iron concentrations show no correlation and have lower, albeit variable, $(Fe_{PY}+Fe_{Carb})/Fe_{T\text{-}XRD}$ and $Fe_{PY}/(Fe_{PY}+Fe_{Carb})$ ratios.

7.2.1 Iron distribution in the OnZap succession

Iron speciation is now routinely used to characterise redox conditions of the depositional environment (Poulton and Canfield, 2005). Underpinned by empirical observations from modern sediments and inferred conditions from Phanerozoic sedimentary rocks, sediments formed within oxic water columns typically have Fe_{HR}/Fe_T values less than 0.22 whereas those formed under anoxic water columns typically exhibit Fe_{HR}/Fe_T ratios that exceed >0.38. The interpretation of intermediate values i.e. where Fe_{HR}/Fe_T ratios are between 0.22–0.38, warrant caution and may represent either oxic or anoxic conditions. This can result from either the transformation of unsulfidised Fe_{HR} to sheet silicate minerals during diagenesis, Fe_{HR} dilution by atypically high sedimentation rates or changes in provenance (Clarkson et al., 2014; Poulton and Canfield, 2011; Raiswell et al., 1994). The extent of pyritisation of the highly reactive iron pool, as determined by the Fe_{PY}/Fe_{HR} ratio of anoxic samples (i.e. $Fe_{HR}/Fe_T > 0.38$), can further differentiate sulfide-rich (euxinic, Fe_{PY}/Fe_{HR} >0.7–0.8) from iron-rich (ferruginous, Fe_{PY}/Fe_{HR} <0.7) depositional conditions (Clarkson et al., 2014; Poulton and Canfield, 2011; Poulton and Raiswell, 2002; Raiswell et al., 1994).

There are, however, several caveats that need to be considered when using Fe-based redox information to infer ancient redox conditions from rocks. Ideally, the sequential leaching method assumes that at each extraction step Fe is wholly liberated from the targeted mineral phase (e.g. oxides, carbonates, magnetite). Incomplete dissolution could result in either misleading Fe distribution patterns or underestimation of iron bound to specific mineral phases. Fe-rich carbonates in particular are known for their recalcitrant nature (Clarkson et al., 2014; Poulton and Canfield, 2011; Poulton and Raiswell, 2002; Raiswell et al., 1994; Raiswell and Canfield, 2012; Slotznick et al., 2018) and can lead to underestimations of iron in carbonate. Even if the sequential extraction works perfectly, recent studies of iron mobility under various metamorphic conditions have shown that even low-grade metamorphism mobilises and redistributes Fe between mineral phases (Slotznick et al., 2018). Especially, the occurrence of pyrrhotite in ancient samples warrants caution, since it can form at the expense of both carbonate and pyrite alteration (Slotznick et al., 2018). Thus, interpretations of Fe speciation data should always be supported by other lines of evidence (Clarkson et al., 2014; Poulton and Canfield, 2005).

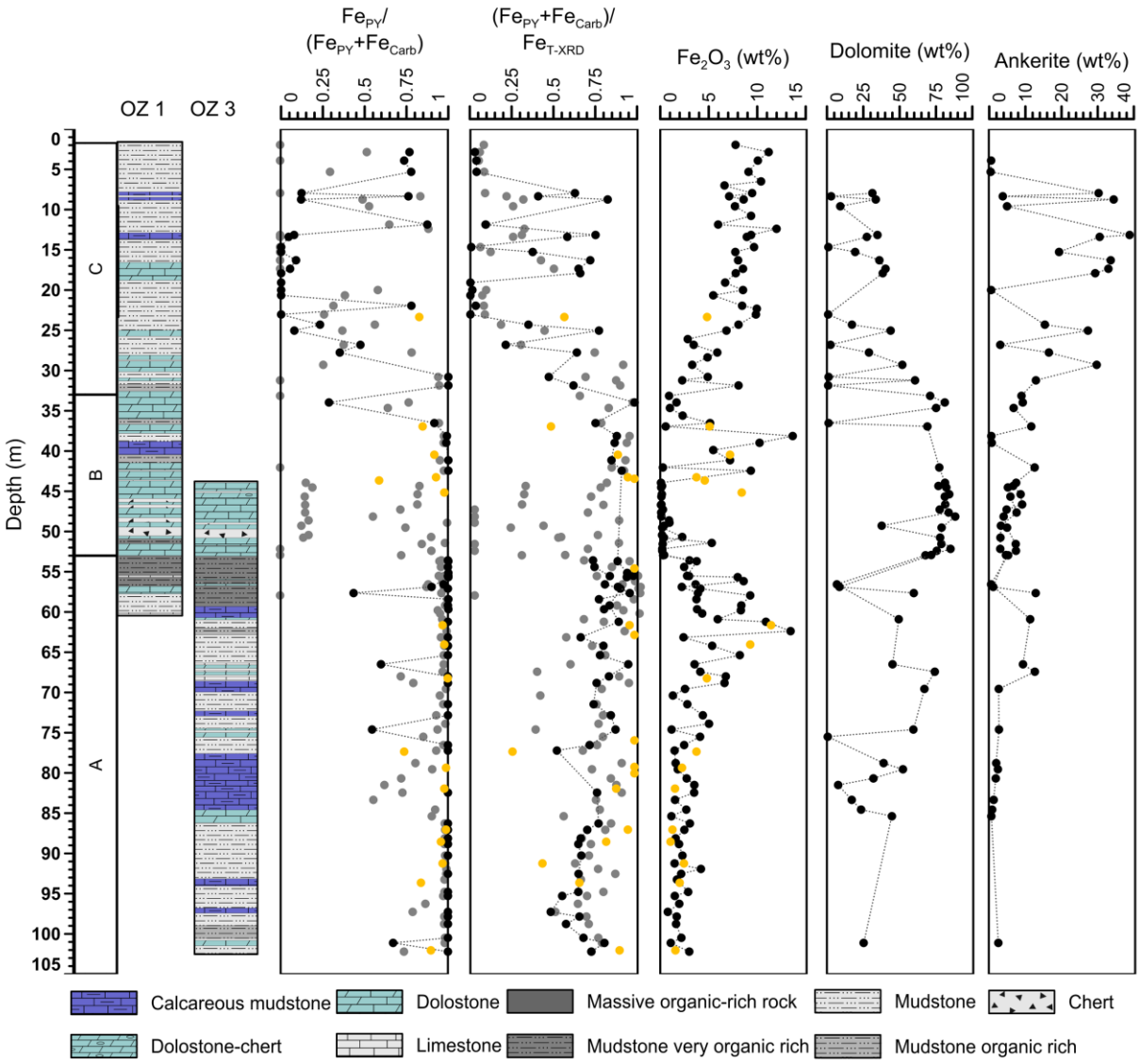

Figure 9. Lihtostratigraphic profiles of the OnZap section divided into Units A, B and C showing iron distribution results, total iron (expressed as Fe_2O_3) and selected mineral concentrations. Black dots on iron distribution profiles represent data points using XRD results; grey (this study) and yellow (from the correlative section in core C-175 studied by Scott et al. 2014) dots represent Fe speciation results using the wet-chemical extraction method. Although the XRD approach has not been empirically calibrated and compared with the traditional Fe speciation method the $(Fe_{PY}+Fe_{Carb})/Fe_{T-XRD}$ is comparable to the Fe_{HR}/Fe_T and $Fe_{PY}/(Fe_{PY}+Fe_{Carb})$ to Fe_{PY}/Fe_{HR} ratios obtained via the latter method.

Taken at face value, the Fe speciation data from the OnZap succession seemingly record an up-section transition from anoxic to more oxic depositional conditions. The organic-rich Units A and B have high Fe_{HR}/Fe_T values, consistent with anoxia, and Fe_{PY}/Fe_{HR} values mostly below 0.7 imply dominantly ferruginous conditions with perhaps occasional euxinia. The dolostone-chert of Unit B exhibits highly variable Fe_{HR}/Fe_T and Fe_{PY}/Fe_{HR} values, likely reflecting its low Fe_T content, which can lead to the overestimation of the highly reactive iron pool (Clarkson et al., 2014; Poulton and Raiswell, 2002). In contrast, low Fe_{HR}/Fe_T ratios of the organic-poor OnZap Unit C imply stable oxic

conditions. However, these results must be assessed with circumspection. Firstly, total sulfur and iron concentrations in OnZap Units A and B display a strong positive correlation. This implies that most iron and sulfur is bound to sulfide minerals, which is more characteristic of euxinic rather than ferruginous conditions. Secondly, considering the occurrence of abundant Fe-rich carbonate phases (dolomite to ankerite solid solution and siderite) in OnZap Unit C, the Fe_{Carb} concentrations measured by sequential extraction were lower than would have been expected. Further, the same interval shows a mismatch between the sum of all extracted iron (including Fe_{PY} calculated from AVS and CRS fractions), and total iron concentrations indicate that some Fe was not accounted for in the Fe speciation method. There are several possible explanations for this: the oxalate acid might have been too weak and/or leaching time too short to dissolve Fe-rich carbonates or quartz cements/coatings surrounding the carbonate crystals may have hindered dissolution. Petrographic evidence does indeed show that quartz fills pore space between mineral crystals and silicification of primary minerals, including carbonates, is common in the OnZap succession.

The exact mechanisms leading to incomplete Fe-rich carbonate dissolution remain to be determined but my analyses show that the XRD derived iron distribution approach is in better agreement with mineralogical, petrographical and bulk chemistry data. Thus, the XRD data provide a more accurate assessment of Fe distribution and redox changes in the OnZap succession than the traditional Fe speciation method. Although the XRD approach to Fe speciation is not empirically calibrated, both methods indicate an up-section transition from anoxic to more variable and possibly oxic redox conditions, providing confidence in this approach.

8. The role of post-depositional processes in the Zaonega Formation

Previous workers (Asael et al., 2013; Črne et al., 2014, 2013a, 2013b; Melezhik et al., 2015, 1999; Qu et al., 2018, 2012) have stressed the widespread occurrence of mafic lavas and sills within the Zaonega Formation being indicative of extensive magmatic activity during sedimentation. Magmatic rocks comprise more than 50% of the Zaonega Formation in the OPH core from the southeast part of the Onega basin and ~35% of the FAR-DEEP 12AB and 13A cores taken in the central-east part of the basin. It is reasonable, then, to conclude that contemporaneous magmatism would have triggered hydrothermal circulation and contact-heat-induced hydrocarbon generation and migration (Črne et al., 2014, 2013a, 2013b; Melezhik et al., 2013a; Qu et al., 2018, 2012). Moreover, interactions between the country rock, hot magmatic bodies and diagenetic or hydrothermal fluids percolating within the subseafloor could have resulted in a range of geochemical reactions causing secondary mineralisation, recrystallisation of primary minerals, oil and gas generation within the sediments (Črne et al., 2014; Melezhik et al., 2013a; Qu et al., 2018, 2012) and thermal breakdown of sedimentary pyrite into pyrrhotite as suggested by Asael et al. (2013).

Close examination of the organic-rich strata that encompass the negative $\delta^{13}C_{org}$ interval in FAR-DEEP 12AB revealed that, despite of mobilisation of hydrocarbons, the stratigraphic $\delta^{13}C_{org}$ record is best explained by secular changes in the primary biomass rather than post-depositional processes (Qu et al., 2018, 2012). This conclusion is based on the fact that the migrated organic matter has a broadly similar carbon isotope composition to its host rock hence was locally sourced, and any post-depositional alteration had a limited (~4‰) effect on the $\delta^{13}C_{org}$ record (Qu et al., 2018, 2012). There is one exception: a massive C_{org}-rich rock interval at 156–136 m depth in the FAR-DEEP 12AB core exhibits a minor positive $\delta^{13}C_{org}$ excursion. This, though, can be explained as due to the upward migration of organic matter and fluidised sediment from lower strata causing a disruption of the otherwise relatively smooth stratigraphic $\delta^{13}C_{org}$ profile of the Zaonega Formation (Paiste et al., paper 3). However, the influence of secondary processes on generating the sulfur isotope composition of pyrite, including closed- versus open-system MSR, thermogenic sulfate reduction (TSR) and mixing processes have not been thoroughly evaluated, which raises the question of the integrity of the sulfur isotope signatures of the Zaonega Formation sedimentary sulfides as recorders of depositional environmental conditions.

8.1 Magmatic influence on the Zaonega sulfur isotope record

Sulfur concentrations in magmatic systems are generally very low (less than 0.2 wt.%) and carry a sulfur isotope composition similar to the mantle ($\delta^{33}S = \delta^{34}S = \delta^{36}S = 0$ ‰; Lesher, 2017; Ono et al., 2007, 2012). In some instances, variations in oxygen fugacity can induce redox reactions in magmatic and hydrothermal systems that could cause up to 4‰ $\delta^{34}S$ fractionation and variations of $\Delta^{33}S$ in the range of 0 ±0.01 to ±0.07‰ in magmatic sulfides (Fiorentini et al., 2012; Ono et al., 2007; Penniston-Dorland et al., 2012; Ripley et al., 2017). Therefore, it is generally thought that sulfur isotope signatures of magmas that significantly deviate from mantle values require incorporation of sulfur from external sources (Fiorentini et al., 2012; Lesher, 2017; Penniston-Dorland et al., 2012; Ripley et al., 2017; Samalens et al., 2017).

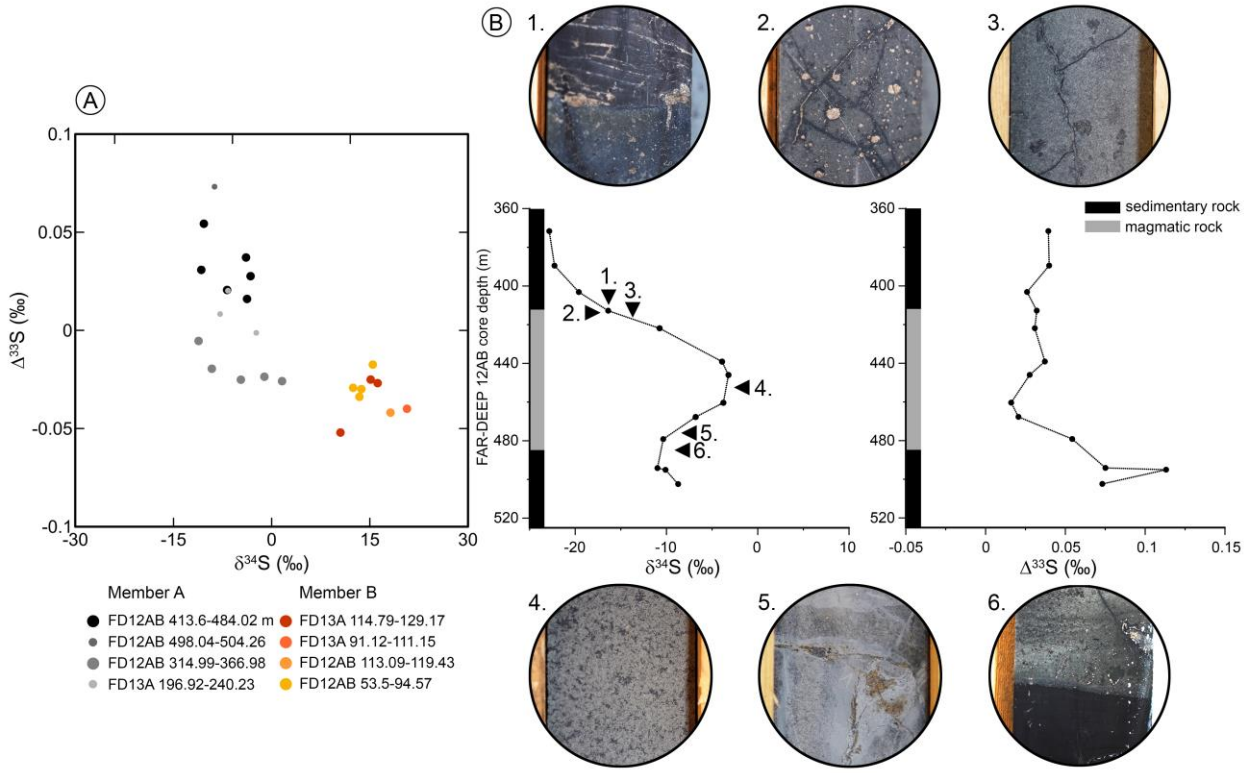

Figure 10. A. Triple isotope plot of sulfide isotope data from magmatic bodies in the Zaonega Formation. Coloured dots represent paired $\Delta^{33}S$-$\delta^{34}S$ data from different magmatic bodies in Members A and B. B. An example of $\delta^{34}S$ (left) and $\Delta^{33}S$ (right) profile through a gabbro (FAR-DEEP 12AB, depth 484-414 m) in Member A. Numbers and black arrows denote locations of core pictures of the contact zones and core area of a gabbroic igneous body.

The $\Delta^{33}S$ and $\delta^{34}S$ composition of sulfide minerals in magmatic bodies display strong dependence on the stratigraphic position within the Zaonega Formation and the sulfur abundance and isotope composition of the surrounding sedimentary rock (Fig. 10). Magmatic bodies that were studied

display centres characterised by very low sulfur concentrations (~0.2 wt.%) and values for both $\Delta^{33}S$ and $\delta^{34}S$ close to 0‰, whereas their margins approach the sulfur isotopic composition and content of the adjacent sedimentary rock. Magmatic bodies in the lower part of Member A display mostly negative $\delta^{34}S$ and positive $\Delta^{33}S$ whereas those in the lower-middle part of Member B are characterised by positive $\delta^{34}S$ and negative $\Delta^{33}S$ (Fig. 10). These relationships suggest that sulfur from the adjacent sedimentary rocks was incorporated into the magmatic bodies during their emplacement. Determining the exact mechanisms is beyond the scope of this study but one explanation could be that sedimentary sulfide minerals formed a partial melt that was assimilated into the mafic magma; such features have been observed elsewhere at intrusive contacts (e.g. Samalens et al., 2017). Nevertheless, based on the sulfur isotope profiles of the magmatic bodies it is unlikely that sulfur derived from magmatic fluids contributed significantly to the sulfur inventory of the depositional environment.

Submarine lava channelisation and intrusion of sills into unconsolidated sediments could promote contact metamorphism and heat-induced alteration of sedimentary pyrites. Petrographical features such as rounded sulfide globules trapped within the margins of the intrusions, numerous sulfide veinlets, and abundant pyrrhotite and sphalerite at the contact aureole are evidence for such alteration. Moreover, pyrrhotite in the FAR-DEEP 13A core has been interpreted as the product of thermal degradation of pyrite (Asael et al., 2013). The presence of AVS in the form of sphalerite and pyrrhotite in the OPH core and lower part of the OnZap succession support that interpretation. This, though, does not appear to have generated any significant isotope effects because the AVS sulfur isotope values exhibit only a few per mil $\delta^{34}S$ differences from the associated CRS fraction. In contrast to the small differences in $\delta^{34}S$ of AVS and CRS, the $\Delta^{33}S$ values of the two sulfide fractions display larger variability but to understand this better requires further detailed petrography and *in situ* analyses by SIMS. In summary, contact metamorphism in the Onega Basin did cause secondary alteration of pyrite adjacent to magmatic bodies but had a limited influence on the primary sulfur isotope record; such alterations can be readily identified via proper screening of the rocks.

9. Synopsis of research

9.1 Paper 1 - Multiple sulphur isotope records tracking basinal and global processes in the 1.98 Ga Zaonega Formation, NW Russia

The main goal of this paper is to provide a high-resolution multi-proxy geochemical and petrographic study of the OnZap drill cores. These cores recovered previously un-documented portions of the upper Zaonega Formation in the Onega Basin thereby enabling a more comprehensive study than previously possible of the putative Shunga Event. The cores form a composite ~102 m thick section that transitions upward from dominantly organic-rich mudstone to carbonate deposition. This transition is accompanied by a decrease in organic matter concentrations and a concomitant shift in $\delta^{13}C_{org}$ from -38‰ to -25‰, which marks the end of the Shunga Event. The $\delta^{34}S$ values of sedimentary pyrites define a profile that centres on ~20‰, without any obvious stratigraphic trends, although transient excursions, both positive and negative, punctuate that relatively stable profile: positive ones are marked by $\delta^{34}S$ of >30‰ ($\Delta^{33}S$ of <-0.05‰) and the attendant negative ones are marked by $\delta^{34}S$ of <5‰ ($\Delta^{33}S$ of > 0.05‰). The pyrite $\Delta^{33}S$-$\delta^{34}S$ display an opposing relationship, typically attributed to closed-system MSR. Integrating lithological, geochemical and mineralogical observations enable inferring that the lower part of the OnZap section accumulated in a complex setting where increased methane flux induced a bloom of methanotrophic organisms that contributed strongly ^{13}C-depleted biomass to the sedimentary organic matter. The addition of carbon sources further stimulated MSR leading to rapid turnover of sulfate and ^{34}S-enriched sulfides. Fractionations imparted by microbial processes could have been further attenuated by limited exchange between pore space and SWS. Contrastingly, the less organic-rich grey mudstones and dolostone beds in the uppermost part of the OnZap succession possibly capture establishment of more normal marine conditions in response to a waning methane flux. This is indicated by the less negative $\delta^{13}C_{org}$ values. The four positive $\delta^{34}S$ (negative $\Delta^{33}S$) excursions can be explained by Rayleigh distillation effects of the local sulfate reservoir whereas the four negative $\delta^{34}S$ (positive $\Delta^{33}S$) excursions could represent more open-system MSR or secondary pyrite crystallisation as a result of post-depositional fluid alteration along bedding planes. Considering that the Zaonega Formation accumulated in a setting that was marked by abundant igneous intrusions and lava flows it is reasonable to consider that the basin could have experienced reconfiguration and partial restriction. In any event, these findings highlight the importance of microbial and basin-specific processes (magmatic activity, hydrocarbon generation and migration,

high organic carbon loading, restriction of the basin, sedimentary processes) in influencing the sulfur isotope record of the Paleoproterozoic Zaonega Formation and urge circumspection before inferring such records constitute an archive of global-scale processes.

9.2 Paper 2 - Biogeochemical sulfur cycling in a semirestricted basin – modelling the pyrite multiple sulfur isotope record of the 1.98 Ga Zaonega Formation

The aim of this paper is to explore in more detail the mechanisms governing the $\Delta^{33}S$, $\delta^{34}S$ and $\Delta^{36}S$ records of the Zaonega Formation. The biogeochemical sulfur cycle interlinks sedimentary and microbial processes that impart distinct isotope fractionations as sulfur mass is partitioned along the pathways that connect its different reservoirs. Thus, sedimentary pyrites reflect the combined effects of biological and abiogenic sulfur cycling that in turn depend on many variables (e.g. organic carbon loading, temperature, iron availability, sulfate concentrations, sedimentation rates), which can be difficult to disentangle. However, modelling allows investigating ways to reduce this complex system to a few key variables in order to trace which factors i.e. microbial metabolic rates, pyrite burial, sulfate exchange between sediments and seawater or basinal sulfate concentrations, had the most influence on generating the pyrite sulfur isotope record.

A well-established steady-state isotope mass balance model developed by Zaback et al. (1993) was adopted and modified to accommodate the multiple sulfur isotope system. After constructing the model, it was applied on the pyrite isotope record of the Zaonega Formation which included new bulk multiple sulfur isotope data from the OPH, FAR-DEEP 12AB and FAR-DEEP 13A cores as well as the data on OnZap cores reported in Paper 1. These cores were obtained from three separate locations across the Onega Basin and, combined, provide a nearly continuous pyrite isotope record of the entire Zaonega Formation and lower part of the overlying Suisari Formation. The stratigraphic succession was divided into Members A, B and C and each was investigated separately with the steady-state isotope mass balance model. This approach revealed a temporal evolution from open-system MSR characterised by large isotope fractionations in the lower part of Member A to the development of sulfate limitation in the middle part of Member B followed by a return to open-system conditions in the upper part of Member C. The model predictions imply that the observed $\Delta^{33}S$, $\delta^{34}S$ and $\Delta^{36}S$ were mainly governed by the rate of sulfate transport to the site of MSR, whereas microbial metabolic rates seem to have a limited effect on the final pyrite isotope composition.

Nevertheless, it is probable that rapid consumption of sulfate due to high organic carbon loading overwhelmed the basinal sulfate pool in Member B inducing Rayleigh distillation effects. A return to more normal marine setting in the upper part of the Zaonega and overlying Suisari Formations is indicated by the steadily decreasing $\delta^{34}S$ values (increasing $\Delta^{33}S$), TOC and TS concentrations. The positive $\delta^{34}S$ and negative $\Delta^{33}S$ trends could signify open-system MSR in more oxidising conditions and a reduced sink for pyrite. Thus, the Zaonega Formation pyrite isotope record and the mass dependent $\Delta^{33}S$-$\delta^{34}S$-$\Delta^{36}S$ relationships can be explained by variations in local sedimentological and biogeochemical conditions endemic to the dynamic basin setting without the need for worldwide changes in ocean chemistry.

9.3 Paper 3 - Global vs. basinal controls on Paleoproterozoic sulfur isotope records: new insights from the Zaonega Formation, NW Russia

The first two papers represented detailed investigations of the sulfur isotope record of the Zaonega and lower part of the Suisari Formations, which set the stage for this third paper: an overall synthesis of the findings of this thesis. The sedimentary strata of the Onega Basin have figured prominently in reconstructions of Paleoproterozoic environmental change, and ones that have produced conflicting interpretations. The Zaonega Formation has been central in many of these efforts and considered as either partially overlapping the LJE or entirely post-LJE leading to interpretations that it housed evidence for global-scale phenomena ranging from inferring that the deep marine realm was oxic to worldwide oceanic deoxygenation, respectively. In strong contrast, other workers have highlighted the significance of local processes in generating the geochemical proxy signals of the Zaonega Formation and hence the need to assess far-more carefully the rock record before invoking global-scale mechanisms as the genesis of those signals.

The paper presents a summary of previous interpretations of geochemical proxies on the Zaonega Formation, its relation to the LJE and more recent insights to the complex depositional setting of the Onega Basin. For the first time new and existing sulfur $\delta^{34}S$ and $\delta^{13}C_{org}$ data from across the Onega Basin - the OPH, FAR-DEEP, new OnZap cores and the C-5190 and C-175 sections from Scott et al. (2014) are integrated and combined into a correlative stratigraphic framework. The combined stable isotope $\delta^{34}S$ and $\delta^{13}C_{org}$ profiles suggest that basinal evolution and microbial feedbacks could have been the main drivers of the observed isotope records that broadly co-vary but exhibit

opposing trends. Lithological evidence suggests increased magmatic activity during deposition of the organic-rich rocks in the middle part of the Zaonega Formation where both $\delta^{34}S$ and $\delta^{13}C_{org}$ isotope profiles show major excursions. Magmatic activity could have stimulated bioproductivity and induced high MSR rates, including sulfate drawdown in the sedimentary column with limited exchange/transport with the basin's sulfate reservoir. This necessitates rethinking interpretations that proposed drawdown of SWS concentrations as a consequence of a global deoxygenation event and, in fact, makes such interpretations unlikely. Further, comparison of the Zaonega results with the Francevillian and younger Paleoproterozoic sedimentary successions demonstrates that similar sulfur isotope profiles were generated millions of years apart in geographically disparate basins. This temporal and spatial disparity suggests a common mechanism but one that was associated with physical (e.g. basin evolution) or biological (e.g. high primary productivity and complex associations of microbial communities) processes that were not due to a temporal singularity in Earth system evolution.

10. Synthesis

The early Paleoproterozoic rise in atmospheric oxygen levels led to large-scale perturbations in the atmosphere-ocean system, intensifying continental weathering, and prompting an increase in the riverine flux of phosphate, sulfate and metals to the oceans. Increased availability of electron acceptors (e.g. SO_4) concomitant with abundant macro- and micronutrients (e.g. PO_4, NO_3, Fe, Cu, Ni, Zn) may have opened new ecological niches to be exploited by complex microbial communities. Rearrangement of ecosystems could in turn impact biogeochemical cycles leaving their distinctive metabolic signatures in the sedimentary rock record. This pivotal time period in Earth's evolution has been captured in the volcano-sedimentary succession of the Onega Basin. The complex depositional setting of the Onega Bain, however, could have significantly influenced the chemostratigraphic record and the information it contains by obscuring geochemical fingerprints left by global processes operating at the backdrop of local environmental change.

The bedded evaporite and shallow-water carbonate deposits that encompass the LJE in the ~2 Ga Tulomozero Formation signify the presence of a sizeable seawater sulfate (SWS) reservoir with an isotope composition of 6–10‰ $\delta^{34}S_{SO4}$, whereas both $\Delta^{33}S_{SO4}$ and $\Delta^{36}S_{SO4}$ have values of 0‰ throughout the entire 800 m thick succession of those evaporites (Blättler et al., 2018). In contrast, sedimentary pyrites from the overlying organic-rich Zaonega Formation record evolving $\delta^{34}S$ values from ~-11‰ and positive ~0.03‰ $\Delta^{33}S$ at its base to ~18‰ $\delta^{34}S$ and -0.03 $\Delta^{33}S$ in the middle and return to ~3‰ $\delta^{34}S$ and ~0‰ $\Delta^{33}S$ at its top. From a simplistic view point the stratigraphic $\delta^{34}S$ and $\Delta^{33}S$ profiles can be explained as follows:

i) After the establishment of a sizeable SWS (10 mM) reservoir at ~2 Ga and deepening of the basin, sulfur cycling similar to modern marine environments characterised the lower part of the Zaonega Formation as evidenced by the negative ~-11‰ $\delta^{34}S$ and positive ~0.03‰ $\Delta^{33}S$ values (Fig. 11a).

ii) During a period of increased magmatism-volcanism and related high bioproductivity, the up-section trend towards increasingly ^{34}S-enriched pyrites (~18‰ $\delta^{34}S$ and ~-0.03‰ $\Delta^{33}S$) and the opposing $\Delta^{33}S$-$\delta^{34}S$ relationship in the upper part of the Zaonega Formation infer rapid reduction of sulfate by MSR and small fractionations from initial sulfate reservoir. Additionally, the anomalously positive, up to 44‰, $\delta^{34}S$ and negative, as low as -0.1‰, $\Delta^{33}S$ that exceed reasonable estimates for SWS isotope composition suggest Rayleigh distillation effects (Fig. 11b).

iii) Shallowing and (partial) closure of the basin is exemplified by the return to less positive ~3‰ $\delta^{34}S$ and ~0‰ $\Delta^{33}S$ in the upper part of the Zaonega and lower part of the Suisari Formations, as the result of lower MSR rates and/or a reduced sink for pyrite.

Importantly, explanation of the sulfur isotope trends in the lower and upper part of the Zaonega Formation does not require processes that are unique to the Paleoproterozoic, many can be viewed through the lens of biogeochemical sulfur cycling as seen in modern marine environments. Sedimentation of the upper part of the Zaonega Formation possibly occurred in a shallowing and semi-restricted basin. This is implied by the increase in the number of thick dolostone beds along with parallel-laminated to ripple cross-laminated grey mudstones and marly Fe-rich dolostones in this part of the succession. Moreover, several hundreds of meters of sub-aqueously extruded basalts (Melezhik et al., 2015), representing the upper part of the Zaonega and Suisari Formations, covered the underlying sedimentary beds shortly after their deposition. Their presence alone confirms significant geodynamical reshaping of the depositional setting. This is further consistent with inferred lacustrine environments by the onset of deposition of the Kondopoga Formation rocks that form the youngest strata of the Paleoproterozoic Onega Basin succession (Galdobina, 1987; Melezhik et al., 2013b). Therefore, it is unlikely that the sulfur isotope record in the upper Zaonega and Suisari Formations would have fully captured a global SWS signature.

Several questions remain. Formation of pyrites with positive $\delta^{34}S$ and mirroring $\Delta^{33}S$ in the middle part of the Zaonega Formation would have required rapid MSR that generated only small differences between sulfate and sulfide, which consequently may have traced changes in the sulfate reservoir. Thus, was the apparent switch from open- to closed-system sulfur cycling a local or global phenomenon? This change in sulfur cycling coincides with a period of syndepositional magmatism that induced oil generation and migration, high primary productivity and extensive methane cycling within the basin, as suggested by the coinciding four-fold increase in TOC abundances and the negative $\delta^{13}C_{org}$ excursion to -42‰. Therefore, resonable to suggest that the ^{34}S-enriched pyrites reflect local rather than global processes. Moreover, pyrites in this ~200 m thick interval display a relatively narrow range of values (~18‰ $\delta^{34}S$ and ~-0.03 $\Delta^{33}S$) whereas the transient positive $\delta^{34}S$ (>30‰) and negative $\Delta^{33}S$ (<-0.05‰) excursions occur over intervals only a few meters thick. Based on modelling the anomalously ^{34}S-enriched sulfides (>30‰ $\delta^{34}S$) would require at least an 80% reduction of the available sulfate pool with initial $\delta^{34}S$ of 6‰ and its rapid repeated contraction and expansion in order to reproduce the pyrite record of the Zaonega Formation. This would be difficult

to explain in a global ocean but could be attributed to the combined effects of biologic and abiogenic sulfur cycling in a semirestricted setting.

In addition, enhanced flux of organic carbon substrates from primary (i.e. photoautotrophic biomass) and secondary sources (i.e. thermogenic methane) to the sedimentary environment could stimulate pore water MSR close to the sediment-water interface where sulfate is readily available. This would generate an open-system with respect to sulfate transport into the sediments but a limited back flux if sulfate consumption exceeds its supply and the produced sulfide is effectively retained in the sediments via pyrite precipitation. Subsequently, the coupling of high MSR and pyrite burial rates could destabilise the local sulfur cycle by invoking oscillating basinal sulfate levels and Rayleigh distillation effects, although, it is unlikely that Rayleigh fractionation alone was governing the observed pyrite isotope trends. In order to sustain ~18‰ $\delta^{34}S$ and ~-0.03‰ $\Delta^{33}S$ of sedimentary sulfides and high pyrite burial (TS up to 11 wt.%) through ~200 m of strata, sulfate had to be sourced from an external reservoir. Therefore, it is reasonable that the Onega Basin was periodically cut off and/or sulfate consumption exceeded its supply from a bigger possibly global sulfate reservoir (Fig. 11). According to such a scenario, the sedimentary pyrite record of the Zaonega Formation does not necessarily reflect large-scale perturbations in the contemporaneous ocean.

Nonetheless, if all sulfate entering pore waters was converted into sulfide and sequestered as pyrite, then the $\delta^{34}S$ and $\Delta^{33}S$ values that converge around ~18‰ and ~-0.03‰, respectively, could represent the SWS isotope composition at the time. Based on model predictions an initial SWS composition between 6 to 15‰ $\delta^{34}S$, 0 to -0.05 ‰ $\Delta^{33}S$ and 0 to 1.9‰ $\Delta^{36}S$ could explain the range of pyrite isotope data in the Zaonega Formation. The upper limit of 15‰ $\delta^{34}S$ and -0.05 ‰ $\Delta^{33}S$ was derived from pyrite isotope data of cores C-175 and C-5190 (Scott et al., 2014). This range of predicted SWS $\delta^{34}S$ values has some interesting implications. On one hand, the lower limit for SWS would suggest that, after the build-up of a substantial oceanic sulfate pool at ~2 Ga, its isotope composition remained stable at least until accumulation of the Zaonega Formation. On the other hand, the upper limit implies, that after ~2 Ga, the SWS evolved towards more positive $\delta^{34}S$ and negative $\Delta^{33}S$ values. Given the possibility that pyrite $\delta^{34}S$ and $\Delta^{33}S$ in the middle Zaonega Formation display small fractionations from sulfate, then the latter scenario could be more likely. Further, if the most positive $\delta^{34}S$ values of up to 18.7‰ in the 1.92 Ga Pilgujärvi Sedimentary Formation (Reuschel et al., 2012a) and the ~17‰ $\delta^{34}S$ estimate from ~1.84 Ga Rove Formation (Poulton et al.,

2004) preserve a SWS isotope signature, then it is possible that the oceanic sulfate reservoir remained relatively stable throughout the Paleoproterozoic.

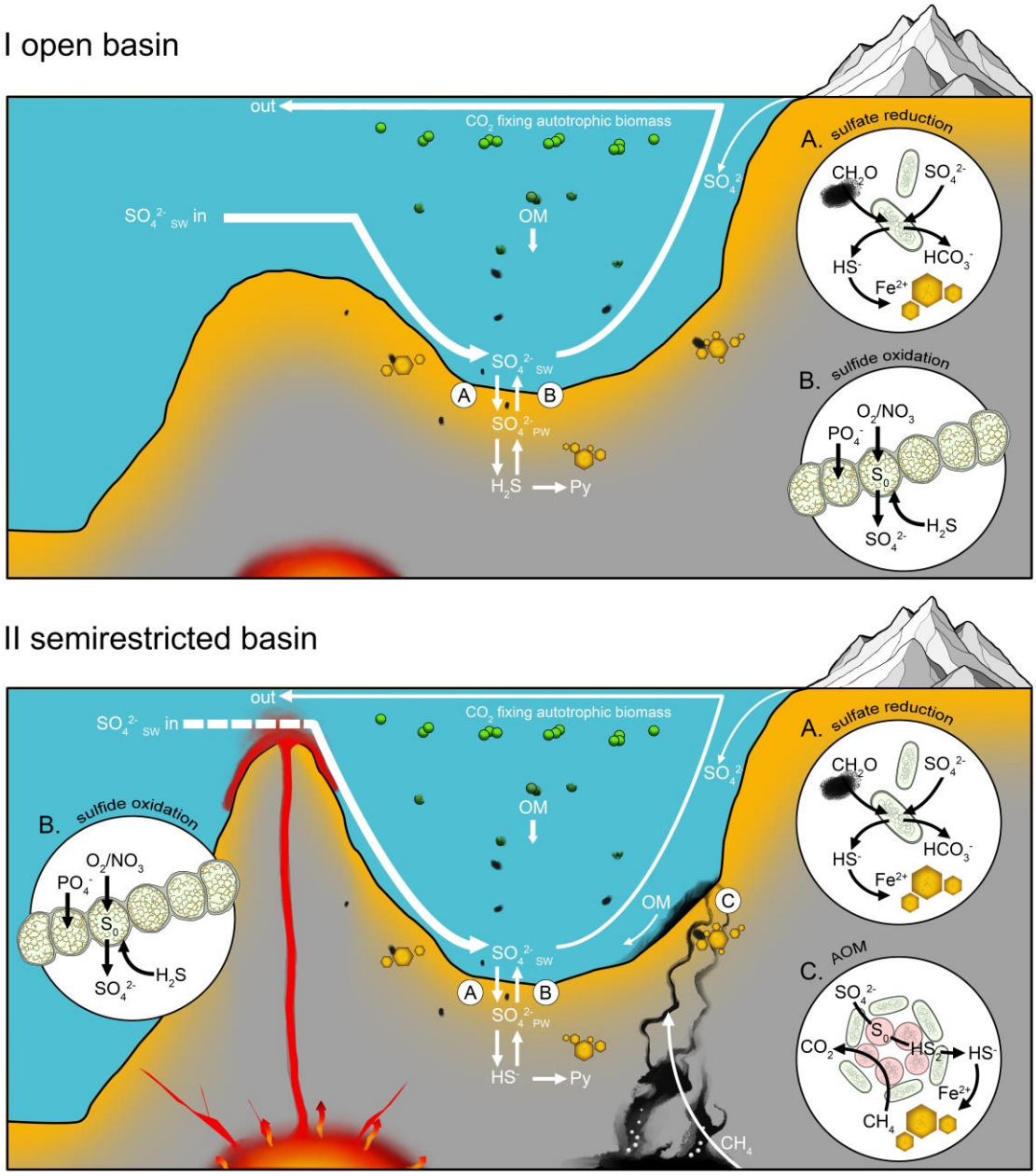

Figure 11. Interpreted open (I) and semirestricted (II) depositional setting of the Zaonega Formation and inferred sulfur metabolisms including A. sulfate reduction, B. sulfide oxidation and C. anaerobic oxidation of methane coupled to sulfate reduction (AOM). White arrows represent flow of sulfur between different reservoirs in the basin (SW = seawater, PW = pore water and Py = pyrite). (I) The lower part of the Zaonega Formation accumulated under open-system conditions where organic matter (OM) was delivered into sediments via sinking particles of CO_2-fixing autotrophic biomass and sulfur cycling occurred under steady-state conditions. (II) The middle Zaonega Formation accumulated during a period of magmatic activity that influenced hydrographic configuration and circulation in the basin and induced hydrocarbon seepage and methanotrophy. These changes led to closed-system sulfur cycling and Rayleigh distillation of the local sulfate reservoir.

This speculative interpretation requires further investigation but could imply a lag time between the build-up of an ocean sulfate reservoir at ~2 Ga and the establishment of necessary conditions for initiating modern-type biogeochemical sulfur cycling in marine settings. There is a caveat to this scenario. In Phanerozoic marine sediments microbial reduction of sulfate produces large $\delta^{34}S$ but small $\delta^{33}S$ fractionations. For that reason, the present day SWS has a positive $\delta^{34}S$ (21‰) and sulfides have typically negative $\delta^{34}S$ values (~-40‰) but both carry a positive $\Delta^{33}S$ signature (0.04‰ for SWS) (Canfield et al., 2010; Masterson et al., 2016; Sim et al., 2011). Paleoproterozoic reconstructions of SWS composition from pyrite records, including the Zaonega and Rove Formations, infer a positive $\delta^{34}S$ but a negative $\Delta^{33}S$ signature for ocean sulfate (Johnston et al., 2006; Scott et al., 2014). It has been proposed that this discrepancy could reflect outgassing of ^{34}S-depleted water column sulfide to the atmosphere (Johnston et al., 2006) or loss to a sulfur sink that has not been accounted for, such as organic sulfur. The role of organic sulfur has been largely overlooked in ancient sulfur cycling since it is difficult to constrain and it could have been lost or gained during diagenesis and kerogen maturation (Werne et al., 2004). This highlights the question: are pyrite isotope records alone reliable indicators for SWS isotope composition? This is particularily relevant since the final isotope signature of pyrite depends on multiple biological and sedimentological factors not to mention postdepositional processes. While it is possible that pyrites in the organic-rich rocks of the middle Zaonega Formation reflect the isotope composition of the contemporaneous SWS, more detailed investigations are required to test this hypothesis.

In summary, the pyrite multiple sulfur isotope record of the Zaonega Formation highlights the complexity in reconstructing ancient sulfur cycling. The transfer of sulfur between different reservoirs interlinks dynamic interactions between microbes and their immediate surroundings and in turn depicts feedbacks between global and local processes. Depending on the addition of substrates, shallowing and/or the establishment of a physical barrier within the Onega Basin, sulfate limitation could have developed due to an increased pyrite sink. Since changes in the depositional environment affect both microbial processes and sedimentation patterns, it is likely that they were mutually important in governing the final $\Delta^{33}S$-$\delta^{34}S$ composition of pyrites in the Zaonega Formation.

Conclusions and future outlook

The overall objective of this thesis was to investigate in detail biogeochemical sulfur cycling in the 1.98 Ga Zaonega Formation. An extensive new isotope dataset was collected and integrated with previous results to demonstrate a broad coupling and negative correlation between $\delta^{34}S$ and $\delta^{13}C_{org}$ records with distinct positive $\delta^{34}S$ and negative $\delta^{13}C_{org}$ excursions characterising the upper part of the Zaonega Formation. These results combined with additional geological and geochemical data were used to assess the role of local- versus global-scale processes in contributing to the geochemical proxy records archived in the Zaonega Formation in the aftermath of the GOE.

Given the accumulation of the Zaonega Formation in a magmatically active setting with numerous sills intruding unconsolidated sediments, as well as a subsequent greenschist facies metamorphic overprint, secondary processes relating to post-depositional alteration of the proxy signals needed to be evaluated. Lithological and petrographical observations revealed the presence of multiple generations of pyrite and the formation of pyrrhotite at the expense of pyrite. Despite the magmatic activity during accumulation of the Zaonega sediments, the importance of lavas and sills as the sulfur source appears insignificant. Total sulfur concentrations and pyrite sulfur isotope data of magmatic bodies, that are interlayered with the organic-rich sediments, suggests that sulfur was more likely incorporated into the magma from the adjacent sediments rather than the opposite.

Nonetheless, magmatic activity had a profound influence on the depositional environment and the microbial communities during accumulation of the Zaonega Formation sediments. Syn-depositional magmatic activity during the middle part of the Zaonega Formation not only generated and mobilised hydrocarbons but also impacted the overall sedimentary system and diagenetic environment by generating sharp redox gradients. Thus, the coupled positive pyrite $\delta^{34}S$ (negative $\Delta^{33}S$) and negative $\delta^{13}C_{org}$ trends in this part of the succession reflect concomitant perturbations in basinal sulfur and carbon cycling as a response to environmental change and microbial feedbacks. Consequently, increased methane flux stimulated AOM coupled to MSR that contributed ^{13}C-depleted biomass to the bulk organic matter ($\delta^{13}C_{org}$ -42‰) and rapid MSR leading to small biological fractionations and ^{34}S-enriched pyrites. Biological and sedimentary processes were mutually important in governing the final pyrite isotope composition since the relative fluxes of sulfate diffusion and sulfide retention in sediments could have further attenuated fractionations between SWS sulfate and sulfide. An inferred waning of the methane flux at the top of the Zaonega

Formation resulted in the re-establishment of a dominantly CO_2-fixing photoautotrophic (~-29‰ $\delta^{13}C_{org}$) microbial community. Despite the return to less negative $\delta^{13}C_{org}$ values at the top of the Zaonega Formation, the $\delta^{34}S$ values of sedimentary pyrite from that strata remain enriched in ^{34}S and the two isotope systems become decoupled. In that shallowing, wide-spread volcanic activity, and likely restriction and, eventually, burial of the basin by basalts of the Suisari Formation, it is highly probable that facies differences and associated sedimentary processes were the main influences of the basin's sulfur cycle.

Additionally, comparison of the Zaonega Formation with other Paleoproterozoic sedimentary basins demonstrate that similar sulfur isotope trends can be generated at discrete and different times in different locations. This could indicate that the underlying mechanisms, i.e. basinal evolution, facies changes and local microbial feedbacks are the main drivers of Paleoproterozoic sulfur cycling and do not require mechanisms that significantly differ from those operating in modern environments.

In summary, this thesis highlights the complexity in interpreting sulfur and carbon isotope records in ancient rock successions. The rock record of the Onega Basin provides a rich opportunity for untangling the environmental information in the aftermath of the GOE. The research on the Tulomozero evaporite-carbonate succession using novel isotope and trace element systematics is likely to make an important contribution assessing the underlying causes of the LJE. A systematic study of redox sensitive trace metals that have very high concentrations in parts of the Zaonega Formation and the applicability of these metals as oxygenation proxies, not only for the Onega Basin but also globally, would be important and of widespread interest. Additionally, timing of deposition of the Zaonega Formation and underlying Tulomozero Formation is still a matter of debate and until resolved its relation to the LJE remains unclear. Moreover, even though the depositional context of the Onega Basin is relatively well established, questions about the closure of the basin and changes in sedimentation patterns require additional detailed scrutiny to more thoroughly assess interpretations of geochemical proxies. This thesis provides new data and new insights into the biogeochemical processes operating in the Zaonega Formation but several questions remain: what were the mechanisms affecting iron distribution patterns within the studied section, what processes were behind the assimilation of sulfur into the magmatic bodies and associated isotope effects, what is the importance of TSR in the observed sulfur isotope variability and formation of different generations of pyrite, and what was the role and isotope signature of organic sulfur within the Zaonega Formation?

References

Aller, R.C., Blair, N.E., Brunskill, G.J., 2008. Early diagenetic cycling, incineration, and burial of sedimentary organic carbon in the central Gulf of Papua (Papua New Guinea). Journal of Geophysical Research 113. https://doi.org/10.1029/2006JF000689

Aller, R.C., Madrid, V., Chistoserdov, A., Aller, J.Y., Heilbrun, C., 2010. Unsteady diagenetic processes and sulfur biogeochemistry in tropical deltaic muds: Implications for oceanic isotope cycles and the sedimentary record. Geochimica et Cosmochimica Acta 74, 4671–4692. https://doi.org/10.1016/j.gca.2010.05.008

Anbar, A.D., Duan, Y., Lyons, T.W., Arnold, G.L., Kendall, B., Creaser, R.A., Kaufman, A.J., Gordon, G.W., Scott, C., Garvin, J., Buick, R., 2007. A Whiff of Oxygen Before the Great Oxidation Event? Science 317, 1903–1906. https://doi.org/10.1126/science.1140325

Asael, D., Tissot, F.L.H., Reinhard, C.T., Rouxel, O., Dauphas, N., Lyons, T.W., Ponzevera, E., Liorzou, C., Cheron, S., 2013. Coupled molybdenum, iron and uranium stable isotopes as oceanic paleoredox proxies during the Paleoproterozoic Shunga Event. Chemical Geology 362, 193–210. https://doi.org/10.1016/j.chemgeo.2013.08.003

Baroni, M., Thiemens, M.H., Delmas, R.J., Savarino, J., 2007. Mass-Independent Sulfur Isotopic Compositions in Stratospheric Volcanic Eruptions. Science 315, 84–87. https://doi.org/10.1126/science.1131754

Baross, J.A., Hoffman, S.E., 1985. Submarine hydrothermal vents and associated gradient environments as sites for the origin and evolution of life. Origins Life Evol Biosphere 15, 327–345. https://doi.org/10.1007/BF01808177

Bau, M., Dulski, P., 1996. Distribution of yttrium and rare-earth elements in the Penge and Kuruman iron-formations, Transvaal Supergroup, South Africa. Precambrian Research 79, 37–55. https://doi.org/10.1016/0301-9268(95)00087-9

Bau, M., Höhndorf, A., Dulski, P., Beukes, N.J., 1997. Sources of Rare-Earth Elements and Iron in Paleoproterozoic Iron-Formations from the Transvaal Supergroup, South Africa: Evidence from Neodymium Isotopes. The Journal of Geology 105, 121–129. https://doi.org/10.1086/606152

Bau, M., Möller, P., 1993. Rare earth element systematics of the chemically precipitated component in early precambrian iron formations and the evolution of the terrestrial atmosphere-hydrosphere-lithosphere system. Geochimica et Cosmochimica Acta 57, 2239–2249. https://doi.org/10.1016/0016-7037(93)90566-F

Bekker, A., 2011. Huronian Glaciation, in: Gargaud, M., Amils, R., Quintanilla, J.C., Cleaves, H.J. (Jim), Irvine, W.M., Pinti, D.L., Viso, M. (Eds.), Encyclopedia of Astrobiology. Springer Berlin Heidelberg, Berlin, Heidelberg, pp. 768–772. https://doi.org/10.1007/978-3-642-11274-4_742

Bekker, A., Holland, H.D., Wang, P.L., Rumble, D., Stein, H.J., Hannah, J.L., Coetzee, L.L., Beukes, N.J., 2004. Dating the rise of atmospheric oxygen. Nature 427, 117–120. https://doi.org/10.1038/nature02260

Bekker, A., Karhu, J.A., Eriksson, K.A., Kaufman, A.J., 2003. Chemostratigraphy of Paleoproterozoic carbonate successions of the Wyoming Craton: tectonic forcing of biogeochemical change? Precambrian Res 120, 279–325. https://doi.org/Pii S0301-9268(02)00164-X Doi 10.1016/S0301-9268(02)00164-X

Bekker, A., Karhu, J.A., Kaufman, A.J., 2006. Carbon isotope record for the onset of the Lomagundi carbon isotope excursion in the Great Lakes area, North America. Precambrian Res 148, 145–180. https://doi.org/10.1016/j.precamres.2006.03.008

Bekker, A., Kaufman, A., Karhu, J., Eriksson, K., 2005. Evidence for Paleoproterozoic cap carbonates in North America. Precambrian Research 137, 167–206. https://doi.org/10.1016/j.precamres.2005.03.009

Bekker, A., Kaufman, A.J., Karhu, J.A., Beukes, N.J., Swart, Q.D., Coetzee, L.L., Eriksson, K.A., 2001. Chemostratigraphy of the Paleoproterozoic Duitschland Formation, South Africa: Implications for Coupled Climate Change and Carbon Cycling. Am J Sci 301, 261–285. https://doi.org/10.2475/ajs.301.3.261

Bekker, A., Planavsky, N.J., Krapež, B., Rasmussen, B., Hofmann, A., Slack, J.F., Rouxel, O.J., Konhauser, K.O., 2014. 9.18 - Iron Formations: Their Origins and Implications for Ancient Seawater Chemistry, in:

Holland, H.D., Turekian, K.K. (Eds.), Treatise on Geochemistry (Second Edition). Elsevier, Oxford, pp. 561–628. https://doi.org/10.1016/B978-0-08-095975-7.00719-1

Bekker, A., Slack, J.F., Planavsky, N., Krapež, B., Hofmann, A., Konhauser, K.O., Rouxel, O.J., 2010. Iron Formation: The Sedimentary Product of a Complex Interplay among Mantle, Tectonic, Oceanic, and Biospheric Processes. Economic Geology 105, 467–508. https://doi.org/10.2113/gsecongeo.105.3.467

Berkner, L.V., Marshall, L.C., 1965. History of Major Atmospheric Components. PNAS 53, 1215–1226. https://doi.org/10.1073/pnas.53.6.1215

Berner, R.A., 1964. An idealized model of dissolved sulfate distribution in recent sediments. Geochimica et Cosmochimica Acta 28, 1497–1503.

Berner, R.A., Raiswell, R., 1983. Burial of organic carbon and pyrite sulfur in sediments over phanerozoic time: a new theory. Geochimica et Cosmochimica Acta 47, 855–862. https://doi.org/10.1016/0016-7037(83)90151-5

Blake, R.E., Chang, S.J., Lepland, A., 2010. Phosphate oxygen isotopic evidence for a temperate and biologically active Archaean ocean. Nature 464, 1029.

Blättler, C.L., Claire, M.W., Prave, A.R., Kirsimäe, K., Higgins, J.A., Medvedev, P.V., Romashkin, A.E., Rychanchik, D.V., Zerkle, A.L., Paiste, K., Kreitsmann, T., Millar, I.L., Hayles, J.A., Bao, H., Turchyn, A.V., Warke, M.R., Lepland, A., 2018. Two-billion-year-old evaporites capture Earth's great oxidation. Science eaar2687. https://doi.org/10.1126/science.aar2687

Bradley, A.S., Leavitt, W.D., Schmidt, M., Knoll, A.H., Girguis, P.R., Johnston, D.T., 2016. Patterns of sulfur isotope fractionation during microbial sulfate reduction. Geobiology 14, 91–101. https://doi.org/10.1111/gbi.12149

Brüchert, V., 2004. Physiological and ecological aspects of sulfur isotope fractionation during bacterial sulfate reduction, in: Special Paper 379: Sulfur Biogeochemistry - Past and Present. Geological Society of America, pp. 1–16. https://doi.org/10.1130/0-8137-2379-5.1

Canfield, D.E., 2001. Biogeochemistry of Sulfur Isotopes. Reviews in Mineralogy and Geochemistry 43, 607–636. https://doi.org/10.2138/gsrmg.43.1.607

Canfield, D.E., 1998. A new model for Proterozoic ocean chemistry. Nature 396, 450–453. https://doi.org/Doi 10.1038/24839

Canfield, D.E., 1991. Sulfate Reduction in Deep-Sea Sediments. Am J Sci 291, 177–188.

Canfield, D.E., Farquhar, J., Zerkle, A.L., 2010. High isotope fractionations during sulfate reduction in a low-sulfate euxinic ocean analog. Geology 38, 415–418. https://doi.org/10.1130/G30723.1

Canfield, D.E., Ngombi-Pemba, L., Hammarlund, E.U., Bengtson, S., Chaussidon, M., Gauthier-Lafaye, F., Meunier, A., Riboulleau, A., Rollion-Bard, C., Rouxel, O., Asael, D., Pierson-Wickmann, A.-C., El Albani, A., 2013. Oxygen dynamics in the aftermath of the Great Oxidation of Earth's atmosphere. Proceedings of the National Academy of Sciences 110, 16736–16741. https://doi.org/10.1073/pnas.1315570110

Canfield, D.E., Raiswell, R., 1999. The evolution of the sulfur cycle. Am J Sci 299, 697–723. https://doi.org/10.2475/ajs.299.7-9.697

Canfield, D.E., Raiswell, R., Westrich, J.T., Reaves, C.M., Berner, R.A., 1986. The use of chromium reduction in the analysis of reduced inorganic sulfur in sediments and shales. Chemical Geology 54, 149–155. https://doi.org/10.1016/0009-2541(86)90078-1

Canfield, D.E., Teske, A., 1996. Late Proterozoic rise in atmospheric oxygen concentration inferred from phylogenetic and sulphur-isotope studies. Nature 382, 127–132. https://doi.org/Doi 10.1038/382127a0

Cates, N.L., Mojzsis, S.J., 2007. Pre-3750 Ma supracrustal rocks from the Nuvvuagittuq supracrustal belt, northern Québec. Earth and Planetary Science Letters 255, 9–21. https://doi.org/10.1016/j.epsl.2006.11.034

Clarkson, M.O., Poulton, S.W., Guilbaud, R., Wood, R.A., 2014. Assessing the utility of Fe/Al and Fe-speciation to record water column redox conditions in carbonate-rich sediments. Chemical Geology 382, 111–122. https://doi.org/10.1016/j.chemgeo.2014.05.031

Clayton, C., 1991. Carbon isotope fractionation during natural gas generation from kerogen. Marine and Petroleum Geology 8, 232–240. https://doi.org/10.1016/0264-8172(91)90010-X

Cloud, J., 1968. Atmospheric and hydrospheric evolution on the primitive earth. Science 160, 729–736. https://doi.org/10.1126/science.160.3829.729

Craig, J.R., 1993. The Metamorphism of Pyrite and Pyritic Ores: An Overview. Mineralogical Magazine 57, 3–18. https://doi.org/10.1180/minmag.1993.057.386.02

Črne, A.E., Melezhik, V.A., Lepland, A., Fallick, A.E., Prave, A.R., Brasier, A.T., 2014. Petrography and geochemistry of carbonate rocks of the Paleoproterozoic Zaonega Formation, Russia: Documentation of C-13-depleted non-primary calcite. Precambrian Res 240, 79–93. https://doi.org/DOI 10.1016/j.precamres.2013.10.005

Črne, A.E., Melezhik, V.A., Prave, A.R., Lepland, A., Romashkin, A.E., Rychanchik, D.V., Hanski, E.J., Luo, Z., 2013a. Zaonega Formation: FAR-DEEP Holes 12A and 12B, and Neighbouring quarries, in: Melezhik, V.A., Prave, A.R., Fallick, A.E., Hanski, E.J., Lepland, A., Kump, L.R., Strauss, H. (Eds.), Reading the Archive of Earth's Oxygenation: Volume 2: The Core Archive of the Fennoscandian Arctic Russia - Drilling Early Earth Project, Frontiers in Earth Sciences. Springer, pp. 946–1007.

Črne, A.E., Melezhik, V.A., Prave, A.R., Lepland, A., Romashkin, A.E., Rychanchik, D.V., Hanski, E.J., Luo, Z., 2013b. Zaonega Formation: FAR-DEEP Hole 13A, in: Melezhik, V.A., Prave, A.R., Fallick, A.E., Hanski, E.J., Lepland, A., Kump, L.R., Strauss, H. (Eds.), Reading the Archive of Earth's Oxygenation: Volume 2: The Core Archive of the Fennoscandian Arctic Russia - Drilling Early Earth Project, Frontiers in Earth Sciences. Springer, pp. 1008–1046.

Crowe, S.A., Paris, G., Katsev, S., Jones, C., Kim, S.-T., Zerkle, A.L., Nomosatryo, S., Fowle, D.A., Adkins, J.F., Sessions, A.L., Farquhar, J., Canfield, D.E., 2014. Sulfate was a trace constituent of Archean seawater. Science 346, 735–739. https://doi.org/10.1126/science.1258966

Cui, H., Kitajima, K., Spicuzza, M.J., Fournelle, J.H., Denny, A., Ishida, A., Zhang, F., Valley, J.W., 2018. Questioning the biogenicity of Neoproterozoic superheavy pyrite by SIMS. American Mineralogist 103, 1362–1400. https://doi.org/10.2138/am-2018-6489

Dale, A.W., Brüchert, V., Alperin, M., Regnier, P., 2009. An integrated sulfur isotope model for Namibian shelf sediments. Geochimica et Cosmochimica Acta 73, 1924–1944. https://doi.org/10.1016/j.gca.2008.12.015

Danielache, S.O., Eskebjerg, C., Johnson, M.S., Ueno, Y., Yoshida, N., 2008. High-precision spectroscopy of ^{32}S, ^{33}S, and ^{34}S sulfur dioxide: Ultraviolet absorption cross sections and isotope effects. Journal of Geophysical Research 113. https://doi.org/10.1029/2007JD009695

Dauphas, N., Cates, N.L., Mojzsis, S.J., Busigny, V., 2007. Identification of chemical sedimentary protoliths using iron isotopes in the >3750 Ma Nuvvuagittuq supracrustal belt, Canada. Earth and Planetary Science Letters 254, 358–376. https://doi.org/10.1016/j.epsl.2006.11.042

Davies, C., Pozzo, M., Gubbins, D., Alfè, D., 2015. Constraints from material properties on the dynamics and evolution of Earth's core. Nature Geoscience 8, 678–685. https://doi.org/10.1038/ngeo2492

Diamond, C.W., Planavsky, N.J., Wang, C., Lyons, T.W., 2018. What the ~1.4 Ga Xiamaling Formation can and cannot tell us about the mid-Proterozoic ocean. Geobiology 16, 219–236. https://doi.org/10.1111/gbi.12282

Djokic, T., Kranendonk, M.J.V., Campbell, K.A., Walter, M.R., Ward, C.R., 2017. Earliest signs of life on land preserved in ca. 3.5 Ga hot spring deposits. Nature Communications 8, 15263. https://doi.org/10.1038/ncomms15263

Dodd, M.S., Papineau, D., Grenne, T., Slack, J.F., Rittner, M., Pirajno, F., O'Neil, J., Little, C.T.S., 2017. Evidence for early life in Earth's oldest hydrothermal vent precipitates. Nature 543, 60–64. https://doi.org/10.1038/nature21377

Eigenbrode, J.L., Freeman, K.H., 2006. Late Archean rise of aerobic microbial ecosystems. PNAS 103, 15759–15764. https://doi.org/10.1073/pnas.0607540103

Eriksson, P.G., Catuneanu, O., Sarkar, S., Tirsgaard, H., 2005. Patterns of sedimentation in the Precambrian. Sedimentary Geology 176, 17–42. https://doi.org/10.1016/j.sedgeo.2005.01.003

Eriksson, P.G., Cheney, E.S., 1992. Evidence for the transition to an oxygen-rich atmosphere during the evolution of red beds in the lower proterozoic sequences of southern Africa. Precambrian Research 54, 257–269. https://doi.org/10.1016/0301-9268(92)90073-W

Evans, D.A., Beukes, N.J., Kirschvink, J.L., 1997. Low-latitude glaciation in the Palaeoproterozoic era. Nature 386, 262.

Farquhar, J., Bao, H., Thiemens, M., 2000. Atmospheric Influence of Earth's Earliest Sulfur Cycle. Science 289, 756–758. https://doi.org/10.1126/science.289.5480.756

Farquhar, J., Johnston, D.T., Wing, B.A., 2007. Implications of conservation of mass effects on mass-dependent isotope fractionations: Influence of network structure on sulfur isotope phase space of dissimilatory sulfate reduction. Geochimica et Cosmochimica Acta 71, 5862–5875. https://doi.org/10.1016/j.gca.2007.08.028

Farquhar, J., Johnston, D.T., Wing, B.A., Habicht, K.S., Canfield, D.E., Airieau, S., Thiemens, M.H., 2003. Multiple sulphur isotopic interpretations of biosynthetic pathways: implications for biological signatures in the sulphur isotope record. Geobiology 1, 27–36. https://doi.org/10.1046/j.1472-4669.2003.00007.x

Farquhar, J., Savarino, J., Airieau, S., Thiemens, M.H., 2001. Observation of wavelength-sensitive mass-independent sulfur isotope effects during SO_2 photolysis: Implications for the early atmosphere. Journal of Geophysical Research: Planets 106, 32829–32839. https://doi.org/10.1029/2000JE001437

Farquhar, J., Zerkle, A.L., Bekker, A., 2014. Geologic and Geochemical Constraints on Earth's Early Atmosphere, in: Treatise on Geochemistry. Elsevier, pp. 91–138. https://doi.org/10.1016/B978-0-08-095975-7.01304-8

Farquhar, J., Zerkle, A.L., Bekker, A., 2011. Geological constraints on the origin of oxygenic photosynthesis. Photosyn. Res. 107, 11–36. https://doi.org/10.1007/s11120-010-9594-0

Fike, D.A., Bradley, A.S., Rose, C.V., 2015. Rethinking the Ancient Sulfur Cycle. Annu Rev Earth Pl Sc 43, 593–622. https://doi.org/10.1146/annurev-earth-060313-054802

Filippov, M.M., Yesipko, O.A., 2016. Geological-geophysical marker horizons of the Paleoproterozoic Onega Structure. Proceedings of the Karelian Research Centre of the Russian Academy of Sciences.

Fiorentini, M.L., Bekker, A., Rouxel, O., Wing, B.A., Maier, W., Rumble, D., 2012. Multiple Sulfur and Iron Isotope Composition of Magmatic Ni-Cu-(PGE) Sulfide Mineralization from Eastern Botswana. Econ Geol 107, 105–116.

Fischer, W.W., Fike, D.A., Johnson, J.E., Raub, T.D., Guan, Y., Kirschvink, J.L., Eiler, J.M., 2014. SQUID-SIMS is a useful approach to uncover primary signals in the Archean sulfur cycle. Proceedings of the National Academy of Sciences 111, 5468–5473. https://doi.org/10.1073/pnas.1322577111

Fralick, P., Planavsky, N., Burton, J., Jarvis, I., Addison, W.D., Barrett, T.J., Brumpton, G.R., 2017. Geochemistry of Paleoproterozoic Gunflint Formation carbonate: Implications for hydrosphere-atmosphere evolution. Precambrian Research 290, 126–146. https://doi.org/10.1016/j.precamres.2016.12.014

Fralick, P.W., Poulton, S.W., Canfield, D.E., 2011. Does the Paleoproterozoic Animikie Basin record the sulfidic ocean transition?: COMMENT. Geology 39, e241–e241. https://doi.org/10.1130/G31747C.1

Freeman, K.H., 2001. Isotopic Biogeochemistry of Marine Organic Carbon. Reviews in Mineralogy and Geochemistry 43, 579–605. https://doi.org/10.2138/gsrmg.43.1.579

Fry, B., Ruf, W., Gest, H., Hayes, J.M., 1988. Sulfur isotope effects associated with oxidation of sulfide by O2 in aqueous solution. Chemical Geology: Isotope Geoscience section 73, 205–210. https://doi.org/10.1016/0168-9622(88)90001-2

Galdobina, L.P., 1987. The Ludikovi superhorizon, in: Sokolov, V. A. (Ed.), Geology of Karelia. Nauka (Science), Leningrad, pp. 59–67.

Goldhaber, M.B., Kaplan, I.R., 1975. Controls and consequences of sulfate reduction rates in recent marine sediments. Soil Science 119.

Gomes, M.L., Hurtgen, M.T., 2013. Sulfur isotope systematics of a euxinic, low-sulfate lake: Evaluating the importance of the reservoir effect in modern and ancient oceans. Geology 41, 663–666. https://doi.org/10.1130/G34187.1

Gomes, M.L., Johnston, D.T., 2017. Oxygen and sulfur isotopes in sulfate in modern euxinic systems with implications for evaluating the extent of euxinia in ancient oceans. Geochimica et Cosmochimica Acta 205, 331–359. https://doi.org/10.1016/j.gca.2017.02.020

Gregory, D.D., Lyons, T.W., Large, R.R., Jiang, G., Stepanov, A.S., Diamond, C.W., Figueroa, M.C., Olin, P., 2017. Whole rock and discrete pyrite geochemistry as complementary tracers of ancient ocean chemistry: An example from the Neoproterozoic Doushantuo Formation, China. Geochimica et Cosmochimica Acta 216, 201–220. https://doi.org/10.1016/j.gca.2017.05.042

Grove, T.., Parman, S.., 2004. Thermal evolution of the Earth as recorded by komatiites. Earth and Planetary Science Letters 219, 173–187. https://doi.org/10.1016/S0012-821X(04)00002-0

Gubbins, D., Masters, G., Nimmo, F., 2008. A thermochemical boundary layer at the base of Earth's outer core and independent estimate of core heat flux. Geophysical Journal International 174, 1007–1018. https://doi.org/10.1111/j.1365-246X.2008.03879.x

Gumsley, A.P., Chamberlain, K.R., Bleeker, W., Soderlund, U., Kock, M.D.O., Larsson, E.R., Bekker, A., 2017. Timing and tempo of the Great Oxidation Event. P Natl Acad Sci USA 114, 1811–1816. https://doi.org/10.1073/pnas.1608824114

Guo, Q., Strauss, H., Kaufman, A.J., Schröder, S., Gutzmer, J., Wing, B., Baker, M.A., Bekker, A., Jin, Q., Kim, S.-T., Farquhar, J., 2009. Reconstructing Earth's surface oxidation across the Archean-Proterozoic transition. Geology 37, 399–402. https://doi.org/10.1130/G25423A.1

Habicht, K.S., Gade, M., Thamdrup, B., Berg, P., Canfield, D.E., 2002. Calibration of sulfate levels in the Archean Ocean. Science 298, 2372–2374. https://doi.org/DOI 10.1126/science.1078265

Halevy, I., Peters, S.E., Fischer, W.W., 2012. Sulfate Burial Constraints on the Phanerozoic Sulfur Cycle. Science 337, 331–334. https://doi.org/10.1126/science.1220224

Hannah, J.L., Stein, H.J., Zimmerman, A., Yang, G., Melezhik, V.A., Filippov, M.M., Turgeon, S.C., Creaser, R.A., 2008. Re-Os geochronology of shungite: A 2.05 Ga fossil oil field in Karelia. Presented at the 33rd International Geological Congress, Goldschmidt Conference Abstracts, Oslo.

Havig, J.R., Hamilton, T.L., Bachan, A., Kump, L.R., 2017. Sulfur and carbon isotopic evidence for metabolic pathway evolution and a four-stepped Earth system progression across the Archean and Paleoproterozoic. Earth-Science Reviews 174, 1–21. https://doi.org/10.1016/j.earscirev.2017.06.014

Hayes, J.M., 1993. Factors controlling 13C contents of sedimentary organic compounds: Principles and evidence. Marine Geology, Marine Sediments, Burial, Pore Water Chemistry, Microbiology and Diagenesis 113, 111–125. https://doi.org/10.1016/0025-3227(93)90153-M

Hayes, J.M., 1983. Geochemical evidence bearing on the origin of aerobiosis, a speculative hypothesis.

Hayes, J.M., Strauss, H., Kaufman, A.J., 1999. The abundance of 13C in marine organic matter and isotopic fractionation in the global biogeochemical cycle of carbon during the past 800 Ma. Chemical Geology 161, 103–125. https://doi.org/10.1016/S0009-2541(99)00083-2

Hayes, J.M., Waldbauer, J.R., 2006. The carbon cycle and associated redox processes through time. Philos Trans R Soc Lond B Biol Sci 361, 931–950. https://doi.org/10.1098/rstb.2006.1840

Hazen, R.M., Papineau, D., Bleeker, W., Downs, R.T., Ferry, J.M., McCoy, T.J., Sverjensky, D.A., Yang, H., 2008. Mineral evolution. American Mineralogist 93, 1693–1720. https://doi.org/10.2138/am.2008.2955

Hessler, A.M., Lowe, D.R., 2006. Weathering and sediment generation in the Archean: An integrated study of the evolution of siliciclastic sedimentary rocks of the 3.2Ga Moodies Group, Barberton Greenstone Belt, South Africa. Precambrian Research 151, 185–210. https://doi.org/10.1016/j.precamres.2006.08.008

Hildebrand, R.S., Whalen, J.B., Bowring, S.A., 2018. Resolving the crustal composition paradox by 3.8 billion years of slab failure magmatism and collisional recycling of continental crust. Tectonophysics 734–735, 69–88. https://doi.org/10.1016/j.tecto.2018.04.001

Holland, H.D., 2006. The oxygenation of the atmosphere and oceans. Philos T R Soc B 361, 903–915. https://doi.org/DOI 10.1098/rstb.2006.1838

Holland, H.D., 1984. The Chemical Evolution of the Atmosphere and Oceans. Princeton University Press.

Holland, H.D., 1973. The Oceans; A Possible Source of Iron in Iron-Formations. Economic Geology 68, 1169–1172. https://doi.org/10.2113/gsecongeo.68.7.1169

Holland, H.D., 1962. Model for the Evolution of the Earth's Atmosphere, in: Engel, A.E.J., James, H.L., Leonard, B.F. (Eds.), Petrologic Studies. Geological Society of America, USA, pp. 447–477. https://doi.org/10.1130/Petrologic.1962.447

Hren, M.T., Tice, M.M., Chamberlain, C.P., 2009. Oxygen and hydrogen isotope evidence for a temperate climate 3.42 billion years ago. Nature 462, 205.

Jacobs, J.A., 1953. The Earth's Inner Core. Nature 172, 297–298. https://doi.org/10.1038/172297a0

Johnston, D.T., 2011. Multiple sulfur isotopes and the evolution of Earth's surface sulfur cycle. Earth-Sci Rev 106, 161–183. https://doi.org/DOI 10.1016/j.earscirev.2011.02.003

Johnston, D.T., Farquhar, J., Canfield, D.E., 2007. Sulfur isotope insights into microbial sulfate reduction: When microbes meet models. Geochimica et Cosmochimica Acta 71, 3929–3947. https://doi.org/DOI 10.1016/j.gca.2007.05.008

Johnston, D.T., Farquhar, J., Wing, B.A., Kaufman, A., Canfield, D.E., Habicht, K.S., 2005. Multiple sulfur isotope fractionations in biological systems: A case study with sulfate reducers and sulfur disproportionators. Am J Sci 305, 645–660. https://doi.org/DOI 10.2475/ajs.305.6-8.645

Johnston, D.T., Poulton, S.W., Fralick, P.W., Wing, B.A., Canfield, D.E., Farquhar, J., 2006. Evolution of the oceanic sulfur cycle at the end of the Paleoproterozoic. Geochimica et Cosmochimica Acta 70, 5723–5739. https://doi.org/DOI 10.1016/j.gca.2006.08.001

Jones, D.S., Fike, D.A., 2013. Dynamic sulfur and carbon cycling through the end-Ordovician extinction revealed by paired sulfate–pyrite δ34S. Earth and Planetary Science Letters 363, 144–155. https://doi.org/10.1016/j.epsl.2012.12.015

Joosu, L., Lepland, A., Kirsimae, K., Romashkin, A.E., Roberts, N.W., Martin, A.P., Crne, A.E., 2015. The REE-composition and petrography of apatite in 2 Ga Zaonega Formation, Russia: The environmental setting for phosphogenesis. Chemical Geology 395, 88–107. https://doi.org/10.1016/j.chemgeo.2014.11.013

Jørgensen, B.B., 1979. A theoretical model of the stable sulfur isotope distribution in marine sediments. Geochimica et Cosmochimica Acta 43, 363–374. https://doi.org/10.1016/0016-7037(79)90201-1

Jørgensen, B.B., Bottcher, M.E., Luschen, H., Neretin, L.N., Volkov, I.I., 2004. Anaerobic methane oxidation and a deep H2S sink generate isotopically heavy sulfides in Black Sea sediments. Geochimica et Cosmochimica Acta 68, 2095–2118. https://doi.org/DOI 10.1016/j.gca.2003.07.017

Joye, S.B., Boetius, A., Orcutt, B.N., Montoya, J.P., Schulz, H.N., Erickson, M.J., Lugo, S.K., 2004. The anaerobic oxidation of methane and sulfate reduction in sediments from Gulf of Mexico cold seeps. Chemical Geology 205, 219–238. https://doi.org/10.1016/j.chemgeo.2003.12.019

Kah, L.C., Lyons, T.W., Frank, T.D., 2004. Low marine sulphate and protracted oxygenation of the Proterozoic biosphere. Nature 431, 834–838. https://doi.org/10.1038/nature02974

Karhu, J.A., 1993. Paleoproterozoic evolution of the carbon isotope ratios of sedimentary carbonates in the Fennoscandian Shield. Geological Survey of Finland, Bulletin 371 1–87.

Karhu, J.A., Holland, H.D., 1996. Carbon isotopes and the rise of atmospheric oxygen. Geology 24, 867–870. https://doi.org/Doi 10.1130/0091-7613(1996)024<0867:Ciatro>2.3.Co;2

Kasting, J., 1993. Earth's early atmosphere. Science 259, 920–926. https://doi.org/10.1126/science.11536547

Kato, Y., Kano, T., Kunugiza, K., 2002. Negative Ce Anomaly in the Indian Banded Iron Formations: Evidence for the Emergence of Oxygenated Deep-Sea at 2.9-2.7 Ga. Resource Geology 52, 101–110. https://doi.org/10.1111/j.1751-3928.2002.tb00123.x

Kirschvink, J.L., Gaidos, E.J., Bertani, L.E., Beukes, N.J., Gutzmer, J., Maepa, L.N., Steinberger, R.E., 2000. Paleoproterozoic snowball Earth: Extreme climatic and geochemical global change and its biological consequences. PNAS 97, 1400–1405. https://doi.org/10.1073/pnas.97.4.1400

Kleine, T., Münker, C., Mezger, K., Palme, H., 2002. Rapid accretion and early core formation on asteroids and the terrestrial planets from Hf–W chronometry. Nature 418, 952–955. https://doi.org/10.1038/nature00982

Knauth, L.P., Epstein, S., 1976. Hydrogen and oxygen isotope ratios in nodular and bedded cherts. Geochimica et Cosmochimica Acta 40, 1095–1108. https://doi.org/10.1016/0016-7037(76)90051-X

Konhauser, K.O., Planavsky, N.J., Hardisty, D.S., Robbins, L.J., Warchola, T.J., Haugaard, R., Lalonde, S.V., Partin, C.A., Oonk, P.B.H., Tsikos, H., Lyons, T.W., Bekker, A., Johnson, C.M., 2017. Iron formations: A global record of Neoarchaean to Palaeoproterozoic environmental history. Earth-Science Reviews 172, 140–177. https://doi.org/10.1016/j.earscirev.2017.06.012

Kopp, R.E., Kirschvink, J.L., Hilburn, I.A., Nash, C.Z., 2005. The Paleoproterozoic snowball Earth: A climate disaster triggered by the evolution of oxygenic photosynthesis. PNAS 102, 11131–11136. https://doi.org/10.1073/pnas.0504878102

Krupenik, V.A., Akhmedov, A.M., Sveshnikova, K.Y., 2011. Isotopic composition of carbon, oxygen and sulfur in the Ludicovian and Jatulian rocks, in: Glushanin, L.V., Sharov, N.V., Shchiptsov, V.V. (Eds.), The Onega Paleoproterozoic Structure (Geology, Tectonics, Deep Structure, Minerogeny). Institute of Geology, Karelian Research Centre RAS, Petrozavodsk, pp. 250–255.

Kump, L.R., 2011. Isotopic Evidence for Massive Oxidation of Organic Matter Following the Great Oxidation Event. Science 334, 1694–1696. https://doi.org/10.1126/science.1213999

Kump, L.R., Barley, M.E., 2007. Increased subaerial volcanism and the rise of atmospheric oxygen 2.5 billion years ago. Nature 448, 1033.

Kump, L.R., Kirsimäe, K., Melezhik, V.A., Brasier, A.T., Fallick, A.E., Salminen, P.E., 2013. 7.9 Terrestrial Environments, in: Melezhik, V.A., Prave, A.R., Hanski, E.J., Fallick, A.E., Lepland, A., Kump, L.R., Strauss, H. (Eds.), Reading the Archive of Earth's Oxygenation: Volume 3: Global Events and the Fennoscandian Arctic Russia - Drilling Early Earth Project, Frontiers in Earth Sciences. Springer Berlin Heidelberg, Berlin, Heidelberg, pp. 1407–1456. https://doi.org/10.1007/978-3-642-29670-3_9

Lahtinen, R., Garde, A.A., Melezhik, V.A., 2008. Paleoproterozoic Evolution of Fennoscandia and Greenland. Episodes 31, 20–28.

Large, R.R., Halpin, J.A., Danyushevsky, L.V., Maslennikov, V.V., Bull, S.W., Long, J.A., Gregory, D.D., Lounejeva, E., Lyons, T.W., Sack, P.J., McGoldrick, P.J., Calver, C.R., 2014. Trace element content of sedimentary pyrite as a new proxy for deep-time ocean-atmosphere evolution. Earth Planet Sc Lett 389, 209–220. https://doi.org/10.1016/j.epsl.2013.12.020

Lasaga, A.C., Otake, T., Watanabe, Y., Ohmoto, H., 2008. Anomalous fractionation of sulfur isotopes during heterogeneous reactions. Earth and Planetary Science Letters 268, 225–238. https://doi.org/10.1016/j.epsl.2008.01.016

Lepland, A., Joosu, L., Kirsimae, K., Prave, A.R., Romashkin, A.E., Crne, A.E., Martin, A.P., Fallick, A.E., Somelar, P., Upraus, K., Mand, K., Roberts, N.M.W., van Zuilen, M.A., Wirth, R., Schreiber, A., 2014. Potential influence of sulphur bacteria on Palaeoproterozoic phosphogenesis. Nat Geosci 7, 20–24. https://doi.org/10.1038/Ngeo2005

Lepland, A., Melezhik, V.A., Papineau, A.E., Romashkin, A.E., Joosu, L., 2013. The Earliest Phosphorites – Radical Change in the Phosphorus Cycle during the Palaeoproterozoic, in: Melezhik, V.A., Prave, A.R., Fallick, A.E., Kump, L.R., Strauss, H., Lepland, A., Hanski, E. (Eds.), Reading the Archive of Earth's Oxygenation: Volume 3: Global Events and the Fennoscandian Arctic Russia - Drilling Early Earth Project, Frontiers in Earth Sciences. Springer, pp. 1275–1296.

Lesher, C.M., 2017. Roles of xenomelts, xenoliths, xenocrysts, xenovolatiles, residues, and skarns in the genesis, transport, and localization of magmatic Fe-Ni-Cu-PGE sulfides and chromite. Ore Geology Reviews 90, 465–484. https://doi.org/10.1016/j.oregeorev.2017.08.008

Lewan, M.D., 1983. Effects of thermal maturation on stable organic carbon isotopes as determined by hydrous pyrolysis of Woodford Shale. Geochimica et Cosmochimica Acta 47, 1471–1479. https://doi.org/10.1016/0016-7037(83)90306-X

Lowenstein, T.K., Hardie, L.A., Timofeeff, M.N., Demicco, R.V., 2003. Secular variation in seawater chemistry and the origin of calcium chloride basinal brines. Geology 31, 857. https://doi.org/10.1130/G19728R.1

Luo, G.M., Ono, S.H., Beukes, N.J., Wang, D.T., Xie, S.C., Summons, R.E., 2016. Rapid oxygenation of Earth's atmosphere 2.33 billion years ago. Sci Adv 2. https://doi.org/UNSP e1600134 10.1126/sciadv.1600134

Lyons, T.W., 1997. Sulfur isotopic trends and pathways of iron sulfide formation in upper Holocene sediments of the anoxic Black Sea. Geochimica et Cosmochimica Acta 61, 3367–3382. https://doi.org/Doi 10.1016/S0016-7037(97)00174-9

Maher, K.A., Stevenson, D.J., 1988. Impact frustration of the origin of life. Nature 331, 612–614. https://doi.org/10.1038/331612a0

Maloof, A.C., Porter, S.M., Moore, J.L., Dudás, F.Ö., Bowring, S.A., Higgins, J.A., Fike, D.A., Eddy, M.P., 2010. The earliest Cambrian record of animals and ocean geochemical change. GSA Bulletin 122, 1731–1774. https://doi.org/10.1130/B30346.1

Marais, D.J.D., 2001. Isotopic Evolution of the Biogeochemical Carbon Cycle During the Precambrian. Reviews in Mineralogy and Geochemistry 43, 555–578. https://doi.org/10.2138/gsrmg.43.1.555

Marin, J., Chaussidon, M., Robert, F., 2010. Microscale oxygen isotope variations in 1.9Ga Gunflint cherts: Assessments of diagenesis effects and implications for oceanic paleotemperature reconstructions. Geochimica et Cosmochimica Acta 74, 116–130. https://doi.org/10.1016/j.gca.2009.09.016

Marmo, J.S., Ojakangas, R.W., 1984. Lower Proterozoic glaciogenic deposits, eastern Finland. GSA Bulletin 95, 1055–1062. https://doi.org/10.1130/0016-7606(1984)95<1055:LPGDEF>2.0.CO;2

Martin, Adam P., Condon, D.J., Prave, A.R., Lepland, A., 2013. A review of temporal constraints for the Palaeoproterozoic large, positive carbonate carbon isotope excursion (the Lomagundi–Jatuli Event). Earth-Science Reviews 127, 242–261. https://doi.org/10.1016/j.earscirev.2013.10.006

Martin, A.P., Condon, D.J., Prave, A.R., Melezhik, V.A., Lepland, A., Fallick, A.E., 2013. Dating the termination of the Palaeoproterozoic Lomagundi-Jatuli carbon isotopic event in the North Transfennoscandian Greenstone Belt. Precambrian Research 224, 160–168. https://doi.org/10.1016/j.precamres.2012.09.010

Martin, A.P., Prave, A.R., Condon, D.J., Lepland, A., Fallick, A.E., Romashkin, A.E., Medvedev, P.V., Rychanchik, D.V., 2015. Multiple Palaeoproterozoic carbon burial episodes and excursions. Earth Planet Sc Lett 424, 226–236. https://doi.org/10.1016/j.epsl.2015.05.023

Masterson, A.L., Farquhar, J., Wing, B.A., 2011. Sulfur mass-independent fractionation patterns in the broadband UV photolysis of sulfur dioxide: Pressure and third body effects. Earth and Planetary Science Letters 306, 253–260. https://doi.org/10.1016/j.epsl.2011.04.004

Masterson, A.L., Wing, B.A., Paytan, A., Farquhar, J., Johnston, D.T., 2016. The minor sulfur isotope composition of Cretaceous and Cenozoic seawater sulfate. Paleoceanography 31, 779–788. https://doi.org/10.1002/2016PA002945

Maynard, J.B., Ritger, S.D., Sutton, S.J., 1991. Chemistry of sands from the modern Indus River and the Archean Witwatersrand basin: Implications for the composition of the Archean atmosphere. Geology 19, 265–268. https://doi.org/10.1130/0091-7613(1991)019<0265:COSFTM>2.3.CO;2

Melezhik, V.A., Fallick, A.E., Brasier, A.T., Lepland, A., 2015. Carbonate deposition in the Palaeoproterozoic Onega basin from Fennoscandia: a spotlight on the transition from the Lomagundi-Jatuli to Shunga events. Earth-Sci Rev 147, 65–98. https://doi.org/10.1016/j.earscirev.2015.05.005

Melezhik, V.A., Fallick, A.E., Filippov, M.M., Deines, Y.E., Črne, A.E., Lepland, A., Brasier, A.T., Strauss, H., 2013a. Giant Palaeoproterozoic Petrified Oil Field in the Onega Basin, in: Reading the Archive of Earth's Oxygenation: Volume 3: Global Events and the Fennoscandian Arctic Russia - Drilling Early Earth Project, Frontiers in Earth Sciences. Springer, pp. 1202–1212.

Melezhik, V.A., Fallick, A.E., Filippov, M.M., Larsen, O., 1999. Karelian shungite—an indication of 2.0-Ga-old metamorphosed oil-shale and generation of petroleum: geology, lithology and geochemistry. Earth-Science Reviews 47, 1–40. https://doi.org/10.1016/S0012-8252(99)00027-6

Melezhik, V.A., Fallick, A.E., Rychanchik, D.V., Kuznetsov, A.B., 2005. Palaeoproterozoic evaporites in Fennoscandia: implications for seawater sulphate, the rise of atmospheric oxygen and local amplification of the delta C-13 excursion. Terra Nova 17, 141–148. https://doi.org/10.1111/j.1365-3121.2005.00600.x

Melezhik, V.A., Hanski, E.J., 2013. Palaeotectonic and Palaeogeographic Evolution of Fennoscandia in the Early Palaeoproterozoic, in: Reading the Archive of Earth's Oxygenation, Frontiers in Earth Sciences. Springer, Berlin, Heidelberg, pp. 111–178. https://doi.org/10.1007/978-3-642-29682-6_5

Melezhik, V.A., Huhma, H., Condon, D.J., Fallick, A.E., Whitehouse, M.J., 2007. Temporal constraints on the Paleoproterozoic Lomagundi-Jatuli carbon isotopic event. Geology 35, 655–658. https://doi.org/10.1130/G23764A.1

Melezhik, V.A., Medvedev, P.V., Svetov, S.A., 2013b. The Onega Basin, in: Reading the Archive of Earth's Oxygenation. Springer Berlin Heidelberg, Berlin, Heidelberg, pp. 387–490. https://doi.org/10.1007/978-3-642-29682-6_9

Meyer, K.M., Kump, L.R., 2008. Oceanic Euxinia in Earth History: Causes and Consequences. Annu. Rev. Earth Planet. Sci. 36, 251–288. https://doi.org/10.1146/annurev.earth.36.031207.124256

Meyer, N.R., Zerkle, A.L., Fike, D.A., 2017. Sulphur cycling in a Neoarchaean microbial mat. Geobiology 15, 353–365. https://doi.org/10.1111/gbi.12227

Meyers, P.A., 2014. Why are the δ13Corg values in Phanerozoic black shales more negative than in modern marine organic matter? Geochemistry, Geophysics, Geosystems 15, 3085–3106. https://doi.org/10.1002/2014GC005305

Morozov, A.F., Hakhaev, B.N., Petrov, O.V., Gorbachev, V.I., Tarkhanov, G.B., Tsvetkov, L.D., Erinchek, Y.M., Akhmedov, A.M., Krupenik, V.A., Sveshnikova, K.Y., 2010. Rock-salts in Palaeoproterozoic strata of the Onega depression of Karelia (based on data from the Onega parametric drillhole). Transection of Academy of Sciences 435, 230–233.

Murakami, T., Sreenivas, B., Sharma, S.D., Sugimori, H., 2011. Quantification of atmospheric oxygen levels during the Paleoproterozoic using paleosol compositions and iron oxidation kinetics. Geochimica et Cosmochimica Acta 75, 3982–4004. https://doi.org/10.1016/j.gca.2011.04.023

Murakami, T., Utsunomiya, S., Imazu, Y., Prasad, N., 2001. Direct evidence of late Archean to early Proterozoic anoxic atmosphere from a product of 2.5 Ga old weathering. Earth and Planetary Science Letters 184, 523–528. https://doi.org/10.1016/S0012-821X(00)00344-7

Nisbet, E.G., Cheadle, M.J., Arndt, N.T., Bickle, M.J., 1993. Constraining the potential temperature of the Archaean mantle: A review of the evidence from komatiites. Lithos 30, 291–307. https://doi.org/10.1016/0024-4937(93)90042-B

Nutman, A.P., Bennett, V.C., Friend, C.R.L., Van Kranendonk, M.J., Chivas, A.R., 2016. Rapid emergence of life shown by discovery of 3,700-million-year-old microbial structures. Nature 537, 535.

Oduro, H., Harms, B., Sintim, H.O., Kaufman, A.J., Cody, G., Farquhar, J., 2011. Evidence of magnetic isotope effects during thermochemical sulfate reduction. Proceedings of the National Academy of Sciences 108, 17635–17638. https://doi.org/10.1073/pnas.1108112108

Oduro, H., Kamyshny, A., Zerkle, A.L., Li, Y., Farquhar, J., 2013. Quadruple sulfur isotope constraints on the origin and cycling of volatile organic sulfur compounds in a stratified sulfidic lake. Geochimica et Cosmochimica Acta 120, 251–262. https://doi.org/10.1016/j.gca.2013.06.039

Ohmoto, H., Watanabe, Y., Lasaga, A.C., Naraoka, H., Johnson, I., Brainard, J., Chorney, A., 2014. Oxygen, iron, and sulfur geochemical cycles on early Earth: Paradigms and contradictions, in: Geological Society of America Special Papers. Geological Society of America, pp. 55–95. https://doi.org/10.1130/2014.2504(09)

Ojakangas, R.W., Marmo, J.S., Heiskanen, K.I., 2001. Basin evolution of the Paleoproterozoic Karelian Supergroup of the Fennoscandian (Baltic) Shield. Sediment Geol 141, 255–285. https://doi.org/Doi 10.1016/S0037-0738(01)00079-3

Ono, S., Shanks, W.C., Rouxel, O.J., Rumble, D., 2007. S-33 constraints on the seawater sulfate contribution in modern seafloor hydrothermal vent sulfides. Geochimica et Cosmochimica Acta 71, 1170–1182. https://doi.org/10.1016/j.gca.2006.11.017

Ono, S., Wing, B., Johnston, D., Farquhar, J., Rumble, D., 2006. Mass-dependent fractionation of quadruple stable sulfur isotope system as a new tracer of sulfur biogeochemical cycles. Geochimica et Cosmochimica Acta 70, 2238–2252. https://doi.org/DOI 10.1016/j.gca.2006.01.022

Ono, S.H., Keller, N.S., Rouxel, O., Alt, J.C., 2012. Sulfur-33 constraints on the origin of secondary pyrite in altered oceanic basement. Geochimica et Cosmochimica Acta 87, 323–340. https://doi.org/10.1016/j.gca.2012.04.016

Ossa Ossa, F., Eickmann, B., Hofmann, A., Planavsky, N.J., Asael, D., Pambo, F., Bekker, A., 2018. Two-step deoxygenation at the end of the Paleoproterozoic Lomagundi Event. Earth and Planetary Science Letters 486, 70–83. https://doi.org/10.1016/j.epsl.2018.01.009

Ovchinnikova, G.V., Kuznetsov, A.B., Melezhik, V.A., Gorokhov, I.M., Vasil'eva, I.M., Gorokhovskii, B.M., 2007. Pb-Pb age of Jatulian carbonate rocks: The Tulomozero Formation of southeast Karelia. Stratigr. Geol. Correl. 15, 359–372. https://doi.org/10.1134/S0869593807040028

Papineau, D., 2010. Global biogeochemical changes at both ends of the proterozoic: insights from phosphorites. Astrobiology 10, 165–181. https://doi.org/10.1089/ast.2009.0360

Papineau, D., Mojzsis, S.J., Schmitt, A.K., 2007. Multiple sulfur isotopes from Paleoproterozoic Huronian interglacial sediments and the rise of atmospheric oxygen. Earth and Planetary Science Letters 255, 188–212. https://doi.org/10.1016/j.epsl.2006.12.015

Partin, C.A., Bekker, A., Planavsky, N.J., Scott, C.T., Gill, B.C., Li, C., Podkovyrov, V., Maslov, A., Konhauser, K.O., Lalonde, S.V., Love, G.D., Poulton, S.W., Lyons, T.W., 2013. Large-scale fluctuations in Precambrian atmospheric and oceanic oxygen levels from the record of U in shales. Earth Planet Sc Lett 369, 284–293. https://doi.org/10.1016/j.epsl.2013.03.031

Pasquier, V., Sansjofre, P., Rabineau, M., Revillon, S., Houghton, J., Fike, D.A., 2017. Pyrite sulfur isotopes reveal glacial–interglacial environmental changes. Proceedings of the National Academy of Sciences 114, 5941–5945. https://doi.org/10.1073/pnas.1618245114

Pavlov, A. a., Kasting, J. f., 2002. Mass-Independent Fractionation of Sulfur Isotopes in Archean Sediments: Strong Evidence for an Anoxic Archean Atmosphere. Astrobiology 2, 27–41. https://doi.org/10.1089/153110702753621321

Penniston-Dorland, S.C., Mathez, E.A., Wing, B.A., Farquhar, J., Kinnaird, J.A., 2012. Multiple sulfur isotope evidence for surface-derived sulfur in the Bushveld Complex. Earth Planet Sc Lett 337, 236–242. https://doi.org/10.1016/j.epsl.2012.05.013

Perttunen, V., Vaasjoki, M., 2001. U-Pb geochronology of the Peräpohja Schist Belt, northwestern Finland. Geological Survey of Finland, Special Paper 33 45–84.

Picard, A., Gartman, A., Clarke, D.R., Girguis, P.R., 2018. Sulfate-reducing bacteria influence the nucleation and growth of mackinawite and greigite. Geochimica et Cosmochimica Acta 220, 367–384. https://doi.org/10.1016/j.gca.2017.10.006

Planavsky, N., Bekker, A., Rouxel, O.J., Kamber, B., Hofmann, A., Knudsen, A., Lyons, T.W., 2010. Rare Earth Element and yttrium compositions of Archean and Paleoproterozoic Fe formations revisited: New perspectives on the significance and mechanisms of deposition. Geochimica et Cosmochimica Acta 74, 6387–6405. https://doi.org/10.1016/j.gca.2010.07.021

Planavsky, N.J., Bekker, A., Hofmann, A., Owens, J.D., Lyons, T.W., 2012. Sulfur record of rising and falling marine oxygen and sulfate levels during the Lomagundi event. P Natl Acad Sci USA 109, 18300–18305. https://doi.org/10.1073/pnas.1120387109

Planavsky, N.J., McGoldrick, P., Scott, C.T., Li, C., Reinhard, C.T., Kelly, A.E., Chu, X., Bekker, A., Love, G.D., Lyons, T.W., 2011. Widespread iron-rich conditions in the mid-Proterozoic ocean. Nature 477, 448–451. https://doi.org/10.1038/nature10327

Planavsky, N.J., Slack, J.F., Cannon, W.F., O'Connell, B., Isson, T.T., Asael, D., Jackson, J.C., Hardisty, D.S., Lyons, T.W., Bekker, A., 2018. Evidence for episodic oxygenation in a weakly redox-buffered deep mid-Proterozoic ocean. Chemical Geology 483, 581–594. https://doi.org/10.1016/j.chemgeo.2018.03.028

Poulton, S.W., Canfield, D.E., 2011. Ferruginous Conditions: A Dominant Feature of the Ocean through Earth's History. Elements 7, 107–112. https://doi.org/10.2113/gselements.7.2.107

Poulton, S.W., Canfield, D.E., 2005. Development of a sequential extraction procedure for iron: implications for iron partitioning in continentally derived particulates. Chemical Geology 214, 209–221. https://doi.org/10.1016/j.chemgeo.2004.09.003

Poulton, S.W., Fralick, P.W., Canfield, D.E., 2004. The transition to a sulphidic ocean [similar] 1.84 billion years ago [WWW Document]. Nature. URL http://link.galegroup.com/apps/doc/A186294134/AONE?sid=googlescholar (accessed 9.8.18).

Poulton, S.W., Raiswell, R., 2002. The low-temperature geochemical cycle of iron: From continental fluxes to marine sediment deposition. Am J Sci 302, 774–805. https://doi.org/DOI 10.2475/ajs.302.9.774

Preuß, A., Schauder, R., Fuchs, G., 1989. Carbon Isotope Fractionation by Autotrophic Bacteria with Three Different CO2 Fixation Pathways. Zeitschrift fur Naturforschung 44c, 397–402.

Priyatkina, N., Khudoley, A.K., Ustinov, V.N., Kullerud, K., 2014. 1.92 Ga kimberlitic rocks from Kimozero, NW Russia: Their geochemistry, tectonic setting and unusual field occurrence. Precambrian Res 249, 162–179. https://doi.org/10.1016/j.precamres.2014.05.009

Puchtel, I.S., Arndt, N.T., Hofmann, A.W., Haase, K.M., Kroner, A., Kulikov, V.S., Kulikova, V.V., Garbe-Schonberg, C.D., Nemchin, A.A., 1998. Petrology of mafic lavas within the Onega plateau, central Karelia: evidence for 2.0 Ga plume-related continental crustal growth in the Baltic Shield. Contributions to Mineralogy and Petrology 130, 134–153. https://doi.org/10.1007/s004100050355

Puchtel, I.S., Brugmann, G.E., Hofmann, A.W., 1999. Precise Re-Os mineral isochron and Pb-Nd-Os isotope systematics of a mafic-ultramafic sill in the 2.0 Ga Onega plateau (Baltic Shield). Earth Planet Sc Lett 170, 447–461. https://doi.org/10.1016/s0012-821x(99)00118-1

Pufahl, P.K., Hiatt, E.E., Kyser, T.K., 2010. Does the Paleoproterozoic Animikie Basin record the sulfidic ocean transition? Geology 38, 659–662. https://doi.org/10.1130/G30747.1

Qu, Y., Crne, A.E., Lepland, A., Van Zuilen, M.A., 2012. Methanotrophy in a Paleoproterozoic oil field ecosystem, Zaonega Formation, Karelia, Russia. Geobiology 10, 467–478. https://doi.org/Doi 10.1111/Gbi.12007

Qu, Y., Lepland, A., van Zuilen, M.A., Whitehouse, M., Črne, A.E., Fallick, A.E., 2018. Sample-scale carbon isotopic variability and diverse biomass in the Paleoproterozoic Zaonega Formation, Russia. Precambrian Research 315, 222–231. https://doi.org/10.1016/j.precamres.2018.07.008

Raiswell, R., Canfield, D.E., 2012. The Iron Biogeochemical Cycle Past and Present. Geochem Perspect 1, 1–220. https://doi.org/10.7185/geochempersp.1.1

Raiswell, R., Canfield, D.E., Berner, R.A., 1994. A Comparison of Iron Extraction Methods for the Determination of Degree of Pyritisation and the Recognition of Iron-Limited Pyrite Formation. Chemical Geology 111, 101–110. https://doi.org/Doi 10.1016/0009-2541(94)90084-1

Rau, G., 1978. Carbon-13 Depletion in a Subalpine Lake: Carbon Flow Implications. Science 201, 901–902. https://doi.org/10.1126/science.201.4359.901

Raven, M.R., Fike, D.A., Gomes, M.L., Webb, S.M., Bradley, A.S., McClelland, H.-L.O., 2018. Organic carbon burial during OAE2 driven by changes in the locus of organic matter sulfurization. Nature Communications 9, 3409. https://doi.org/10.1038/s41467-018-05943-6

Raven, M.R., Sessions, A.L., Adkins, J.F., Thunell, R.C., 2016. Rapid organic matter sulfurization in sinking particles from the Cariaco Basin water column. Geochimica et Cosmochimica Acta 190, 175–190. https://doi.org/10.1016/j.gca.2016.06.030

Reddy, S.M., Evans, D.A.D., 2009. Palaeoproterozoic supercontinents and global evolution: correlations from core to atmosphere: Fig. 1. Geological Society, London, Special Publications 323, 1–26. https://doi.org/10.1144/SP323.1

Rees, C.E., Jenkins, W.J., Monster, J., 1978. The sulphur isotope geochemistry of ocean water sulphate. Geochimica et Cosmochimica Acta 42, 377–381. https://doi.org/10.1016/0016-7037(78)90268-5

Reinhard, C.T., Raiswell, R., Scott, C., Anbar, A.D., Lyons, T.W., 2009. A Late Archean Sulfidic Sea Stimulated by Early Oxidative Weathering of the Continents. Science 326, 713–716. https://doi.org/10.1126/science.1176711

Reuschel, M., Melezhik, V.A., Strauss, H., 2012a. Sulfur isotopic trends and iron speciation from the c. 2.0 Ga Pilgujärvi Sedimentary Formation, NW Russia. Precambrian Research 196–197, 193–203. https://doi.org/10.1016/j.precamres.2011.12.009

Reuschel, M., Melezhik, V.A., Whitehouse, M.J., Lepland, A., Fallick, A.E., Strauss, H., 2012b. Isotopic evidence for a sizeable seawater sulfate reservoir at 2.1 Ga. Precambrian Res 192–95, 78–88. https://doi.org/DOI 10.1016/j.precamres.2011.10.013

Ries, J.B., Fike, D.A., Pratt, L.M., Lyons, T.W., Grotzinger, J.P., 2009. Superheavy pyrite (34Spyr > 34SCAS) in the terminal Proterozoic Nama Group, southern Namibia: A consequence of low seawater sulfate at the dawn of animal life. Geology 37, 743–746. https://doi.org/10.1130/G25775A.1

Ripley, E.M., Wernette, B.W., Ayre, A., Li, C., Smith, J.M., Underwood, B.S., Keays, R.R., 2017. Multiple S isotope studies of the Stillwater Complex and country rocks: An assessment of the role of crustal S in the origin of PGE enrichment found in the J-M Reef and related rocks. Geochimica et Cosmochimica Acta 226–245.

Robert, F., Chaussidon, M., 2006. A palaeotemperature curve for the Precambrian oceans based on silicon isotopes in cherts. Nature 443, 969–972. https://doi.org/10.1038/nature05239

Romero, A.B., 2003. Mass-independent sulfur isotopic compositions in present-day sulfate aerosols. Journal of Geophysical Research 108. https://doi.org/10.1029/2003JD003660

Roscoe, S.M., Minter, W.E.L., 1993. Pyritic paleoplacer gold and uranium deposits, in: Mineral Deposit Modeling, Special Paper-Geological Association of Canada. Presented at the International conference, Mineral deposit modeling, Geological Association of Canada, St. John's, Newfoundland, pp. 103–124.

Rosing, M.T., 1999. 13C-Depleted Carbon Microparticles in >3700-Ma Sea-Floor Sedimentary Rocks from West Greenland. Science 283, 674–676. https://doi.org/10.1126/science.283.5402.674

Roy, S., 2006. Sedimentary manganese metallogenesis in response to the evolution of the Earth system. Earth-Science Reviews 77, 273–305. https://doi.org/10.1016/j.earscirev.2006.03.004

Russell, M.J., Hall, A.J., 1997. The emergence of life from iron monosulphide bubbles at a submarine hydrothermal redox and pH front. Journal of the Geological Society 154, 377–402. https://doi.org/10.1144/gsjgs.154.3.0377

Rybacki, K.S., Kump, L.R., Hanski, E.J., Melezhik, V.A., 2013. 7.4 An Apparent Oxidation of the Upper Mantle versus Regional Deep Oxidation of Terrestrial Surfaces in the Fennoscandian Shield, in: Melezhik, V.A., Prave, A.R., Hanski, E.J., Fallick, A.E., Lepland, A., Kump, L.R., Strauss, H. (Eds.), Reading the Archive of Earth's Oxygenation. Springer Berlin Heidelberg, Berlin, Heidelberg, pp. 1151–1167. https://doi.org/10.1007/978-3-642-29670-3_4

Rye, R., Holland, H.D., 1998. Paleosols and the evolution of atmospheric oxygen: a critical review. Am J Sci 298, 621–672.

Sackett, W.M., 1978. Carbon and hydrogen isotope effects during thermo-catalytic production of hydrocarbons in laboratory simulation experiments. Geochimica et Cosmochimica Acta 42, 571–580.

Samalens, N., Barnes, S.J., Sawyer, E.W., 2017. The role of black shales as a source of sulfur and semimetals in magmatic nickel-copper deposits: Example from the Partridge River Intrusion, Duluth Complex, Minnesota, USA. Ore Geol Rev 81, 173–187. https://doi.org/10.1016/j.oregeorev.2016.09.030

Savarino, J., Romero, A., Cole-Dai, J., Thiemens, M.H., 2003. UV induced mass-independent sulfur composition in stratospheric volcanic eruptions. Geochim. Cosmochim. Acta 67.

Schidlowski, M., 2001. Carbon isotopes as biogeochemical recorders of life over 3.8 Ga of Earth history: evolution of a concept. Precambrian Research 106, 117–134. https://doi.org/10.1016/S0301-9268(00)00128-5

Schoell, M., 1983. Genetic-characterization of natural gases. American Association of Petroleum Geologists 67, 546.

Schröder, S., Bekker, A., Beukes, N.J., Strauss, H., Niekerk, H.S.V., 2008. Rise in seawater sulphate concentration associated with the Paleoproterozoic positive carbon isotope excursion: evidence from sulphate evaporites in the ∼2.2–2.1 Gyr shallow-marine Lucknow Formation, South Africa. Terra Nova 20, 108–117. https://doi.org/10.1111/j.1365-3121.2008.00795.x

Scott, C., Lyons, T.W., Bekker, A., Shen, Y., Poulton, S.W., Chu, X., Anbar, A.D., 2008. Tracing the stepwise oxygenation of the Proterozoic ocean. Nature 452, 456.

Scott, C., Wing, B.A., Bekker, A., Planavsky, N.J., Medvedev, P., Bates, S.M., Yun, M., Lyons, T.W., 2014. Pyrite multiple-sulfur isotope evidence for rapid expansion and contraction of the early Paleoproterozoic seawater sulfate reservoir. Earth Planet Sc Lett 389, 95–104. https://doi.org/DOI 10.1016/j.eps1.2013.12.010

Scott, C.T., Bekker, A., Reinhard, C.T., Schnetger, B., Krapež, B., Rumble, D., Lyons, T.W., 2011. Late Archean euxinic conditions before the rise of atmospheric oxygen. Geology 39, 119–122. https://doi.org/10.1130/G31571.1

Seal, R.R., 2006. Sulfur isotope geochemistry of sulfide minerals. Rev Mineral Geochem 61, 633–677. https://doi.org/DOI 10.2138/rmg.2006.61.12

Sheen, A.I., Kendall, B., Reinhard, C.T., Creaser, R.A., Lyons, T.W., Bekker, A., Poulton, S.W., Anbar, A.D., 2018. A model for the oceanic mass balance of rhenium and implications for the extent of Proterozoic ocean anoxia. Geochimica et Cosmochimica Acta 227, 75–95. https://doi.org/10.1016/j.gca.2018.01.036

Shen, B., Dong, L., Xiao, S., Kowalewski, M., 2008. The Avalon Explosion: Evolution of Ediacara Morphospace. Science 319, 81–84. https://doi.org/10.1126/science.1150279

Shields-Zhou, G., Och, L., 2011. The case for a Neoproterozoic Oxygenation Event: Geochemical evidence and biological consequences. GSA Today 21, 4–11. https://doi.org/10.1130/GSATG102A.1

Sim, M.S., Bosak, T., Ono, S., 2011. Large Sulfur Isotope Fractionation Does Not Require Disproportionation. Science 333, 74–77. https://doi.org/10.1126/science.1205103

Slotznick, S.P., Eiler, J.M., Fischer, W.W., 2018. The effects of metamorphism on iron mineralogy and the iron speciation redox proxy. Geochimica et Cosmochimica Acta 224, 96–115. https://doi.org/10.1016/j.gca.2017.12.003

Sperling, E.A., Rooney, A.D., Hays, L., Sergeev, V.N., Vorob'eva, N.G., Sergeeva, N.D., Selby, D., Johnston, D.T., Knoll, A.H., 2014. Redox heterogeneity of subsurface waters in the Mesoproterozoic ocean. Geobiology 12, 373–386. https://doi.org/10.1111/gbi.12091

Sperling, E.A., Wolock, C.J., Morgan, A.S., Gill, B.C., Kunzmann, M., Halverson, G.P., Macdonald, F.A., Knoll, A.H., Johnston, D.T., 2015. Statistical analysis of iron geochemical data suggests limited late Proterozoic oxygenation. Nature 523, 451–454. https://doi.org/10.1038/nature14589

Stepanova, A.V., Samsonov, A.V., Larionov, A.N., 2014. The final episode of middle Proterozoic magmatism in the Onega structure: data on trans-Onega dolerites. Proceedings of the Karelian Research Centre of the Russian Academy of Sci-ences 1, 3–16.

Strauss, H., Melezhik, V.A., Lepland, A., Fallick, A.E., Hanski, E.J., Filippov, M.M., Deines, Y.E., Illing, C.J., Črne, A.E., Brasier, A.T., 2013. Enhanced Accumulation of Organic Matter: The Shunga Event, in: Melezhik, V.A., Prave, A.R., Hanski, E.J., Fallick, A.E., Lepland, A., Kump, L.R., Strauss, H. (Eds.), Reading the Archive of Earth's Oxygenation. Springer Berlin Heidelberg, Berlin, Heidelberg, pp. 1195–1273. https://doi.org/10.1007/978-3-642-29670-3_6

Taylor, S.R., McLennan, S.M., Armstrong, R.L., Tarney, J., 1981. The Composition and Evolution of the Continental Crust: Rare Earth Element Evidence from Sedimentary Rocks [and Discussion]. Philosophical Transactions of the Royal Society of London. Series A, Mathematical and Physical Sciences 301, 381–399.

Thode, H.G., Ding, T., Crocket, J.H., 1991. Sulphur-isotope and elemental geochemistry studies of the Hemlo gold mineralization, Ontario: sources of sulphur and implications for the mineralization process. Can. J. Earth Sci. 28, 13–25. https://doi.org/10.1139/e91-002

Twist, D., Cheney, E.S., 1986. Evidence for the transition to an oxygen-rich atmosphere in the Rooiberg Group, South Africa — A note. Precambrian Research 33, 255–264. https://doi.org/10.1016/0301-9268(86)90045-8

Ueno, Y., Johnson, M.S., Danielache, S.O., Eskebjerg, C., Pandey, A., Yoshida, N., 2009. Geological sulfur isotopes indicate elevated OCS in the Archean atmosphere, solving faint young sun paradox. PNAS 106, 14784–14789. https://doi.org/10.1073/pnas.0903518106

van Breugel, Y., Schouten, S., Paetzel, M., Nordeide, R., Sinninghe Damsté, J.S., 2005. The impact of recycling of organic carbon on the stable carbon isotopic composition of dissolved inorganic carbon in a

stratified marine system (Kyllaren fjord, Norway). Organic Geochemistry 36, 1163–1173. https://doi.org/10.1016/j.orggeochem.2005.03.003

Wagner, T., Boyce, A.J., 2006. Pyrite metamorphism in the Devonian Hunsruck Slate of Germany: Insights from laser microprobe sulfur isotope analysis and thermodynamic modeling. Am J Sci 306, 525–552. https://doi.org/10.2475/07.2006.02

Warke, M.R., Schröder, S., 2018. Synsedimentary fault control on the deposition of the Duitschland Formation (South Africa): Implications for depositional settings, Paleoproterozoic stratigraphic correlations, and the GOE. Precambrian Research 310, 348–364. https://doi.org/10.1016/j.precamres.2018.03.001

Watanabe, Y., Farquhar, J., Ohmoto, H., 2009. Anomalous Fractionations of Sulfur Isotopes During Thermochemical Sulfate Reduction. Science 324, 370–373. https://doi.org/10.1126/science.1169289

Weber, F., Gauthier-Lafaye, F., 2013. No proof from carbon isotopes in the Francevillian (Gabon) and Onega (Fennoscandian shield) basins of a global oxidation event at 1980–2090 Ma following the Great Oxidation Event (GOE). Comptes Rendus Geoscience 345, 28–35. https://doi.org/10.1016/j.crte.2012.12.003

Weiss, M.C., Sousa, F.L., Mrnjavac, N., Neukirchen, S., Roettger, M., Nelson-Sathi, S., Martin, W.F., 2016. The physiology and habitat of the last universal common ancestor. Nature Microbiology 1, 16116.

Werne, J.P., Hollander, D.J., Lyons, T.W., Sinninghe Damsté, J.S., 2004. Organic sulfur biogeochemistry: Recent advances and future research directions, in: Special Paper 379: Sulfur Biogeochemistry - Past and Present. Geological Society of America, pp. 135–150. https://doi.org/10.1130/0-8137-2379-5.135

Werne, J.P., Lyons, T.W., Hollander, D.J., Formolo, M.J., Sinninghe Damsté, J.S., 2003. Reduced sulfur in euxinic sediments of the Cariaco Basin: sulfur isotope constraints on organic sulfur formation. Chemical Geology, Isotopic records of microbially mediated processes 195, 159–179. https://doi.org/10.1016/S0009-2541(02)00393-5

Whiticar, M.J., 1999. Carbon and hydrogen isotope systematics of bacterial formation and oxidation of methane. Chemical Geology 161, 291–314. https://doi.org/Doi 10.1016/S0009-2541(99)00092-3

Wilde, S.A., Valley, J.W., Peck, W.H., Graham, C.M., 2001. Evidence from detrital zircons for the existence of continental crust and oceans on the Earth 4.4 Gyr ago. Nature 409, 175–178. https://doi.org/10.1038/35051550

Wing, B.A., Halevy, I., 2014. Intracellular metabolite levels shape sulfur isotope fractionation during microbial sulfate respiration. Proceedings of the National Academy of Sciences 111, 18116–18125. https://doi.org/10.1073/pnas.1407502111

Wortmann, U.G., Paytan, A., 2012. Rapid Variability of Seawater Chemistry Over the Past 130 Million Years. Science 337, 334–336. https://doi.org/10.1126/science.1220656

Xiao, S., Schiffbauer, J.D., McFadden, K.A., Hunter, J., 2010. Petrographic and SIMS pyrite sulfur isotope analyses of Ediacaran chert nodules: Implications for microbial processes in pyrite rim formation, silicification, and exceptional fossil preservation. Earth and Planetary Science Letters 297, 481–495. https://doi.org/10.1016/j.epsl.2010.07.001

Young, G.M., Brunn, V. von, Gold, D.J.C., Minter, W.E.L., 1998. Earth's Oldest Reported Glaciation: Physical and Chemical Evidence from the Archean Mozaan Group (~2.9 Ga) of South Africa. The Journal of Geology 106, 523–538. https://doi.org/10.1086/516039

Zaback, D.A., Pratt, L.M., Hayes, J.M., 1993. Transport and reduction of sulfate and immobilization of sulfide in marine black shales. Geology 21, 141–144. https://doi.org/10.1130/0091-7613(1993)021<0141:TAROSA>2.3.CO;2

Zerkle, A.L., Claire, M.W., Domagal-Goldman, S.D., Farquhar, J., Poulton, S.W., 2012. A bistable organic-rich atmosphere on the Neoarchaean Earth. Nature Geoscience 5, 359.

Zerkle, A.L., House, C.H., Brantley, S.L., 2005. Biogeochemical signatures through time as inferred from whole microbial genomes. Am J Sci 305, 467–502. https://doi.org/DOI 10.2475/ajs.305.6-8.467

Zerkle, A.L., Jones, D.S., Farquhar, J., Macalady, J.L., 2016. Sulfur isotope values in the sulfidic Frasassi cave system, central Italy: A case study of a chemolithotrophic S-based ecosystem. Geochimica et Cosmochimica Acta 173, 373–386. https://doi.org/10.1016/j.gca.2015.10.028

Zerkle, A.L., Kamyshny, A., Kump, L.R., Farquhar, J., Oduro, H., Arthur, M.A., 2010. Sulfur cycling in a stratified euxinic lake with moderately high sulfate: Constraints from quadruple S isotopes. Geochimica et Cosmochimica Acta 74, 4953–4970. https://doi.org/10.1016/j.gca.2010.06.015

Paper 1

Multiple sulphur isotope records tracking basinal and global processes in the 1.98 Ga Zaonega Formation

K. Paiste, A. Lepland, A. L. Zerkle, K. Kirsimäe, G. Izon, N. K. Patel, F. McLean, T. Kreitsmann, K. Mänd, T. H. Bui, A. E. Romashkin, D. V. Rychanchik, A. R. Prave

Accepted manuscript in Chemical Geology
https://doi.org/10.1016/j.chemgeo.2018.09.025

Paper 2

Biogeochemical sulfur cycling in a semirestricted basin – modelling the pyrite multiple sulfur isotope record of the 1.98 Ga Zaonega Formation

K. Paiste, B. A. Wing, A. L. Zerkle, K. Kirsimäe, A. Pellerin, A. R. Prave, A. E. Romashkin, A. Lepland

Manuscript to be submitted to Earth and Planetary Science Letters

Paper 3

Global vs. basinal controls on Paleoproterozoic sulfur isotope records: new insights from the Zaonega Formation, NW Russia

K. Paiste, A. Lepland, A. L. Zerkle, B. A. Wing, K. Kirsimäe, T. Kreitsmann, K. Mänd, A. E. Romashkin, D. V. Rychanchik, A. R. Prave

Manuscript to be submitted to Earth-Science Reviews